IDŐJÁRÁS

QUARTERLY JOURNAL
OF THE HUNGARIAN METEOROLOGICAL SERVICE

CONTENTS

G. Götz: Application of nonlinear dynamics in atmospheric sciences. Part II. Some examples 65

D. S. Lee and *J. W. S. Longhurst*: The urban modification of acid deposition 87

I. Csiszár: The effect of the droplet size distribution on the reflectivity of boundary layer clouds 107

Zs. Bacsi and *M. Hunkár*: Assessment of the impacts of climate change on the yields of winter wheat and maize, using crop models 119

Á. T. Meszlényi: Cloud motion winds derived from METEOSAT infrared images 135

Book review 143

News 145

Contents of journal Atmospheric Environment Vol. 28 Nos. 3–6 147

VOL. 98 * NO. 2 * APRIL–JUNE 1994

IDŐJÁRÁS

Quarterly Journal of the Hungarian Meteorological Service

Editor-in-Chief
E. MÉSZÁROS

Editor
T. TÄNCZER

Technical Editor
Mrs. M. ANTAL

EDITORIAL BOARD

ANTAL, E. (Budapest)
BOTTENHEIM, J. (Downsview, Ont.)
CZELNAI, R. (Budapest)
DÉVÉNYI, D. (Budapest)
DRĂGHICI, I. (Bucharest)
FARAGÓ, T. (Budapest)
FISHER, B. (London)
GEORGII, H.-W. (Frankfurt a. M.)
GÖTZ, G. (Budapest)
HAMAN, K. (Warsaw)
HASZPRA, L. (Budapest)
IVÁNYI, Z. (Budapest)
KALNAY, E. (Washington, D.C.)
KOLB, H. (Vienna)
KONDRATYEV, K.Ya. (St. Petersburg)
MAJOR, G. (Budapest)
MILOSHEV, G. (Sofia)
MÖLLER, D. (Berlin)
PANCHEV, S. (Sofia)
PRÁGER, T. (Budapest)
PRETEL, J. (Prague)
PRUPPACHER, H.R. (Mainz)
RÁKÓCZI, F. (Budapest)
RENOUX, A. (Paris-Créteil)
ŠAMAJ, F. (Bratislava)
SPÄNKUCH, D. (Potsdam)
STAROSOLSZKY, Ö. (Budapest)
VARGA-HASZONITS, Z. (Budapest)
WILHITE, D.A. (Lincoln, NE)
WIRTH, E. (Budapest)

Editorial Office: P.O. Box 39, H–1675 Budapest

Subscription from customers in Hungary should be sent to the Financial Department of the Hungarian Meteorological Service Kitaibel Pál u. 1, 1024 Budapest. The subscription rate is HUF 2000.

Abroad the journal can be purchased from the distributor: KULTURA, P.O. Box 149, H–1389 Budapest. The annual subscription rate is USD 56.

IDŐJÁRÁS

Quarterly Journal of the Hungarian Meteorological Service
Vol. 98, No. 2, April–June 1994

Application of nonlinear dynamics in atmospheric sciences Part II. Some examples

G. Götz

Hungarian Meteorological Service
P.O. Box 38, H-1525 Budapest, Hungary

(Manuscript received 1 March 1994; in final form 20 April 1994)

Abstract—The purpose of this review article is to demonstrate the applicability of chaos theory in the study of the nature of atmospheric behavior. Selected examples are chosen to illustrate how the theory of nonlinear dynamics has improved our understanding of the behavior of the atmosphere, and how new ideas and insights are shaping our way of investigating the prediction problem. The examples presented cover a wide range of the frequency domain of atmospheric variability, extending from the phenomenon of cellular convection up to the glacial-interglacial fluctuations of the Quaternary ice age. Special attention is devoted to the nonlinear dynamical aspects of a global climate change. Finally, the existence of low-dimensional atmospheric attractors, a highly debated subject in these days, is discussed.

Key-words: strange attractor, chaos, fractals, predictability.

1. Introduction

The basic goal of dynamical systems theory is to understand the asymptotic consolidated behavior of a given bounded deterministic system as $t \to \infty$. It is now an accepted notion that many *nonlinear* dissipative dynamical systems do not approach stationary, periodic or quasi-periodic final states as transients monotonically die out. Instead, with appropriate values of their control parameters, they tend towards *strange attractors* in the phase space, on which the spectra of the trajectories are not composed solely of discrete frequencies, but have a continuous, broad-band nature. This noise-like consolidated behavior of a deterministic system has been termed *chaotic* or *strange behavior.*

Strange attractors are not smooth topological manifolds, and do not have integer dimension. Typically, a strange attractor arises when the flow of the

dissipative system does not contract a volume element in all directions of the phase space, but stretches it in some. In order to remain confined to a bounded domain, the volume element gets folded at the same time, so that it has after some time a multisheeted structure. A closer study shows that a choatic attractor finally becomes locally Cantor-set like in some directions, and is accordingly a *fractal construction* in the sense of *Mandelbrot* (1977).

Another property of choatic systems is *sensitive dependence on initial conditions*: initially nearby trajectories diverge at a rate characteristic of the system until, for all practical purposes, they are uncorrelated. In practice, the initial state of a system can never be specified exactly, but only to within some tolerance $\epsilon > 0$. Therefore, no matter how precisely the initial condition is known, the long-term behavior of the system can never be predicted. It is the discovery of this property of chaotic systems, also known as *dynamical instability* with respect to small perturbations, that has eliminated one of the basic tenets of science, the Laplacian idea of long-term deterministic predictability.

In order to make quantitative the notion of 'sensitive dependence on initial conditions', Lyapunov exponents are most frequently used. The Lyapunov exponents λ_i ($i = 1, 2, \ldots, n$) of an n-dimensional dynamical system are determined by $\epsilon_i(t) \approx \epsilon(0)\, e^{\lambda_i t}$, and describe the distortion of a sufficiently small hypersphere in the phase space of radius $\epsilon(0)$ at time $t = 0$ into at ellipsoid of principal semi-axes $\epsilon_i(t)$ at $t = t$. Thus, Lyapunov exponents quantify the long-term average dynamical stability properties of the system's behavior on an attractor by measuring the exponential rates of convergence ($\lambda_i < 0$) or divergence ($\lambda_i > 0$) of initially nearby trajectories. A positive exponent indicates chaotic behavior and a loss of predictability.

One limitation of the Lyapunov exponents is that while they describe the stretching needed to generate a strange attractor, they do not say much about the folding. To eliminate this drawback, the dimension of the attractor is used. There are several ways to generalize the concept of dimension to the fractional case (*Farmer et al.*, 1983; *Grassberger* and *Procaccia*, 1983a,b). The relevant definitions are of two general types, those that depend only on metric properties (e.g. the fractal dimension), and those that depend on the frequency with which a typical trajectory visits different regions of the attractor (e.g. the information dimension and the correlation dimension). Another type of dimension is the Lyapunov dimension, which is defined in terms of Lyapunov exponents, and is usually far easier to calculate than any other definition.

The concept of deterministic randomness has initiated a rapidly developing interdisciplinary field of research called *nonlinear dynamics*. As it was discussed in some details in Part I of this paper (*Götz,* 1992), the atmosphere should be considered as a nonlinear system forced by differential heating of the solar radiation, and kept bounded by dissipation of its total energy due to outgoing thermal radiation and the diffusive effects of friction. Therefore, it seems evident that chaos theory has its natural applications in atmospheric sciences,

leading to new ideas and insights, and offering inspiration for further research. The purpose of this part of the article is to give some examples of these applications aiming at a better understanding of weather and climate processes.

2. *The chaotic behavior of atmospheric processes*

In this section, the asymptotic final-state characteristics of some selected macro-scale motion systems of the atmosphere are discussed, and the problem of predictability in nonlinear dynamics is briefly reviewed.

2.1 The Rayleigh-Bénard convection

Historically the irregular and apparently random behavior of a simple deterministic dynamical system was first demonstrated by *Lorenz* (1963) in his work on Rayleigh-Bénard convection, i.e. the flow occurring in a layer of fluid of uniform depth, when the temperature difference between the upper and lower surfaces is maintained at a constant value. The simplified equations governing this forced dissipative hydrodynamic flow are

$$\left.\begin{aligned} dx/dt &= \sigma y - \sigma x, \\ dy/dt &= rx - y - xz, \\ dz/dt &= xy - bz. \end{aligned}\right\} \tag{1}$$

In this third-order autonomous dynamical system, the state variable x is proportional to the intensity of the convective motion, y is proportional to the temperature difference between the ascending and descending currents, while z is proportional to the distortion of the vertical temperature profile from linearity. Among the control parameters of the system, r is the Rayleigh number, i.e. the forcing parameter, which is proportional to the imposed vertical temperature gradient, σ is the Prandtl number of the fluid, and b is related to the aspect ratio of the domain. The variation of the volume V of a small region in the phase space of the system, as each point in the region is displaced in accordance with (1), is

$$dV/dt = -V(\sigma + b + 1). \tag{2}$$

Hence each small volume shrinks to zero as $t \to \infty$, at a rate independent of the state variables. This does not imply that each small volume shrinks to a point; it may simply become flattened into a surface. Consequently, all sufficiently close trajectories become 'attracted' asymptotically to a specific subset of the phase space having zero volume.

Eqs. (1) possess the steady-state solution $x = y = z = 0$, representing the state of no convection. The criterion for the onset of convection is $r = 1$. When $r > 1$, Eqs. (1) have two additional steady-state solutions $x = y = \pm\sqrt{b(r-1)}$, $z = r - 1$. If $\sigma > b + 1$, the states of steady convection are linearly unstable for sufficiently high Rayleigh numbers.

The surprising, previously unknown behavioral form of the deterministic system (1) appears at the slightly supercritical control parameter value of the thermal forcing $r = 28$. For $b = 8/3$ and $\sigma = 10$, and using a standard fourth-order Runge-Kutta scheme with time increment $\Delta t = 0.01$ to integrate the equations, the graph of x as a function of t obtained for the first 4500 iterations is shown in *Fig. 1*. The initial instability of the state of rest is evident; the strength of the convection grows rapidly. After reaching its early peak, it undergoes systematic amplified oscillation. Then a critical state is reached, and thereafter x changes sign at seemingly irregular intervals, reaching sometimes one, sometimes two, and sometimes three or more extremes of one sign before changing sign again. Projections of the transient-free solution trajectory onto the xy-, xz- and yz-planes of the phase space corresponding to iterations 4001 to 9000 are shown in *Fig. 2*. Characteristically, the trajectory travels around one of the two unstable fixed points of the system (which represent the states of steady convection), and crosses from one spiral to the other at irregular intervals. One of the main conclusions is that there are certain thermally (or mechanically) forced nonconservative hydrodynamical systems exhibiting *irregular behavior* when there is *no* obviously related irregularity in the forcing process (*Lorenz,* 1963). The peculiar geometrical object in Fig. 2, resembling an owl's mask or butterfly's wing, is now known as the *Lorenz attractor* of the Lorenz equations (1).

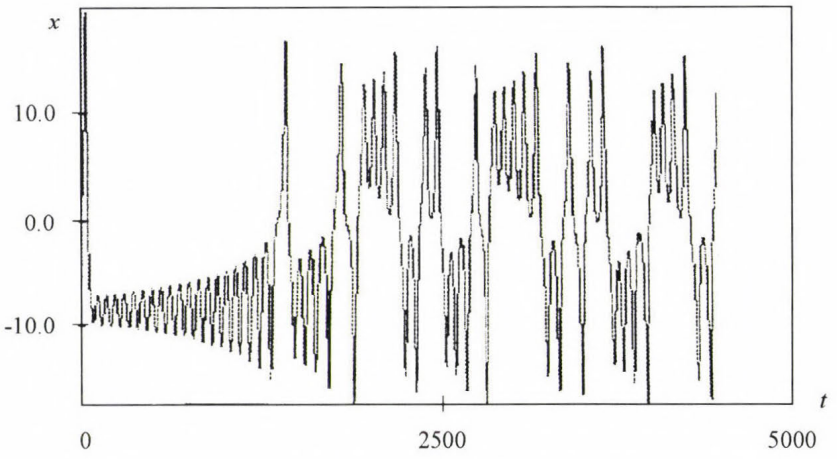

Fig. 1. Numerical solution of the Rayleigh-Bénard convection equations. Graph of x as a function of time for the first 4500 iterations.

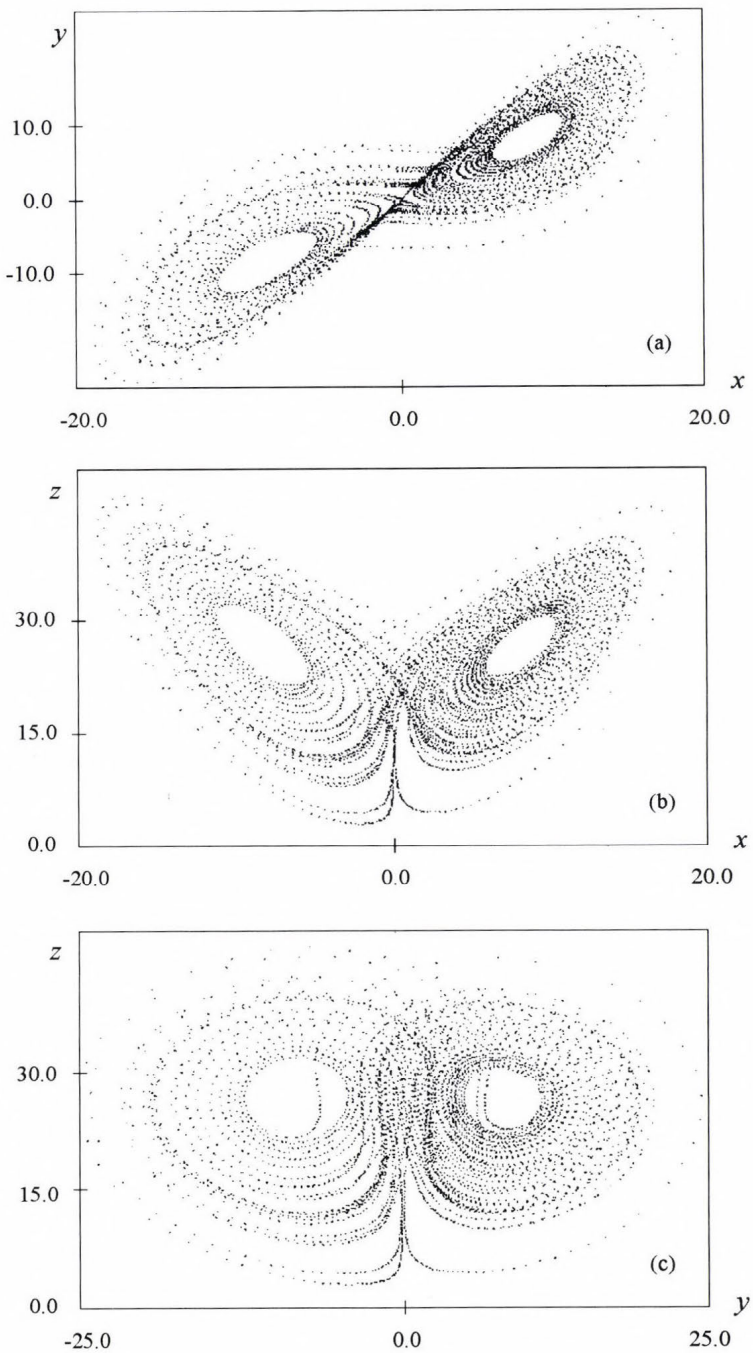

Fig. 2. Numerical solution of the Rayleigh-Bénard convection equations. Projections (*a*) on the *xy*-, (*b*) on the *xz*-, and (*c*) on the *yz*-planes in the phase space of the segment of the trajectory from iteration 4001 to iteration 9000.

To quantify the phase space topology of the Lorenz attractor, first we note from Eq. (2) that the net divergence of the flow is $1/V\,(dV/dt) = -(\sigma + b + 1) = -41/3$. When using the method described by *Nese et al.* (1987), we find the Lyapunov exponents $\lambda_1 = 0.93$, $\lambda_2 = 0$, $\lambda_3 = -14.60$. The Lyapunov dimension of the attractor embedded in the three-dimensional phase space is given by

$$d_L = 2 + \frac{\lambda_+}{|\lambda_-|} = 2.063\,.$$

The existence of one positive Lyapunov exponent indicates the presence of chaos. The relative magnitudes of λ_1 and λ_3 indicate that the contraction of a phase space volume in one principal direction is occurring much faster than the rate of expansion of the volume along another principal axis. This is quantified by the small fractional component of the Lyapunov dimension which, on the other hand, measures the 'strangeness' of the Lorenz attractor.

In his famous paper, *Lorenz* (1963) had not used the terms 'chaos' and 'strange attractor'; they emerged some ten years later. The phrase *strange attractor* first appeared in the article by *Ruelle* and *Takens* (1971), and the word *chaos*, that came to stand for deterministic disorder, was coined and introduced to the mathematical literature by *James A. Yorke* in a paper written with his student *Tien-Yien Li* (*Li* and *Yorke*, 1975). Lorenz's work became widely known only about a decade later than it had been published in a meteorological journal but thereafter, in the thousands of articles that made up the technical literature of chaos, few were cited more often than his one.

2.2 *The general circulation of the atmosphere*

In recent years, it has become increasingly recognized that a deeper understanding of the general circulation of the atmosphere is an essential condition to further major progress in the science of meteorology (*Lorenz,* 1991a). The construction of low-order models of the large-scale atmospheric flow for qualitative analysis of its inherent behavioral characteristics constitutes one possible avenue towards achieving this aim.

Lorenz (1984, 1987) has developed such a model of the general circulation which may well be the simplest possible model capable of representing its most prominent feature, i.e. the nonlinear interaction between the zonal flow (Hadley circulation) and the superposed stationary or migratory disturbances. The model is defined by three ordinary differential equations

$$\left.\begin{aligned} dx/dt &= -y^2 - z^2 - ax + aF, \\ dy/dt &= xy - cxz - y + G, \\ dz/dt &= cxy + xz - z. \end{aligned}\right\} \qquad (3)$$

Here x denotes the intensity of the globally averaged westerly current, which

is identified through the geostrophic relation with the large-scale poleward temperature gradient, while y and z denote the strengths of the cosine and sine phases of a chain of superposed waves, which can be identified with the Rossby waves that transport heat poleward, thus reducing the temperature contrast. The control parameter $c > 1$ allows the displacement of the waves by the westerly current to occur more rapidly than their amplification, while the parameter $a < 1$ allows the westerly current to damp less rapidly than the waves; a suitable choice includes $c = 4$ and $a = 0.25$. F represents the cross-latitude external heating symmetric with respect to the earth's axis, while G represents the asymmetric external thermal forcing due to the heating contrast between the oceans and continents. The time unit equals the damping time for the waves, which is assumed to be five days.

The Eqs. (3) constitute a bounded dynamical system, since it is easily shown that the total energy $(x^2 + y^2 + z^2)/2$ will decrease if it exceeds a certain value. From (3), we also find that the variation of the volume V of an infinitesimal region of the phase space is given by

$$dV/dt = -V(a + 2 - 2x). \tag{4}$$

The right side of (4) is negative only when $x < (1 + a/2)$. Thus, in contrast to the fully dissipative systems, where dV/dt is always negative, there is no assurance that small volumes will shrink to zero, and in particular, that attractors will have zero volume.

For suitable choices of the parameters a, c, F, and G, Eqs. (3) produce chaos, which was studied in details by *Masoller et al.* (1992). Such choices of parameters include $a = 1/4$, $c = 4$, $F = 8$, and $G = 5/4$. Variations of the state variable x in this case will be qualitatively the same as those shown in Fig. 1, i.e. again we will see aperiodic behavior of the system. Therefore, the chief lesson about the atmosphere to be learned from the model is that such fluctuations of the weather need not require external irregularity or even external variability (*Lorenz,* 1984).

Projections of the solution trajectory of Eqs. (3) onto the selected planes of the phase space exhibit the same characteristic configuration of the strange attractor as those displayed in Fig. 2. The solution trajectory moves around the two lobes in an entirely random fashion, but with certain preferred metastable types of behavior: the trajectory spends an extended time (several weeks) in one of the regimes before crossing to the other regime at irregular intervals. We can think about one regime as representing zonal flow, and the other regime as being blocked flow. Therefore, the succession of these episodes may be regarded as modeling the atmospheric index cycle.

As it is known, a linear or quasi-linear description of the large-scale flow of the atmosphere has permitted a qualitative explanation of many of the observed features of the global circulation, but has left others entirely unexplained. In particular, it has not accounted for the persistence of large amplitude

flow anomalies such as blocking. Nor has it explained the existence of the persistent or recurrent weather patterns or types exemplified by the *Grosswetterlage* of *Baur* (1951). Such multiple metastable equilibria (or weather regimes) were first found numerically by *Charney* and *DeVore* (1979) who used another simple nonlinear model in which the external asymmetries were orographic rather than thermal.

The Lyapunov exponents of the dynamical system (3) prove to be $\lambda_1 = 0.18$, $\lambda_2 = 0$, $\lambda_3 = -0.52$. The Lyapunov dimension of the attractor is $d_L = 2.346$. The fractional component of d_L is larger than in the case of the Rayleigh-Bénard convection, indicating that the strange attractor of the general circulation is a more complex construction. The first Lyapunov exponent indicates that, on the average, the *e*-folding time of a small error ϵ in the initial condition is $t = 1/\lambda_1 = 5.55$ time units, or about 28 days. We might add that by real atmospheric standards this growth is unreasonably small. For example, by analyzing the time series of daily surface pressure over the North Atlantic Ocean, *Zeng et al.* (1992) found $\lambda_1 = 0.098$, $\lambda_2 = 0.044$, $\lambda_3 = 0.004$ day^{-1}, i.e. an *e*-folding time of initial error $t = (\lambda_1 + \lambda_2 + \lambda_3)^{-1} = 6.8$ days. (The divergence of initially nearby trajectories in more than one direction in the phase space has been termed *hyper-chaos*.)

2.3 The El Niño-Southern Oscillation phenomenon

An El Niño-Southern Oscillation (ENSO) event may be defined as the appearance of anomalously warm water in the eastern equatorial Pacific. Associated with this is a weakening, and sometimes a reversal, of the trade wind field. An ENSO event has major economic consequences, and much observational and modeling efforts has therefore been devoted to it. The theory elaborated by *Vallis* (1986) differs from others in that the aperiodic occurrence and the variations in intensity of the ENSO are generated internally and deterministically within a simple chaotic dynamical system.

The equatorial ocean is imagined to be a box of fluid characterized by temperatures in the east and west (T_E and T_W), and a current u. The current in the basin of size ΔX is driven by a surface wind, which is in part generated by the temperature gradient $(T_E - T_W)/\Delta X$, so describing a parameterized Walker circulation (i.e. $T_E < T_W$ produces a westward surface wind, because of the tendency of air to rise over warm water), and the temperature field is advected by the current. Thus the nonlinear governing equations of the dynamical system are

$$du/dt = B(T_E - T_W)/2\Delta X - C(u - u^*), \tag{5}$$

$$dT_W/dt = u(\bar{T} - T_E)/2\Delta X - A(T_W - T^*), \tag{6}$$

$$dT_E/dt = u(T_W - \bar{T})/2\Delta X - A(T_E - T^*). \tag{7}$$

Here, the temperature decay time scale A, the influence of ocean temperatures on the wind field B, and the frictional decay time scale C are constants; $-u^* = \text{const}$ is the speed of the mean tropical easterlies, $\bar{T} = \text{const}$ is the temperature below the thermocline, while $T^* = \text{const}$ is the temperature to which the ocean would relax in the absence of motion. In Eq. (5), the terms $B\,(T_E - T_W)/\Delta X + Cu^*$ represent wind-produced stress, and $-Cu$ represents mechanical damping. In Eqs. (6) and (7), the first term on each right-hand side represents horizontal advection, while the second term represents forcing and thermal damping.

With $u^* \neq 0$, Eqs. (5) to (7) have the same structure as the Lorenz equations (1). The physical system resembles that of ordinary convection in that the velocity of circulation is maintained by a horizontal temperature gradient: this sets up a direct circulation in the atmosphere, which forces the ocean. The unusual aspect here is that the oceanic part of the system is able to overturn with warmer water above the cool deep ocean, i.e. a stable configuration because work must be done on the system. Overturning and instability can occur here because the dominant driving of the ocean is mechanical, namely wind stress.

For constant T^*, C and A, all stationary solutions become unstable when B, the thermal forcing of the wind field, is sufficiently large. The system can no longer stably reside anywhere and oscillates apparently randomly between the two least unstable stationary states. Numerical integration of the Eqs. (5) to (7) yields aperiodic behavior plausibly reproducing the basic ENSO event cycle (*Fig. 3*). The system stays in the neighborhood of one unstable stationary solution for many model years before flipping to an ENSO event. These ENSO

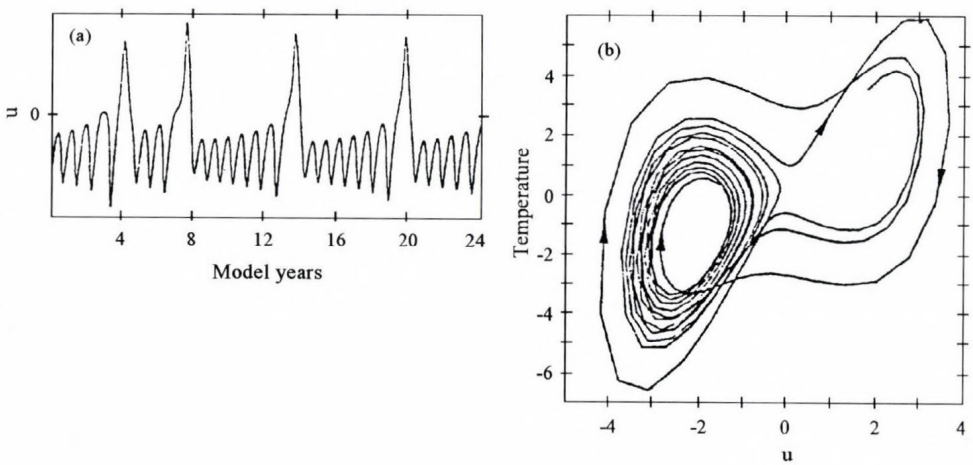

Fig. 3. Numerical solution of the ENSO equations with parameter values $C = 1/4$ month^{-1}, $A = 1$ year^{-1}, $u^* = -0.45$ m s^{-1}, $\Delta X = 7500$ km, and $T^* = 12$°C. (*a*) Graph of u as a function of time. (*b*) Trajectory of the system projected onto the u,$(T_E - T_W)$-plane, over a period of 12 model years. Arrows indicate the direction of the flow. (After *Vallis*, 1986)

states are trajectories around another stationary, but highly unstable, solution and the system quickly returns to its normal, less unstable state.

In summary, this theoretical model clearly demonstrates the underlying dynamics and thereby the possibility of a *purely internal mechanism* for the ENSO. It shows that external triggering or stochastic forcing is not necessarily essential, although such effects may have a role in the real system. Recently, *Elsner* and *Tsonis* (1993) have analyzed a time series describing the ENSO, using the latest techniques of chaos theory. They carried out a strictly empirical investigation of the intrinsic nonlinearity within the atmosphere-ocean system. From the results, nonlinear dynamics in the ENSO have been established at a high confidence level.

2.4 The phase-spatial variation of predictability

The rate at which adjacent trajectories diverge on a chaotic attractor is, in general, not constant, but rather this local divergence rate depends on time and therefore, on location in phase space. Thus, for applications requiring short-term prediction, using only the Lyapunov exponents to measure predictability is inadequate, because any phase-spatially dependent predictability information is essentially eliminated by long-term averaging over the attractor. The local predictability of the Lorenz system (1) from both temporal and phase-spatial viewpoints was studied by *Nese* (1989) to demonstrate how local divergence rates might be used to identify regions of high or low predictability in phase space.

The distribution of local predictability on the Lorenz attractor is summarized qualitatively in *Fig. 4*. We find that initially nearby trajectories converge most rapidly on average as they approach the vicinity of the z-axis on the tops of the wings. Adjacent trajectories diverge most rapidly on average on the bottoms of the wings of the attractor as trajectories swing away from the vicinity of the unstable origin (0,0,0) representing the state of no convection. However, even on a portion of the attractor where predictability is low, there still may be a sense of predictability, because the divergence of nearby trajectories may be a uniform characteristic of that region of the phase space. In these cases, the short-term error growth can be estimated.

Predictability near the z-axis and origin is influenced by two opposing effects. For relatively large values of z, almost all pairs of adjacent trajectories converge temporarily owing to the stabilizing influence of the z-axis, which is part of the two-dimensional stable manifold of the unstable steady state (0,0,0). On the other hand, closer to the origin, the potential for extremely rapid divergence of neighboring trajectories exists, with one trajectory circling each wing. However, this potential is only occasionally realized. Thus the region near the origin, which is the principal source of long-term forecast errors, is only moderately unpredictable in terms of average local divergence rates.

Nonetheless, when catastrophic separation of initially nearby trajectories occurs, the consequences in terms of forecast errors are extremely severe.

The *stable manifold* of a steady state is the set of points **x** in the phase space such that the forward trajectory starting from **x** approaches the steady state. Similarly, the *unstable manifold* of a steady state is the set of points **x** such that the trajectory going backward in time starting from **x** approaches the steady state. Within this context, *Legras* and *Ghil* (1985) suggested a relationship be-

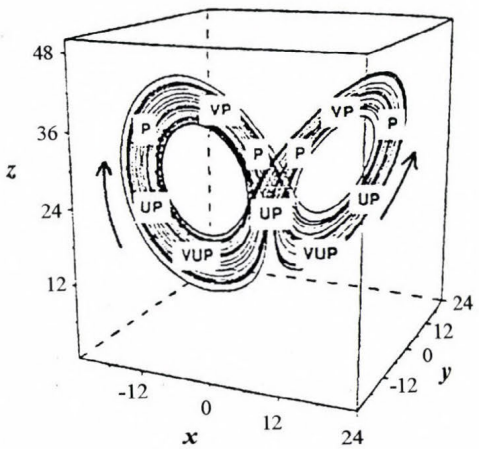

Fig. 4. Distribution of local predictability on the Lorenz attractor in a three-dimensional perspective. The abbreviations VP, P, UP, and VUP denote very predictable, predictable, unpredictable, and very unpredictable regions, respectively. Arrows indicate the direction of the flow. (After *Nese*, 1989)

tween the temporal variation of predictability and the dynamics of weather regimes (quasi-stationary states of the general circulation). They found that at the onset of weather regimes, the rate of divergence of nearby trajectories has a small value, and it has a large value at the transitions between two types of the flow. They explained this variation of the predictability by the local dynamics of the unstable steady state generating quasi-stationary states: persistencies are associated with gradual capture of the trajectory into a contracting phase flow region near the stable manifold of the unstable steady state, and rapid transients with strong instabilities along the unstable manifold.

In order to investigate further the dynamical aspects of the temporal variation of predictability, *Mukougawa et al.* (1991) introduced the *Lorenz index*, which is a measure of the ensemble average of the *linear growth rate* of infinitesimally small initial errors. This index does not depend on the amplitude nor the configuration of initial errors, but directly represents the instability characteristics of the flow. The authors computed the Lorenz index along the stable and unstable manifold of the three unstable stationary points in the Lorenz system, and found that none of these steady states has the property suggested by *Legras* and *Ghil* (1985). This is also implied by the phase-spatial organization of the Lorenz index in *Fig. 5*; we see that the Lorenz index is a smooth function of the state variables, and does not show any distinctive

organization (e.g., a local maximum or minimum value) around the unstable stationary points of the Lorenz system. Therefore, the unstable steady states do not have the same local dynamics.

The nonlinear prediction problem is currently one of the most exciting topics and a very active research area (*c.f.*, *Elsner* and *Tsonis*, 1992).

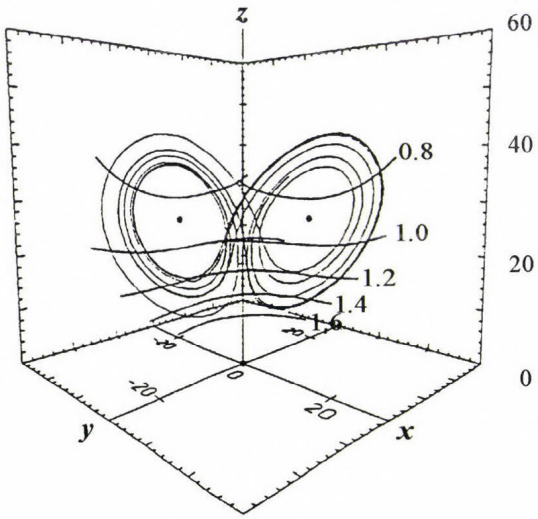

Fig. 5. Distribution of the Lorenz index on the Lorenz attractor in a three-dimensional perspective. A part of the trajectory is indicated by the solid line. The locations of the three unstable stationary points are denoted by dots. (After *Mukougawa et al.*, 1991)

3. Chaotic behavior on climatic time scales

When a dynamical system is an atmospheric model, the points on the attractor represent those states which are compatible with the climate. Physically unrealistic states correspond to points in the phase space which are not on the attractor, while extreme states correspond to points which are in domains of the attractor rarely visited by a trajectory. Within this context, the question of climate becomes a problem of quantifying the attractor, and climate change a matter of how modifications of the boundary conditions lead to altered attractors.

In this section, climate variations on time scales ranging from years to ice-age cycles are interpreted from the viewpoint of nonlinear dynamics, and a modified perspective on global climatic change of anthropogenic origin is outlined.

3.1 Interannual variability

As possible causes for variations in climate, climatologists have often invoked the presumed variations of certain external influences. However, recent numerical studies have uncovered a multitude of autonomous dynamical systems

that undergo variations on a wide range of time scales, without the aid of any varying external influences (see, e.g., *James* and *James*, 1989; *Geller*, 1989). Therefore, some climatic variations may be internally, rather than externally produced, i.e., they are simply the natural internal oscillations in the intricate climate system. Of course the activity of this system requires external thermal forcing, but this is not to say that *variations* in the system require *variations* in the external heating.

In a recent study, *Lorenz* (1990) examined a mechanism that in theory can produce changes on time scales of years, with no variations in external conditions other than the normal seasonal cycle. He presumed that F, representing the cross-latitude external-heating contrast in the geostrophic baroclinic model (3), is greater in winter than in summer. Therefore he identified $F = 6$ with a summer condition, and $F = 8$ with a winter condition. Depending upon the initial conditions, two types of the perpetual summer circulation can develop with the thermal forcing $F = 6$: strong periodic oscillations of the westerly flow x (called *active summer*), and oscillations of x with a much smaller amplitude and a much shorter period than in the former (this type of activity is referred to as *inactive summer*). Extension of the solutions indicated that each type of oscillation, once established, is stable and persists for ever, so that the system can be looked upon as an intransitive system. On the other hand, in the winter case with $F = 8$, different initial conditions lead to strong fluctuations that exhibit chaotic behavior. However, without a *continuous* seasonal change of F, there is no sign of pronounced variations with periods of years or longer.

When a continuous seasonal heating cycle is included by letting F vary sinusoidally between the extreme values 5 and 9, strong interannual variation can appear, with irregular alternations between active and inactive summers. The mechanism that produces the year-to-year variations involves chaotic behavior during the colder months, which assures that a randomly chosen circulation pattern will be present when the warmer months begin. This allows one possible circulation pattern to develop during one summer, while an alternative pattern may develop during another.

Since both summer cases with $F = 6$ are periodic solutions of the Eqs. (3), the two attractors, which *Lorenz* (1990) has called the *strong attractor* and the *weak attractor*, are closed loops (limit cycles) that a trajectory traverses during a single period. A detailed analysis has revealed that the boundary separating the basins of attractions of the two attractors has an extremely complex, fine-scale distribution in the phase space: the two basins are intricately intertwined, and magnification of successively smaller and smaller regions has unveiled a Cantor-set-like, fractal nature of the basin boundary. The existence of such a *fractal basin boundary* can present a serious problem when one attempts to predict the future state of a dynamical system (*Grebogi et al.*, 1987; *Ott*, 1993).

As an extension of Lorenz's work, *Pielke* and *Zeng* (1993) integrated the Eqs. (3) for about 1100 years. Their calculations have revealed that the seasonal cycle itself is sufficient to generate decadal and century time scale variations in climate that are of the same order as interannual variations. No long-term external mechanisms are required to account for substantial long-term deviations in the climatic state. These long-term natural variabilities cannot be predicted deterministically because of the chaotic property of the system (see also *Palmer*, 1993a).

3.2 Long-term variability

The Quaternary ice age has been characterized by repeated alternations between relatively warm interglacial periods and much colder glacial periods. The marked cyclic character of the glaciations has promted many investigators to view long-term climatic variations as a sustained self-oscillation of the limit cycle type. Such self-oscillations were shown to arise quite naturally from the coupling between mean ocean temperature and sea ice, or mean surface temperature and continental ice sheet. Under the presence of a weak external periodic forcing due to Earth-Sun orbital geometry changes, a phase locking can take place, enabling the limit cycle oscillator to adopt the frequency of the forcing or a multiple thereof (see, e.g., *Nicolis*, 1987; *Saltzman* and *Verbitsky*, 1992). Thus, according to this hypothesis, the main climatic variations during the Quaternary are caused by an *internal* property of the climate system, with external forcing playing a relevant role only in determining the phases of the cycles.

As an illustrative example, we recall the work of *Tsonis* and *Elsner* (1990). They considered a simple model of the climate system in which long-term forced damped, nonlinear oscillations are described by the following equation:

$$d^2x/dt^2 + kdx/dt + \beta(x^3 - x) = A\cos\omega t. \tag{8}$$

Here, x is a variable of the climatic state (e.g., global temperature, or ice-sheet extent), k indicates the damping, A is the amplitude of the external forcing, ω is the angular frequency, and $\beta\ (x^3 - x)$ is the nonlinear restoring force. Physically, the damping is related to the tendency of the system to react to changes dictated by some external force (which may be thought of as some astronomical forcing) and the restoring force.

For $k = 0.15$, $\beta = 0.5$, $\omega = 0.833$ and $A = 0.1$ the system exhibits two periodic attractors I and G, which in the one-sided Poincaré map are fixed points $x = \pm 1$, $dx/dt = 0$. In this simplified situation, attractor I may be thought of as describing the dynamics of weather in the interglacial climate, and attractor G in the glacial climate. Depending upon the initial conditions, the system settles down in one of the two attractors.

Numerical experiments on the forced damped pendulum equation show that

fractal basin boundaries are extremely common for this system, causing high sensitivity to initial conditions even if all solutions are found periodic (*Ott*, 1993). Thus, in the presence of noise it is quite possible that a trajectory converging to one attractor will be forced to a point in the fractal boundary which will bring the trajectory to the other attractor. This will indicate a jump from one attractor to the other. Such jumps happen in the system (8) when a random-noise term is added to the right-hand side of the equation. The noise may be thought of as related to short-term internal or external fluctuations. An example of the chaotic evolution of the system is presented in *Fig. 6a*, while *Figs. 6b* and *6c* show the corresponding time variation of x. Fig. 6c indicates, in agreement with several deep-sea core records which represent average climatic conditions over thousands of years, that the climate system has two modes of oscillation. Each oscillation involves a jump from one mode of operation to the other.

The jumps may provide an explanation for the rapid deglaciations and why glacial periods do not last as long as interglacial epochs. In order for that to happen, the coexisting basins of attractions have to be asymmetric. In such a case one attractor will be more attracting than the other, and the residence time on each of the attractors will not be the same. In the case of system (8), the mean residence time of the trajectory for attractor I has indeed proven to be greater than for attractor G.

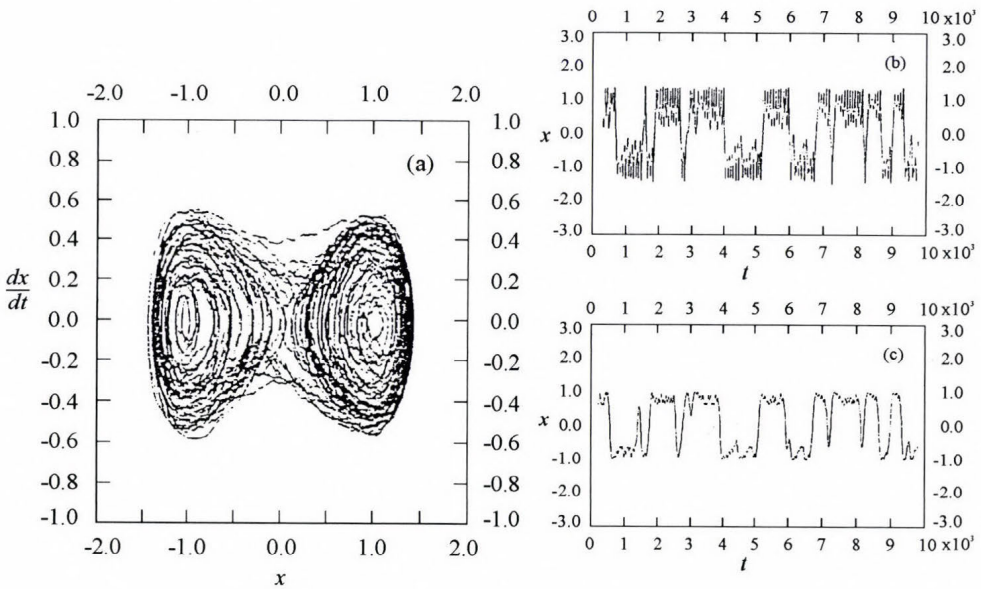

Fig. 6. Numerical solution of the forced damped, nonlinear oscillation equation. (*a*) Trajectory of the system in the phase space whose coordinates are x and dx/dt. (*b*) Graph of x as a function of time. (*c*) A smoothed version of the graph in (*b*). (After *Tsonis* and *Elsner*, 1990)

3.3 A nonlinear dynamical look at climate change

Many of the existing conceptual paradigms about anthropogenic climate change involve linear dynamical thinking. This is embodied in a general perception of the phrases *greenhouse effect* and *global warming* as effectively synonymous. Linear thinking is also implicit in the belief that the effect of increasing atmospheric carbon dioxide concentration will be manifested through a pattern of atmospheric variability that is quite unlike any naturally occurring pattern of variability, e.g. that the greenhouse signal is orthogonal to and independent of the background noise.

In order to put forward a nonlinear dynamical perspective on climate change, *Palmer* (1993b) used the Lorenz model (1) to study predictions of the second kind (i.e., how the statistical properties of the atmosphere change as some control parameter, carbon dioxide content for example, is altered). To do this, he added to the right-hand side of the Eqs. (1) the components of some fixed additional forcing vector **F**, whose strength was governed by a parameter α, and tried to understand conceptually the change in the climate of the Lorenz model as α was increased from zero.

Now, an erroneous linear-thinking analysis of this problem might go as follows. Whilst it is difficult to predict without detailed calculation how an individual trajectory portion might be influenced by the imposed additional forcing, the time-mean state of the system might respond in rough proportion to the forcing **F** itself. The variability in the model might then be approximated by assuming that, relative to the new time-mean state, it is largely unchanged. It might therefore be concluded that the original attractor ($\alpha = 0$) is approximately translated in the direction of the forcing vector **F** to some new position, when $\alpha > 0$.

The actual result of such an additional forcing is shown in *Fig. 7* in terms of the probability distribution function (PDF). This quantity gives the probability of finding the state vector of the system at a given point in the xy-plane of the phase space. *Fig. 7a* gives the values of the PDF with $\alpha = 0$, showing clearly the two weather regimes: the state vector is most likely to be found in two preferred regions of the phase space. We can see that the PDF is symmetric, so that the probability of the trajectory being found in one regime is equal to the probability of its being found in the other regime. *Fig. 7b* shows a PDF when $\alpha > 0$, and the forcing vector **F** is oriented from one regime to the other in the xy-plane. In this case, the PDF is no longer symmetric, the state of the system is more likely to be found in the regime towards which the forcing vector **F** points. However, the phase-space coordinates of the PDF maxima are virtually identical to those in the model with $\alpha = 0$, i.e., the structure of the regime centroids in both the model with $\alpha = 0$ and in the model with forcing $\alpha\mathbf{F}$ is unchanged.

Nonlinear dynamics might also raise questions about the validity of the *Gaia*

hypothesis introduced by *Lovelock* and *Margulis* (1974). It postulated the Earth to be a self-regulating system comprising the biota and their environment with the capacity to maintain the climate and the chemical composition at a steady state favorable for life. A simple model, referred to as Daisyworld, was later developed to illustrate the Gaia concept (*Watson* and *Lovelock*, 1983). Daisyworld is defined as a cloudless planet with negligible atmospheric greenhouse gases, on which the only plants are two species of daisy of different colors. The growth rate of the daisies depends on only one environmental variable, temperature, which the daisies in turn modify because they absorb different amount of solar radiation. The authors concluded that, regardless of the details of the interaction, the effect of daisies is to maintain stable climatic conditions.

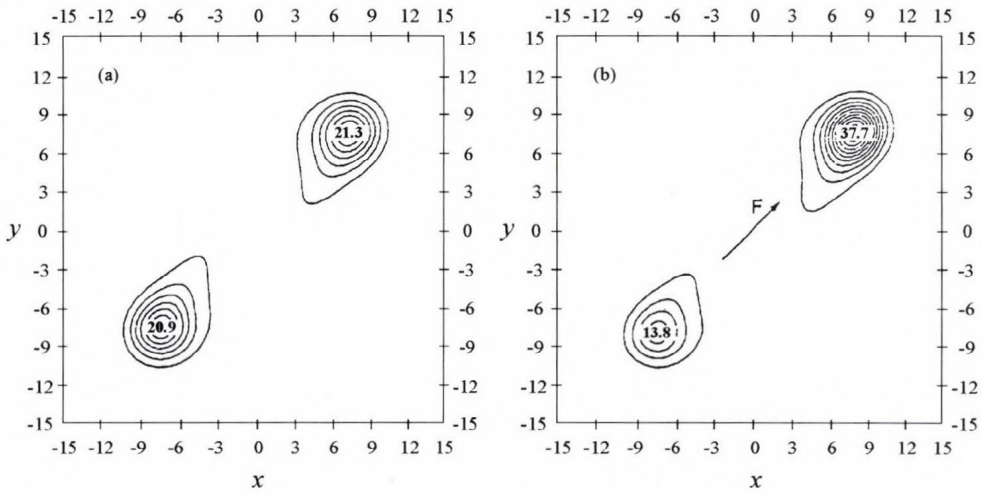

Fig. 7. Probability distribution function of the Lorenz model in the *xy*-plane (*a*) from the model without additional forcing, and (*b*) with a constant additional forcing $F_x = F_y = 1/\sqrt{2}$, $F_z = 0$. (After *Palmer*, 1993b)

In Daisyworld, the comparative growth of the daisies is governed by the logistic map

$$x_{n+1} = rx_n(1 - x_n), \tag{9}$$

where x ($0 \leq x \leq 1$) represents the population density of a given species of daisy, while the growth-rate parameter r depends on the area covered by the given species and on the local temperature. The surprising fact that the iterative mapping of a nonlinear discrete-time equation as simple as Eq. (9) can exhibit apparently aperiodic fluctuations was first described by *May* (1974); population values that look like samples from some random process appear for the control

parameter $r > 3.57$. The presence of chaos in Daisyworld was revealed by *Zeng et al.* (1990). Their results show that this imaginary planet is not always in a steady state as predicted by the Gaia hypothesis; instead, the state of Daisyworld is extremely sensitive to minor fluctuations in the temperature or the areas covered by daisies when in its chaotic regime. Therefore, the biota do not always stabilize the climate, and the remarks made by *Lovelock* (1986), that the inclusion of a negative feedback from the environment appears to lead to steady-state behavior, are also not true in general.

4. Reconstruction of weather and climate attractors

In this section, we present the remarkable fact that allows a strange attractor to be reconstructed from a sampled time series of just one component of the state. The physics behind such a reconstruction is that a nonlinear system is characterized by self-interaction, so that a time series of a single variable can carry the information about the dynamics of the entire multivariable system.

Among the different procedures that have been developed for obtaining a strange attractor, the method of delay coordinates (*Takens*, 1981) is most widely used. Let us suppose that we can only measure one scalar component $y(t)$ of the d-dimensional state vector $\mathbf{x}(t)$. It can be shown that, if n is sufficiently large, then the n-dimensional delay coordinate vector time series

$$y(t_i) = \{y(t_i), y(t_i - \tau), \ldots, y(t_i - (n-1)\tau)\}$$

will be a faithful representation of $\mathbf{x}(t_i)$ where τ is some fixed time interval, and n is the number of delays. In other words, the time trajectory traveling along the sequence of points $\mathbf{y}(t_1)$, $\mathbf{y}(t_2)$,..., $\mathbf{y}(t_n)$ will typically produce a qualitatively similar structure on the Poincaré surface of section in the **y**-space as would be seen had we made our Poincaré section in the original phase space **x**. In this case we say that we have *embedded* the d-dimensional **x**-space into the n-dimensional delay coordinate **y**-space.

Different methods have been suggested to estimate the dimension of the reconstructed attractor, including the correlation-integral method (*Grassberger* and *Procaccia*, 1983a,b) which is most frequently used in atmospheric studies. If the method is correctly applied, the correlation dimension then provides a measure of the number of independent modes excited by the system, that is, it gives the minimum number of coupled nonlinear ordinary differential equations necessary to describe the system (*Procaccia*, 1988a; *Sundermeyer* and *Vallis*, 1993).

Although the method gives no hint as to where these equations might come from and what they might look like, many studies in the field of atmospheric science have concentrated on computing the dimensions of

weather and climate attractors from observational data. To mention just a few, *Nicolis* and *Nicolis* (1984) analyzed the time series of the isotope record of deep-sea cores, and obtained a dimensionality between 3 an 4 for the climate system. Subsequently, *Fraedrich* (1986, 1987), *Essex et al.* (1987), and *Keppenne* and *Nicolis* (1989) analyzed weather data, and have likewise concluded the existence of low-dimensional attractors. From the results obtained for the precipitation and sea-surface temperature, *Hense* (1987) hypothesized the existence of a strange attractor with a fractal dimension between 2.5 and 6.0 for the Southern Oscillation. According to *Tsonis* and *Elsner* (1988), even from the 10-second averages of the vertical wind velocity over a time interval of 11 hours, recorded at Boulder, Colorado, a 7.3-dimensional attractor can be derived.

These unexpected results, suggesting that both long-term climatic processes and phenomena occurring on very short time scales have only a few important modes that govern their dynamics, can stem from one of two reasons. Either there is something fundamental in atmospheric dynamics that we do not understand, which leads to an unexpected simplification of its behavior, or the method of analysis does not apply or is outside its range of validity. Therefore, the existence of low-dimensional atmospheric attractors is currently a highly debated subject. Doubts as to their appropriateness have been expressed even by the originators of the method (*Grassberger*, 1986; *Procaccia*, 1988b), as well as by *Ruelle* (1990). These comments have inspired *Lorenz* (1991b) to apply the procedure to 'data' generated by a mathematical system whose dimension can be evaluated by other means. In this way, he could identify conditions, apparently satisfied by the studies that use real data, in which the method would yield systematic underestimates. Lorenz therefore could see no reason to believe that the global weather and climate systems possess low-dimensional attractors.

In an overview of most recent developments concerning data requirements in estimating the dimension of weather and climate attractors, *Tsonis et al.* (1993) have concluded that due to existing algorithm weaknesses all results present just evidence rather than proof of existence. On the other hand, it should be kept in mind that in weather and climate studies we deal with coarse data in which small-scale processes are absent. These large-scale coarse data are likely to obey to a closed dynamics, which need not appeal to the small-scale processes. Consequently, real-data studies reporting on low-dimensional attractors may not be altogether meaningless; they just need to be reinterpreted.

5. Conclusions

Chaos is a ubiquitous nonlinear phenomenon which permeates all fields of science. Though identified as an important research area only recently, chaos

has been with us from time immemorial. It almost certainly has graced the eyes of many scientists long ago, only to be dismissed as physical noise (*Chua*, 1987). We now know that chaos can readily occur in all natural and living systems where nonlinearity is present. Indeed, chaos has been reported from virtually every scientific discipline: astronomy, biology, biophysics, chemistry, engineering, geology, mathematics, medicine, plasmas, and even social sciences.

In this part of our paper, some examples of the applications of chaos theory to the atmosphere have been presented. In the overview, we have focused our attention mainly on large-scale processes, although areas of application include smaller scale phenomena as well. We now know that the Landau-Hopf route to turbulence is unlikely to occur in nature. Instead, routes through consecutive bifurcations, period doubling cascade, and intermittency have been proposed. Multifractal models of the energy-cascade process have been developed for the understanding of fully developed turbulence. Theories of deterministic chaos have been applied to data in the atmospheric boundary layer, the pulse of thunderstorm rainfall, and some special microphysical systems. More applications can be found in the review article by *Zeng et al.* (1993).

In summary, the grammar of chaos seems to provide a useful way of describing *the nature of dynamically complex phenomena.* Simple models may capture qualitative aspects of a variety of complex atmospheric processes. Whether, and in what sense, the new ideas and physical insights inspired by chaos theory can be used to improve the finite-time prediction of weather and climate is currently one of the most exciting research topics comprising a number of still open questions for the near future.

Acknowledgment—The author would like to thank *Gábor Radnóti* for providing Figs. 1 and 2.

References

Baur, F., 1951: Extended range weather forecasting. In *Compendium of Meteorology* (ed.: *T.F. Malone*). American Meteorological Society, Boston, pp. 814-833.

Charney, J.G. and *DeVore, J.G.*, 1979: Multiple flow equilibria in the atmosphere and blocking. *J. Atmos. Sci. 36*, 1205-1216.

Chua, L.O., 1987: Chaotic systems. *Proc. Inst. Electrical and Electronics Engineers 75*, 979-980.

Elsner, J.B. and *Tsonis, A.A.*, 1992: Nonlinear prediction, chaos, and noise. *Bull. Amer. Meteor. Soc. 73*, 49-60.

Elsner, J.B. and *Tsonis, A.A.*, 1993: Nonlinear dynamics established in ENSO. *Geophys. Res. Lett. 20*, 213-216.

Essex, C., Lookman, T. and *Nerenberg, M. A.H.*, 1987: The climate attractor over short timescales. *Nature 326*, 64-66.

Farmer, J.D., Ott, E. and *Yorke, J.A.*, 1983: The dimension of chaotic attractors. *Physica 7D*, 153-180.

Fraedrich, K., 1986: Estimating the dimensions of weather and climate attractors. *J. Atmos. Sci. 43*, 419-432.

Fraedrich, K., 1987: Estimating weather and climate predictability on attractors. *J. Atmos. Sci. 44*, 722-728.

Geller, M.A., 1989: Variations without forcing. *Nature 342*, 15-16.

Götz, G., 1992: Application of nonlinear dynamics in atmospheric sciences. Part I. Theoretical background. *Időjárás 96*, 121-130.

Grassberger, P., 1986: Do climatic attractors exist? *Nature 323*, 609-612.

Grassberger, P. and *Procaccia, I.*, 1983a: Characterization of strange attractors. *Phys. Rev. Lett. 50*, 346-349.

Grassberger, P. and *Procaccia, I.*, 1983b: Measuring the strangeness of strange attractors. *Physica 9D*, 189-208.

Grebogi, C., Ott, E. and *Yorke, J.A.*, 1987: Chaos, strange attractors, and fractal basin boundaries in nonlinear dynamics. *Science 238*, 632-638.

Hense, A., 1987: On the possible existence of a strange attractor for the Southern Oscillation. *Beitr. Phys. Atmos. 60*, 34-47.

James, I.N. and *James, P.M.*, 1989: Ultra-low-frequency variability in a simple atmospheric circulation model. *Nature 342*, 53-55.

Keppenne, C. and *Nicolis, C.*, 1989: Global properties and local structure of the weather attractor over Western Europe. *J. Atmos. Sci. 46*, 2356-2370.

Legras, B. and *Ghil, M.*, 1985: Persistent anomalies, blocking and variations in atmospheric predictability. *J. Atmos. Sci. 42*, 433-471.

Li, T.-Y. and *Yorke, J.A.*, 1975: Period three implies chaos. *Amer. Math. Mon. 82*, 985-992.

Lorenz, E.N., 1963: Deterministic nonperiodic flow. *J. Atmos. Sci. 20*, 130-141.

Lorenz, E.N., 1984: Irregularity: A fundamental property of the atmosphere. *Tellus 36A*, 98-110.

Lorenz, E.N., 1987: Deterministic and stochastic aspects of atmospheric dynamics. In *Irreversible Phenomena and Dynamical Systems Analysis in Geosciences* (eds.: *C. Nicolis* and *G. Nicolis*). D. Reidel, Dordrecht, pp. 159-179.

Lorenz, E.N., 1990: Can chaos and intransitivity lead to interannual variability? *Tellus 42A*, 378-389.

Lorenz, E.N., 1991a: The general circulation of the atmosphere: An evolving problem. *Tellus 43AB*, 8-15.

Lorenz, E.N., 1991b: Dimension of weather and climate attractors. *Nature 353*, 241-244.

Lovelock, J.E., 1986: Geophysiology: A new look at earth science. *Bull. Amer. Meteor. Soc. 67*, 392-397.

Lovelock, J.E. and *Margulis, L.*, 1974: Atmospheric homeostasis by and for the biosphere: The Gaia hypothesis. *Tellus 26*, 2-10.

Mandelbrot, B. B., 1977: *Fractals–Form, Chance, and Dimension*. W. H. Freeman, San Francisco, 365 pp.

Masoller, C., Sicardi Schifino, A.C. and *Romanelli, L.*, 1992: Regular and chaotic behavior in the new Lorenz system. *Phys. Lett. A167*, 185-190.

May, R.M., 1974: Biological populations with nonoverlapping generations: Stable points, stable cycles, and chaos. *Science 186*, 645-647.

Mukougawa, H., Kimoto, M. and *Yoden, S.*, 1991: A relationship between local error growth and quasi-stationary states: Case study in the Lorenz system. *J. Atmos. Sci. 48*, 1231-1237.

Nese, J.M., 1989: Quantifying local predictability in phase space. *Physica D 35*, 237-250.

Nese, J.M., Dutton, J.A. and *Wells, R.*, 1987: Calculated attractor dimensions for low-order spectral models. *J. Atmos. Sci. 44*, 1950-1972.

Nicolis, C., 1987: Long-term climatic variability and chaotic dynamics. *Tellus 39A*, 1-9.

Nicolis, C. and *Nicolis, G.*, 1984: Is there a climatic attractor? *Nature 311*, 529-532.

Ott, E., 1993: *Chaos in Dynamical Systems*. Cambridge University Press, Cambridge, 385 pp.

Palmer, T.N., 1993a: Extended-range atmospheric prediction and the Lorenz model. *Bull. Amer. Meteor. Soc. 74*, 49-65.

Palmer, T.N., 1993b: A nonlinear perspective on climate change. *Weather 48*, 314-326.

Pielke, R.A. and *Zeng, X.*, 1993: Long term variability of climate. In *Research Activities in Atmospheric and Oceanic Modelling*, Report No. 18 (ed.: *G.J. Boer*). WMO/TD-No. 533, pp. 7.437.44.

Procaccia, I., 1988a: Universal properties of dynamically complex systems: The organization of chaos. *Nature 333*, 618-623.

Procaccia, I., 1988b: Complex or just complicated? *Nature 333*, 498-499.

Ruelle, D., 1990: Deterministic chaos: The science and the fiction. *Proc. Roy. Soc. A 427*, 241-248.

Ruelle, D. and *Takens, F.*, 1971: On the nature of turbulence. *Commun. Math. Phys. 20*, 167-192.

Saltzman, B. and *Verbitsky, M.Y.*, 1993: Multiple instabilities and modes of rhythmicity in the Plio-Pleistocene: A general-theory of late Cenozoic climatic change. *Clim. Dyn. 9*, 1-15.

Sundermeyer, M. and *Vallis, G.K.*, 1993: Correlation dimensions of primitive equation and balanced models. *J. Atmos. Sci. 50*, 2556-2564.

Takens, F., 1981: Detecting strange attractors in turbulence. In *Dynamical Systems and Turbulence* (eds.: *D.A. Rand* and *L.-S. Young*). Springer Lecture Notes in Mathematics, Vol. 898. Springer-Verlag, New York, pp. 366-381.

Tsonis, A. A. and *Elsner, J. B.*, 1988: The weather attractor over very short timescales. *Nature 333*, 545-547.

Tsonis, A.A. and *Elsner, J.B.*, 1990: Multiple attractors, fractal basins and longterm climate dynamics. *Beitr. Phys. Atmos. 63*, 171-176.

Tsonis, A.A., *Elsner, J.B.* and *Georgakakos, K.P.*, 1993: Estimating the dimensions of weather and climate attractors: Important issues about the procedure and interpretation. *J. Atmos. Sci. 50*, 2549-2555.

Vallis, G.K., 1986: El Niño: A chaotic dynamical system? *Science 232*, 243-245.

Watson, A.J. and *Lovelock, J.E.*, 1983: Biological homeostasis of the global environment: The parable of Daisyworld. *Tellus 35B*, 284-289.

Zeng, X., Pielke, R.A. and *Eykholt, R.*, 1990: Chaos in Daisyworld. *Tellus 42B*, 309-318.

Zeng, X., Pielke, R.A. and *Eykholt, R.*, 1992: Estimating the fractal dimension and the predictability of the atmosphere. *J. Atmos. Sci. 49*, 649-659.

Zeng, X., Pielke, R.A. and *Eykholt, R.*, 1993: Chaos theory and its applications to the atmosphere. *Bull. Amer. Meteor. Soc. 74*, 631-644.

IDŐJÁRÁS

Quarterly Journal of the Hungarian Meteorological Service
Vol. 98, No. 2, April–June 1994

The urban modification of acid deposition

D. S. Lee[1] and **J. W. S. Longhurst**[2]

[1] *AEA Technology, National Environmental Technology Centre*
Culham, Oxfordshire OX14 3DB, United Kingdom
[2] *Atmospheric Research and Information Centre,*
Department of Environmental and Geographical Sciences
Manchester Metropolitan University
Chester Street, Manchester M1 5GD, United Kingdom

(Manuscript received 22 April 1994; in final form 24 May 1994)

Abstract—This paper describes the urban modification of precipitation composition in a densely populated region of the United Kingdom. Bulk deposition was compared to wet deposition at a city centre site. Significant differences were found between the collectors, dry deposition contributing less than 20% of the deposition of sulphur and nitrogen species to the bulk collector. However, this sampling artifact was not found to be greatly different to that observed at rural sites in the U.K., confirming the use of carefully sited bulk collectors for these species as valid. Acidity, however, is better assessed with wet-only collectors. Significant spatial variability of concentrations of non-marine sulphate, nitrate, ammonium, calcium and hydrogen ions were found, using a network of 18 bulk collectors. Non-marine sulphate and nitrate were primarily the result of long-range transport with dry deposition of aerosols postulated as being the most likely cause of small, but significant, local variability. Ammonium and calcium in precipitation had local urban sources of precursor species which contributed to their spatial variability which was much stronger than that of non-marine sulphate and nitrate. The spatial variation of acidity was the result of neutralisation by calcium species rather than acidic emissions from local sources. All ions in precipitation showed seasonal variability which was not different to that observed at two nearby rural sites, with the exception of calcium at one of the rural sites, confirming the predominance of meteorology as the controlling factor on seasonal variations. The deposition of ammonium was found to be more episodic than non-marine sulphate or nitrate and back trajectories of two episodes showed that both low pressure and high pressure systems could lead to large deposition.

Key-words: acid deposition, urban rainfall composition, urban bulk/wet deposition.

1. Introduction

The chemical composition of precipitation has been the subject of much discussion over the past two decades because of the impact of wet deposited

sulphur and nitrogen compounds on terrestrial and aquatic ecosystems (*Longhurst et al.*, 1993a; 1993b). However, the effects of emissions from fossil fuel combustion and industrial activity on precipitation composition were recognised as long ago as the late 19th century by Robert Angus Smith (*Smith*, 1852; 1872). Smith described the composition of precipitation at Manchester, Liverpool, Glasgow, London and various rural locations in his book '*Air and Rain–the Beginnings of a Chemical Climatology*' (*Smith*, 1872). Whilst acid deposition was first specifically mentioned in the context of the urban environment by *Smith* (1872), little attention has been paid to acidic deposition in the urban environment other than the work of Gorham and Cauer in the 1940s and 50s (*Gorham*, 1955, 1958; *Cauer*, 1949, 1956).

This paper describes some of the findings of a study of precipitation composition in Greater Manchester, a large urban area of the United Kingdom (*Fig. 1*) with a population of approximately 2.58 million. The aim of the study was to investigate the spatial and temporal variability of precipitation composition and to assess the urban modification of regional precipitation composition and deposition (*Longhurst et al.*, 1987).

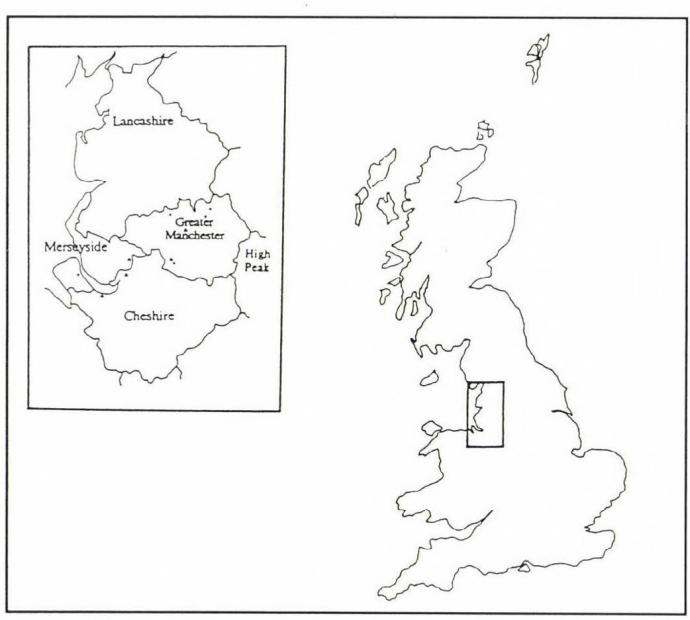

Fig. 1. The north-west of England in relation to the rest of Great Britain.

2. Methods

Samples were collected between January 1987 and December 1988 on a weekly basis from 18 bulk precipitation collectors and despatched to the labo-

ratory for analysis within 24 hours of collection. The network in relation to the geographical extents of Greater Manchester is shown by the crosses in Fig. 3 (see page 94).

An IL 457 spectrophotometer was used for the determination of Ca^{2+}, Mg^{2+} and Zn^{2+}. Sodium and K^+ were determined using a Corning 410 flame photometer. Chloride, SO_4^{2-} and NO_3^- were analysed using a Perkin Elmer ion chromatograph with an LC21 conductivity detector and a Waters IC Pak anion column linked to a LC1-100 Laboratory computing integrator. Hydrogen carbonate and pH were determined within 24 hours of receipt at the laboratory using an Orion EA940 Autochemistry Module fitted with a Ross 8162 electrode. Ammonium was analysed within 24 hours of receipt at the laboratory spectrophotometrically using a Chem Labs Instruments Ltd. autoanalyser.

3. Results and discussion

3.1 Regional emissions estimates

Estimates of emissions of SO_2, NO_x, HCl and NH_3 for Greater Manchester and the north-west of England are given in *Table 1* (see Fig. 1 for geographical extent). These estimates were derived from data on power generation, incinerator plant capacity, fuel usage, animal and human population statistics (*Lee* and *Longhurst*, 1993). The emissions from motor vehicles make up 52% of the NO_x emissions from the north-west of England, whilst those from fossil fuel fired power stations are 20%. The emissions of fossil fuel fired power stations make up 58% of SO_2 emissions from the north-west. A large fossil fuel fired power station is the largest known point source for emissions of SO_2, NO_x and HCl. The largest contribution to NH_3 emissions in the region is from cattle. Humans may contribute some NH_3 to atmospheric emissions (*Atkins* and *Lee*, 1993), as may some other non-agricultural sources (*Lee* and *Dollard*, 1994) but the magnitude of these emissions is highly uncertain.

3.2 Wet and dry deposition

Bulk collectors are continuously open to the atmosphere and collect both wet and dry deposition in the form of gases and aerosols. Bulk deposition collectors provide acceptable estimates of wet deposition at rural background sites but it has been suggested that they are unsuitable for sampling in urban environments (*Gatz*, 1991). Wet-only collectors are expensive and require power, and the operation of a large urban network would be prohibitively expensive. In order to estimate the dry deposition component to the bulk collectors, i.e. the sampling artifact, a wet-only collector was collocated with a bulk collector at one of the sites in the city centre. A comparison of data al-

Table 1. Estimates of emissions of SO_2, NO_x, NH_3 and HCl from Greater Manchester, the north-west of England and the United Kingdom

Source	Greater Manchester* (Gg)	North-west of England* (Gg)	United Kingdom++ (Gg)
SO_2			
Power stations	17	164	2644
Domestic & other	48	119	1055
NO_x			
Power stations	6	41	785
Vehicles & other	70	171	1905
NH_3			
Agriculture	1.2	18.5	300-400#
Industry & other	0.6	1.6	70-100+
HCl			
Power stations	2.0	18.6	244¶
Incinerators & domestic coal burning	3.8	8.7	16¶

* *Lee* and *Longhurst* (1993)
++ *DoE* (1990)
# various estimates, see *Lee* and *Dollard* (1994) for review
+ *Lee* and *Dollard* (1994)
¶ *Lightowlers* and *Cape* (1988)

lowed estimates of the contribution of dry deposition to the bulk collector to be made which are given in *Table 2*. Dry deposition contributed between 15 and 17% to total (wet plus dry) deposition and concentrations of non-marine SO_4^{2-}, NO_3^- and NH_4^+ in the bulk collector and 47% to that of Ca^{2+}. Statistical analyses revealed significant differences between concentrations of ions found in the bulk and wet-only collectors (*Lee* and *Longhurst*, 1992a), but the calculated dry deposition component from gases and aerosols for non-marine SO_4^{2-}, NO_3^- and NH_4^+ found at this urban site was not greatly different to that found at rural sites in the U.K. by *Stedman et al.* (1990). In this particular urban area, the use of bulk collectors did not introduce an unacceptable sampling artifact for S and N species. For acidity, however, it is apparent that the use of a bulk collector introduces a sampling artifact. At the city-centre site, the wet-only collector indicates precipitation weighted mean concentrations of H^+ ion twice those indicated by the use of a bulk collector. It is suggested that such a comparison

Table 2. Measurements of precipitation composition from the collocated bulk and wet-only collectors at the city centre site

	Bulk	Wet	%wet	%dry
Concentration				
non-marine SO_4^{2-}	124.9	106.0	84.9	15.1
NO_3^-	43.9	37.4	85.2	14.8
NH_4^+	58.2	48.2	82.8	17.2
H^+	18.4	37.1	-	-
Ca^{2+}	114.3	61.1	53.4	46.6
Deposition				
non-marine SO_4-S	2.218	1.894	85.4	14.6
NO_3-N	0.683	0.585	85.6	14.4
NH_4-N	0.904	0.754	83.4	16.6
Ca	2.537	1.365	53.8	46.2
mm	1109.7	1116.6	-	-

concentration units = μeq l^{-1}
deposition units = g m^{-2}

would be a requirement for sampling, particularly in more heavily polluted environments where dry deposition may be important. It should, of course, be pointed out that the sampling artifact does not represent dry deposition to natural and urban surfaces.

3.3 Spatial variability

The values of the mean concentrations of non-marine SO_4^{2-}, NO_3^-, NH_4^+ and H^+ across the network are shown in relation to the regional fields of precipitation composition across the U.K. in *Fig. 2* (*RGAR*, 1990). The mean urban network values were not greatly different to those predicted by the U.K. national acid deposition network, which uses bulk collectors sited at rural locations. However, this comparison of data obscures much of the detail from the urban network as the ions in precipitation showed significant spatial variability. Concentrations of non-marine SO_4^{2-}, NO_3^-, NH_4^+, H^+ and Ca^{2+} showed significant spatial variability (*Table 3*) and are shown in *Fig. 3*. This spatial variability demonstrates the potential for local effects of the urban environment and its atmospheric emissions on precipitation composition.

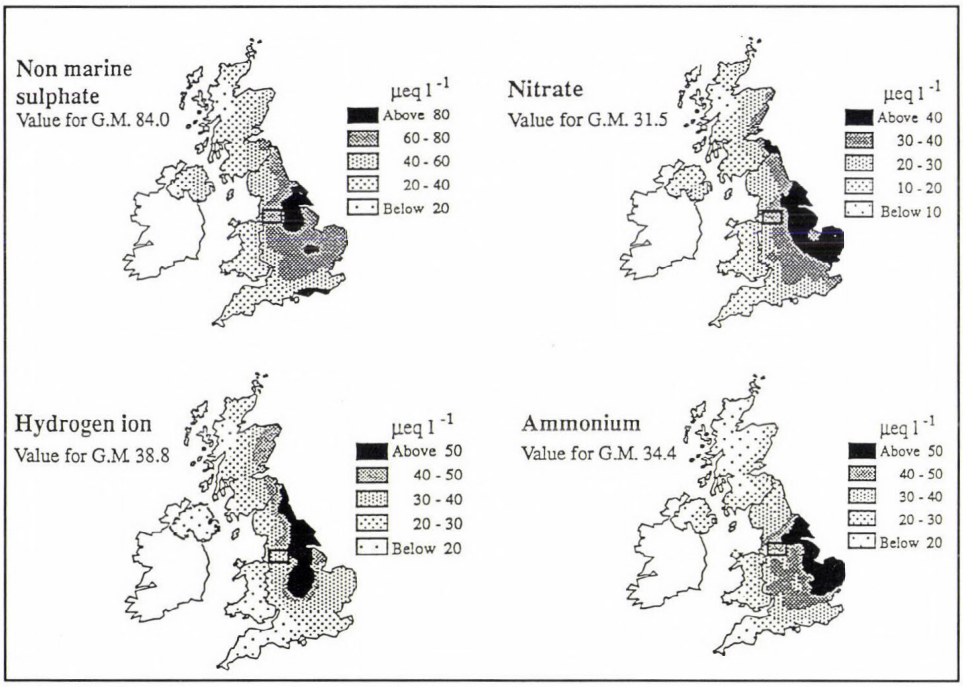

Fig. 2. Mean network values of non-marine sulphate, nitrate, hydrogen and ammonium ions in relation to regional fields of precipitation composition (in μeq l^{-1}).

The spatial variability of non-marine SO_4^{2-} is thought to mainly be the result of the dry deposition of sulphate particles rather than SO_2 gas as the correlation between the dry deposition component of non-marine SO_4^{2-}, evaluated by the difference between the bulk and the wet-only collector, was not significant (*Lee* and *Longhurst*, 1992a). Local variation in the formation of sulphate, and its subsequent removal from the atmosphere, is not feasible on the spatial scale of the network as the oxidation rate is too slow.

Nitrate concentration showed significant spatial variability across the conurbation but this was relatively weak compared to that of other ions in precipitation. Coincident measurements of NO_2 gas concentrations using passive diffusion tube samplers were made at 17 of the 18 sites but the spatial variability of NO_2 was found to be significantly different to that of NO_3^- in precipitation ($r = 0.323$, $P \leq 0.005$). It is concluded that NO_2 gas is not scavenged by precipitation which is in agreement with our current understanding of the atmospheric chemistry of NO_2 and its removal. The spatial variability of NO_3^- in precipitation may be the result of the dry deposition and scavenging of NH_4NO_3 and HNO_3 in the north-east of the study area.

Ammonium concentration was highly variable across the network, which was not random. It is thought that the spatial variability of concentration and

Table 3. Oneway analysis of variance results for periods 1987-1988, 1987, 1988

	1987-1988	1987	1988
non-marine	3.50	2.35	1.66
SO_4^{2-}	< 0.01	< 0.01	0.04
NO_3^-	4.03	2.82	1.95
	< 0.01	< 0.01	0.01
H^+	12.50	6.14	7.52
	< 0.01	< 0.01	< 0.01
NH_4^+	14.70	8.07	9.66
	< 0.01	< 0.01	< 0.01
Ca^{2+}	17.15	8.57	9.51
	< 0.01	< 0.01	< 0.01
mm	1.39	0.80	1.06
	0.13	0.70	0.38

The upper figure is the F ratio, the lower the significance

deposition was not the result of very local sources adjacent to the collectors such as slurry spreading or animal husbandry, as care was taken to locate the collectors away from such sources. Large agricultural sources of NH_3 lie to the south and west of the conurbation in central western England and Wales (*Kruse et al.*, 1989) and the conurbation itself may also be a significant source, as sewage treatment plants and humans, and other urban activities result in emissions of NH_3 (*Lee et al.*, 1992, *Atkins* and *Lee*, 1993, *Lee* and *Dollard*, 1994). The predominant wind direction is from the south-west and the enhanced concentrations and deposition of NH_4^+ in the north-east of the study area may be the result of dry deposition and/or below-cloud scavenging of NH_3 from sources both within and outside the study area.

Calcium concentration showed significant spatial variability with the highest concentrations in the centre of the conurbation. This pattern of variability is thought to be the result of local sources which are intrinsic features of the urban environment. Calcium particles in the atmosphere are generally > 2 μm in diameter so that these large particles are likely to be removed by dry deposition and below-cloud scavenging.

Acidity also showed strong spatial variability which was inversely correlated with Ca^{2+} concentration (*Table 4*). It is likely that calcium compounds in the atmosphere reduce the acidity of precipitation and that the significant spatial variability of H^+ ion concentration is a function of neutralisation by calcium compounds rather than elevated acidity in the fringes of the conurbation.

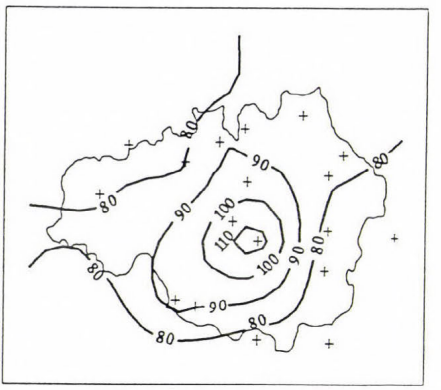

Non-marine sulphate concentrations

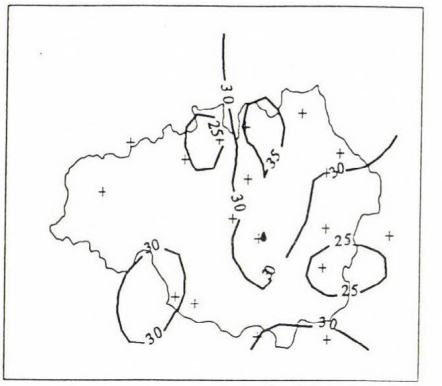

Nitrate concentrations

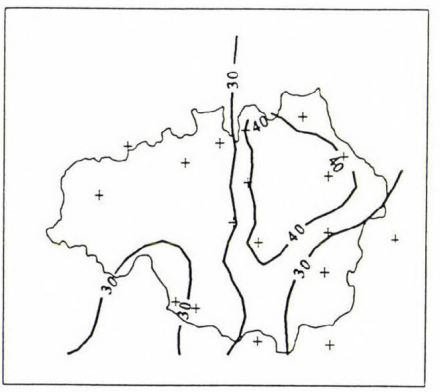

Ammonium concentrations

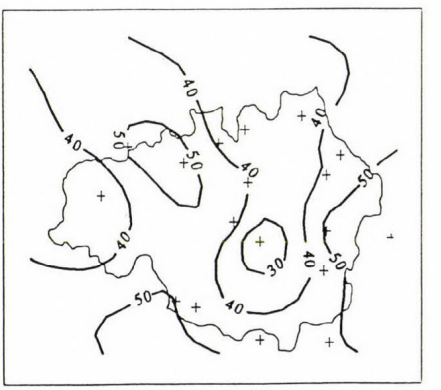

Hydrogen ion concentrations

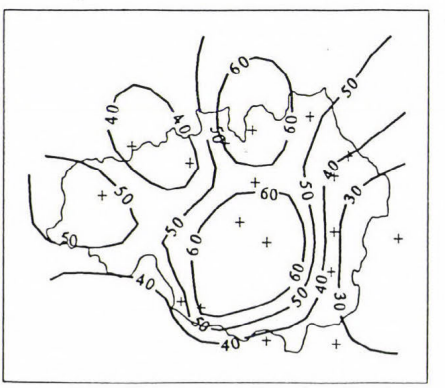

Calcium concentrations

Fig. 3. Concentration fields of non-marine sulphate, nitrate, ammonium, hydrogen and calcium ions across Greater Manchester (in μeq l^{-1}).

Table 4. Correlations between spatial fields of ions in precipitation

	non-marine SO_4^{2-}	NO_3^-	H^+	NH_4^+
NO_3^-	0.296	-	-	-
H^+	- 0.537	- 0.346	-	-
NH_4^+	0.339	0.744*	- 0.329	-
Ca^{2+}	0.836*	0.330	- 0.772*	0.163

* significance less than or equal to 0.005

3.4 Relationships between ions in precipitation

Correlation coefficients calculated between the variables have shown that the data are highly intercorrelated, which hampers interpretation (*Lee*, 1993). Principal Components Analysis (PCA) provides a means of reducing such a large multivariate data set into a series of uncorrelated components which are made up of the original variables. Concentrations of ions in precipitation show a significant inverse correlation with precipitation amount, so that a first-order partial correlation matrix, controlling for precipitation, was used as the basis for the PCA. The PCA was performed on the data from the whole network, rather than by site, and the results are given in *Table 5*. Composite variables of the eigenvectors were selected on the basis of the variable loadings being greater than, or equal to 0.5, (*Gorsuch*, 1983; *Harman*, 1976). The first eigenvector consisted of a marine component (Na^+, Cl^-, Mg^{2+} and K^+) which accounted for 40% of the variation in the data, the second eigenvector of an anthropogenic Ca^{2+}/non-marine SO_4^{2-} component which accounted for 22%, and the third eigenvector of an anthropogenic NH_4^+/NO_3^-, which accounted for 13% of the variation in the data.

Calcium and non-marine sulphate

An analysis of spatial variability clearly shows that Ca^{2+} concentrations are lower at the edge of the urban area (Fig. 3). This phenomenon is not unique to Greater Manchester. Elevated concentrations of Ca^{2+} in urban precipitation have been noted for other cities (e.g. *Clarke* and *Lambert*, 1987; *Lipfert* and *Dupuis*, 1984; *Vermette et al.*, 1988). Calcium is a major component of the fabric of the urban environment, particularly with respect to buildings, and the prevalence of exposed mineral surfaces in towns and cities may have an influence on urban precipitation composition (*Argese* and *Bianchini*, 1989). The wind mediated suspension of coarse particles derived from urban sources such

as erosion of exposed surfaces, extraction industries, construction activities, transportation and combustion may be the source of Ca^{2+} particles in the urban atmosphere. Resuspension of particles occurs as the result of wind (*Nicholson*, 1988) and traffic, both in wet and dry conditions (*Nicholson* and *Branson*, 1990).

Table 5. Results from principal components analysis

Eigenvector	Eigenvalue	% var.	Cum. %
1	3.60853	40.1	40.1
2	2.01505	22.4	62.5
3	1.16865	13.0	75.5
4	0.79473	8.8	84.3

	Eigenvector 1	Eigenvector 2	Eigenvector 3	Eigenvector 4
Cl^-	0.96123			
Na^+	0.92269			
Mg^{2+}	0.87398			
K^+	0.52185			
nm SO_4^{2-}		0.87560		
Ca^{2+}		0.83507		
NH_4^+			0.92410	
NO_3^-			0.74480	
H^+				0.97199

Table 4 shows that the spatial pattern of Ca^{2+} is significantly correlated with that of non-marine SO_4^{2-}. The spatial variability of non-marine SO_4^{2-} (which is significant, but relatively weak) may be the result of an urban source for a fraction of the sulphate. It is suggested that the dry deposition of SO_4^{2-} particles to the bulk collectors results in the spatial variability of non-marine SO_4^{2-}.

Many buildings and other surfaces in towns have been exposed to SO_2, both in the present and the past, which may result in strong sulphation (*Butlin*, 1991). As weathering and other erosive processes occur, particles of both $CaCO_3$ and $CaSO_4$ may be available for suspension.

Other workers have suggested that a relationship between Ca^{2+} and non-marine SO_4^{2-} may be possible in terms of SO_2 reacting with Ca^{2+} bearing

particles in the atmosphere (*Gentilizza* and *Vadjic*, 1986; *Argese* and *Bianchini*, 1989; *Altwicker* and *Mahar*, 1984; *Hooper* and *Peters*, 1989; *Van Borm et al.*, 1989; *Clarke et al.*, 1984). *Buttler* (1988) found conversion rates of samples of $CaCO_3$ to $CaSO_4$ of up to 20% per day from ambient SO_2 at a rural site in the U.S.A. This rate is much slower than the oxidation rate of SO_2 in the atmosphere by either dry or wet oxidation processes which are of the order of per cent per hour (*RGAR*, 1990). Furthermore, any reaction between $CaCO_3$ and SO_2 on particles in the atmosphere will also be limited by the diffusion of the gas into the particle matrix. Thus, the available evidence would suggest that suspension of eroded $CaSO_4$ particles from urban surfaces is more likely to contribute to the spatial variability of SO_4^{2-} particles than atmospheric reaction between SO_2 and $CaCO_3$ particles and subsequent removal of the reaction products.

The origin and form of these SO_4^{2-} particles, however, remains unconfirmed. Other work on particle composition has identified the presence of $CaCO_3$ in the urban atmosphere (*Clarke* and *Karani*, 1992) but *Van Borm et al.* (1989) found that most of the calcium particles are in the sulphate form, rather than the carbonate. *Clarke* and *Karani* (1992) did not, however, quantify the sulphate fraction of the particle phase.

Nitrate and ammonium

The results from the principal components analysis has shown that there is a statistical association between NH_4^+ and NO_3^-. Ammonia may be removed from the atmosphere by wet and dry deposition and atmospheric reactions (*ApSimon et al.*, 1987). It is possible that the elevated concentrations of NH_4^+ in the north-west of the conurbation may be the result of scavenging of NH_3 emissions from animal sources within the conurbation, combined with other sources such as a large sewage treatment plant in the west of the conurbation, humans and other urban sources.

The concentration fields of NO_3^- and NH_4^+ are significantly correlated but the spatial variability of NO_3^- is much weaker than that of NH_4^+ (Tables 3 and 4). The spatial variability of NO_3^- may be the result of the dry deposition of HNO_3. Both NH_3 and HNO_3 are reactive gases with large deposition velocities but HNO_3 is a secondary pollutant formed from the day-time reaction of OH radicals with NO_2 and the night-time reaction with O_3, so that dry deposition is thus unlikely to contribute to spatial variability of concentration and deposition on a local scale, whereas NH_3 is a primary pollutant and is more likely to be spatially variable. The reversible reaction between these two gases to form NH_4NO_3 is also likely to be a sink. The strong correlation between NH_4^+ and NO_3^- concentrations may be the result of this chemical interaction and subsequent precipitation scavenging of NH_4NO_3. This explanation is, however, somewhat speculative.

Neutralisation of acidity by calcium compounds

The acidity of precipitation is a balancing term which responds to concentrations of other ions so that any local source effect increasing H^+ ion concentration would be the result of associated acid nitrate, sulphate or chloride. Furthermore, the acidity will also be altered by the neutralising effect of NH_3, the buffering of NH_4^+ salts or alkaline particles in the atmosphere. This neutralisation effect may mask any acidity enhancement. The spatial pattern of Ca^{2+} concentration appears to 'mirror' that of H^+ ion and they are inversely correlated (Table 4). Thus, it would seem that Ca compounds in the urban atmosphere reduce the acidity of precipitation, so that the spatial variability of the deposition and concentration of H^+ ion is the result of the spatial variability of calcium. The effect of the reduction of acidity from alkaline calcium compounds in the urban atmosphere was also noted by *Casado et al.* (1992) in the urban atmosphere of Vitoria, Spain. However, this apparent neutralisation by Ca compounds is difficult to explain as it has previously been argued that the relationship between Ca^{2+} and non-marine SO_4^{2-} may be the result of SO_2 oxidation on urban surfaces with subsequent suspension and deposition of these particles. Calcium sulphate would not effectively neutralise acidity, whereas $CaCO_3$ would. The only explanation that can be offered is the presence of both these chemical forms which may vary in their spatial distributions. It is suggested that the site of the neutralisation is more likely to be the collector itself, rather than the atmosphere, as the precipitation weighted mean concentration of H^+ ion from the wet-only collector is twice that found in the bulk collector. A likely explanation for this is that Ca^{2+} particles are dry deposited onto the funnel of the bulk collector and are washed in after precipitation events with subsequent neutralisation.

3.5 Temporal variability

Monthly network mean concentrations of non-marine SO_4^{2-}, NO_3^-, NH_4^+, H^+ and Ca^{2+} ions are shown in *Fig. 4*. Mean network concentrations of non-marine SO_4^{2-}, NO_3^-, NH_4^+, and Ca^{2+} ions show more variability in 1988 than in 1987. The exception to this is H^+ ion concentration, for which the converse situation is apparent. It is also apparent that concentrations of NH_4^+ and Ca^{2+} ions are more variable than those of non-marine SO_4^{2-}, NO_3^- and H^+.

Seasonal variability has been shown to exist for concentrations of the major anthropogenic ions in precipitation (i.e. non-marine SO_4^{2-}, NO_3^-, NH_4^+, and H^+) at rural sites across the U.K. where a maximum in concentration is observed in late spring, and a minimum in early winter (*RGAR*, 1983; 1987; 1990; *Skeffington*, 1984) so that the seasonal pattern found at the urban sites is consistent with that found at other rural sites in the U.K.

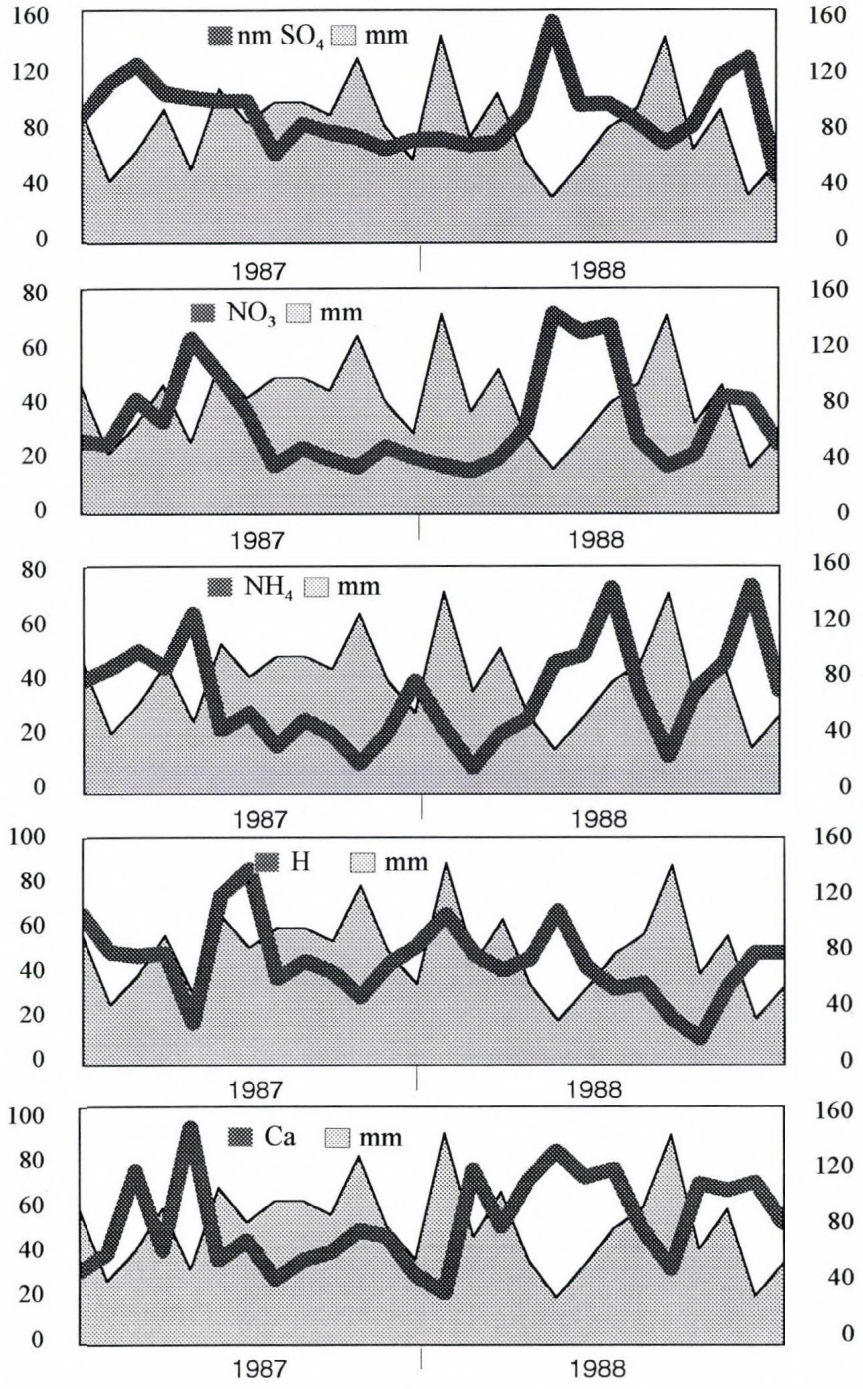

Fig. 4. Four-weekly precipitation weighted mean concentrations (in μeq l^{-1}, left ordinates) of non-marine sulphate, nitrate, ammonium, hydrogen and calcium ions and the precipitation (in mm, right ordinates) 1987-1988 (mean network values).

The temporal variability of concentrations of various ions in precipitation from the urban network was also compared to data collected from two nearby rural sites, Wardlow Hay Cop in Derbyshire and Hebden Bridge in West Yorkshire, some 30 and 15 km distant from the conurbation, and are shown in *Fig. 5*. For concentrations of all species, similarities can be seen between the mean urban network data and data from the two rural sites, with the exception of Ca^{2+} concentration at Wardlow Hay Cop. It is thought that much of the Ca^{2+} ion in precipitation at this site originates from large dust particles from local limestone quarrying, which is extensive in this part of the country, and account for the observed differences (*Lee* and *Longhurst*, 1992b). This comparison of time series plots supports the suggestion of the larger scale influence of meteorology on the temporal variability of species concentration in precipitation (*Davies et al.*, 1990), a factor which also prevails over Greater Manchester.

Whilst the urban area of Greater Manchester is thought to influence spatial patterns of deposition by local emissions adding to meso-scale emissions, temporal variability is considered to be the result of the larger scale influence of meteorology. Identification of the origin of air masses, particularly those which lead to the largest deposition of species, aids the identification of source regions.

One way in which deposition can be considered, is by the identification of episodes. The temporal nature of deposition has so far only been considered in terms of annual cycles. However, wet deposition is made up of discrete events.

In this investigation, bulk deposition was collected on a weekly basis and hence it was only possible to define 'episode weeks' (i.e. those weeks for which 30% of the annual deposition fell) for the whole network rather than individual events. The deposition of non-marine SO_4-S, NO_3-N and NH_4-N were calculated in terms of percentage deposition per week for 1988 and shown in *Fig. 6*. Deposition which lies on or above the horizontal lines shown in these figures indicates the individual weeks which contributed 30% of the annual deposition. The episodicity of a species is defined as the ratio of the number of episode weeks to the number of individual rain days. Across the network, NH_4-N deposition was the most episodic at 13%, the episodicity of NO_3-N was 15% and non-marine SO_4-S was the least episodic at 19%. From Fig. 6 it appears that episode weeks of NH_4-N and NO_3-N tend to occur together, mostly independent of non-marine SO_4-S deposition, particularly in the summer. However, this can only remain speculative as episode weeks are made up of several rain events and it was not possible to attribute deposition quantitatively to any particular trajectory. Two weeks which illustrate the ability of quite different synoptic weather condition to lead to large deposition were weeks 28 and 43. Composite back trajectories constructed for these weeks in which particular conditions prevailed are shown in *Figs. 7* and *8*. In Fig. 7, conditions were dominated by a strong frontal Atlantic low pressure system. As the

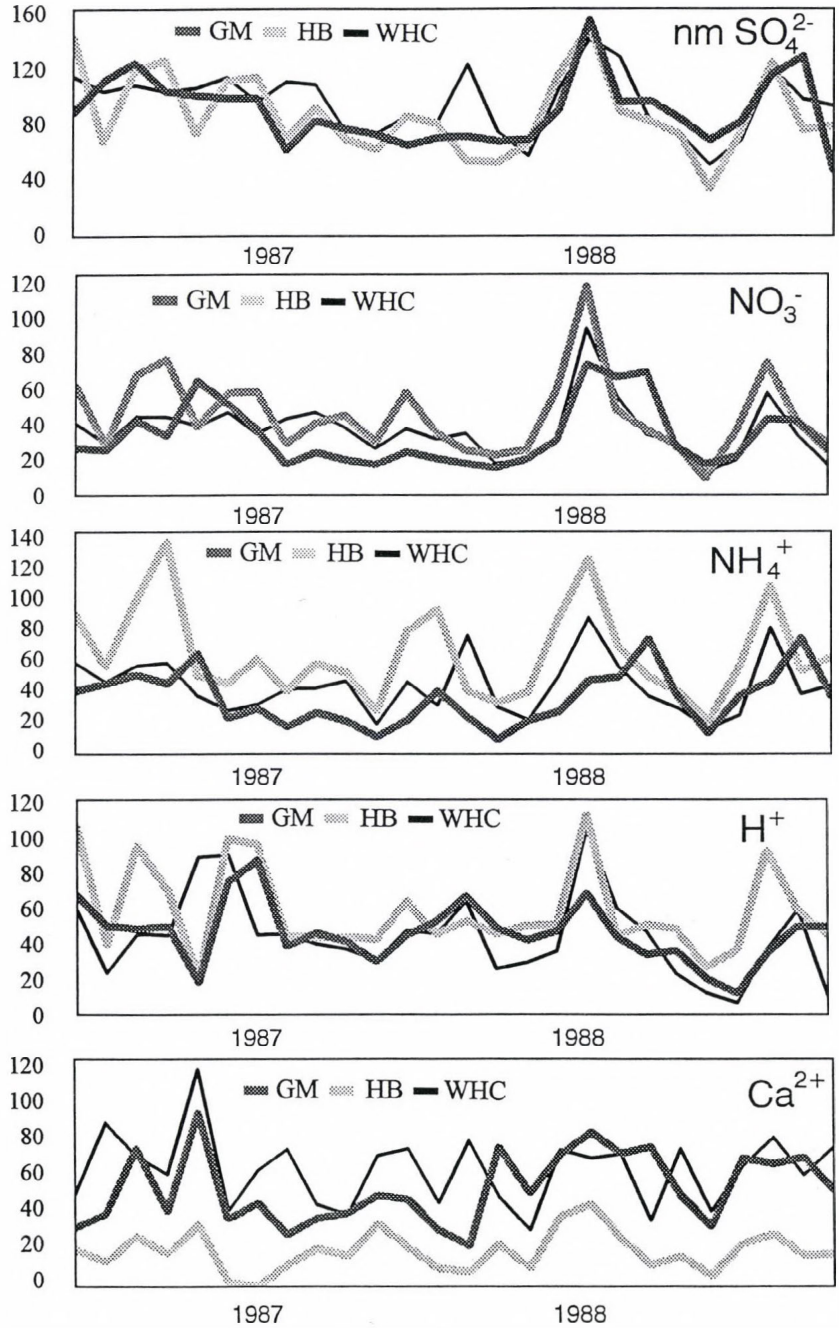

Fig. 5. Four-weekly precipitation weighted mean concentrations (in μeq l^{-1}) of non-marine sulphate, nitrate, ammonium, hydrogen and calcium ions 1987–1988, from the Greater Manchester network and two nearby rural sites, Hebden Bridge and Wardlow Hay Cop.

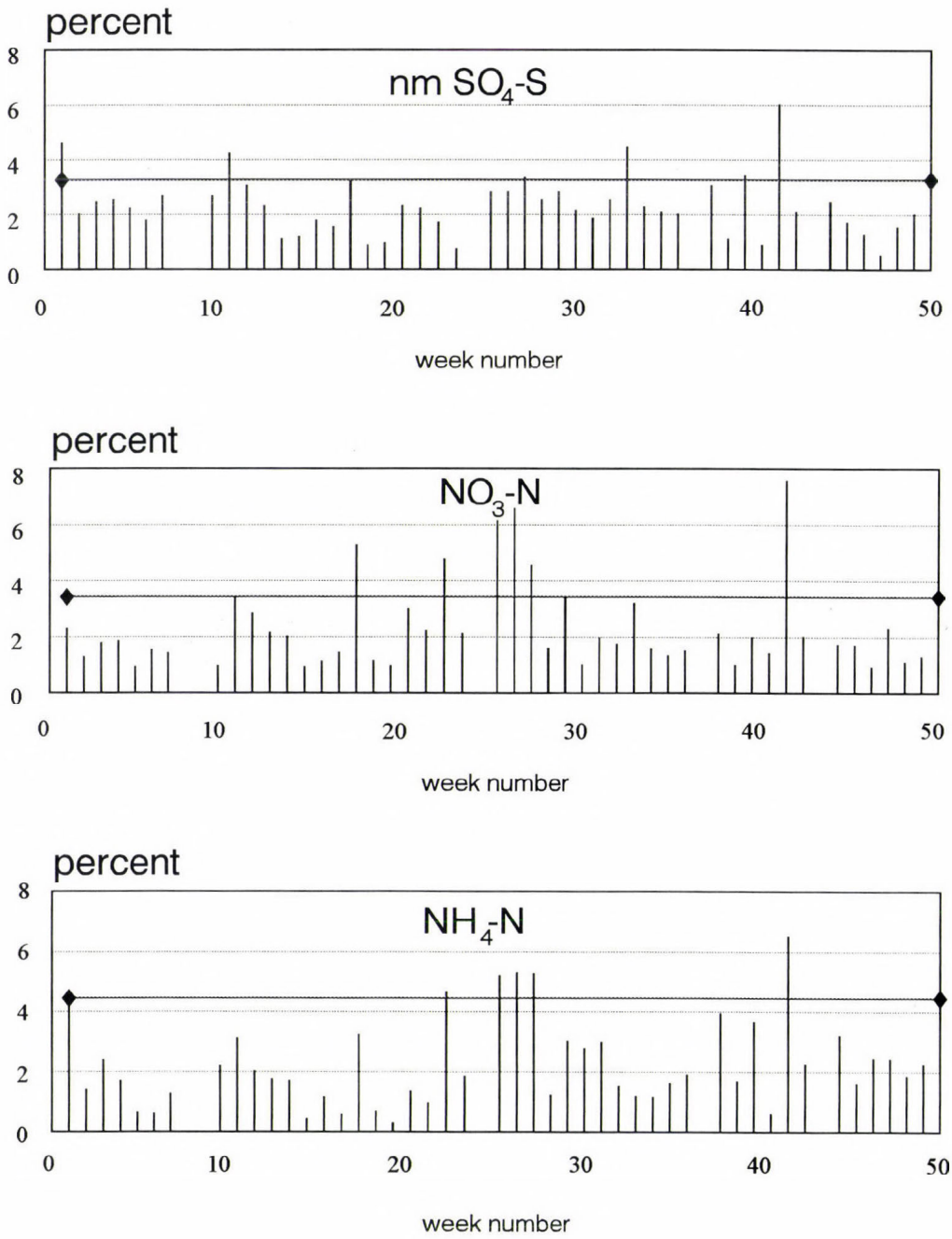

Fig. 6. Weekly network deposition of non-marine sulphate (S), nitrate (N) and ammonium (N). Horizontal lines indicate threshold value for 'episode weeks'.

trajectories indicate, this system drew in air from Europe, which resulted in large concurrent deposition of non-marine SO_4-S, NH_4-N and NO_3-N. In week 43, however, the trajectories which lead to rain events and a large deposition episode of non-marine SO_4-S, NH_4-N and NO_3-N were the result of a high pressure system which drew in air masses directly from central Europe in an easterly flow (Fig. 8).

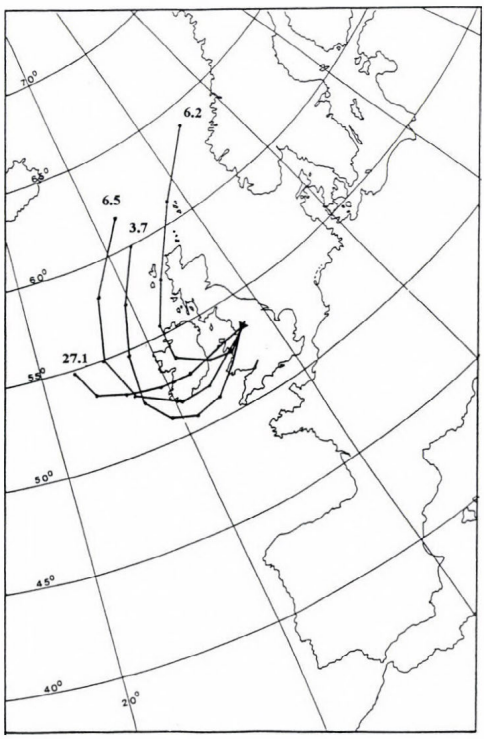

Fig. 7. Composite trajectories for episode week, Atlantic frontal system, showing precipitation amounts for each trajectory (mm).

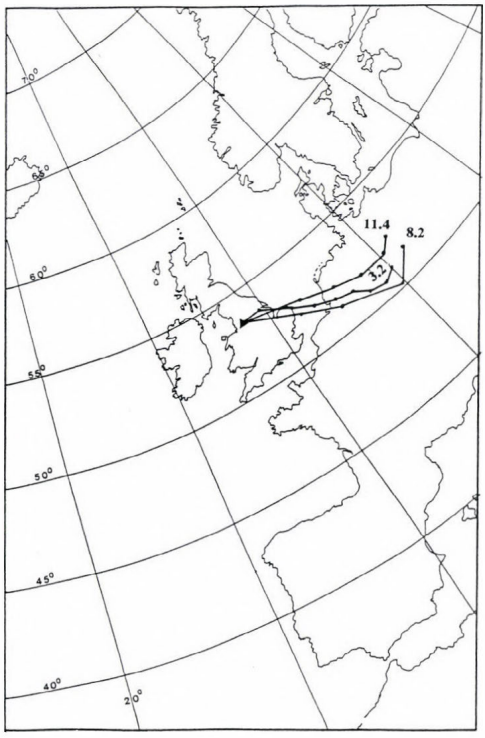

Fig. 8. Composite trajectories for episode week, high pressure system, showing precipitation amounts for each trajectory (mm).

4. Conclusions

Concentrations of non-marine SO_4^{2-}, NO_3^-, NH_4^+, and H^+ in precipitation over Greater Manchester are not greatly different to those predicted by interpolation of data from a national rural network. However, all these ions exhibit significant spatial variability, particularly NH_4^+, Ca^{2+} and H^+. The use of bulk precipitation collectors in the urban environment did not introduce a sampling artifact which was greater than that found at more rural sites in the U.K. for S and N species.

Local sources of SO_2 and NO_x did not result in enhanced concentrations of SO_4^{2-} and NO_3^- in precipitation over the study area, these ions were the result of more regional scale atmospheric chemistry. It is postulated that local sources of Ca^{2+} and NH_3 had an impact on urban precipitation composition. Calcium is thought to have its origin in the suspension of calcium-bearing particles from the erosion of urban surfaces and emissions from construction and industrial activities. Ammonia has urban sources but the magnitude of these are, as yet, uncertain. It is likely, however, that the steep gradient of NH_4^+ ions in precipitation are the result of local sources. Urban precipitation is not generally more acidic than rural precipitation but was found to be rather less so in the centre of the conurbation, as measured by the bulk collector. However, a comparison of data from the wet-only and bulk collectors at the city centre site would indicate that the site of neutralisation is the bulk collector rather than the atmosphere. Calcium carbonate aerosol is probably the main neutralising compound.

The temporal variation of concentrations of the major ions in rainfall was very similar to that observed at two rural monitoring sites, demonstrating that synoptic scale meteorology controls the seasonal variations of all the major ions in urban precipitation. Episodes of deposition were observed, of which NH_4-N, was the most episodic. By constructing back trajectories for selected weeks, it was shown that both high and low pressure systems could result in deposition episodes of S and N species, but that the origin of the emissions was European in both instances.

Acknowledgements–This work was funded by *Tameside Metropolitan Borough Council* on behalf of the *Association of Greater Manchester Authorities Planning and Transportation Committee*. Data from the national network sites were provided *Warren Spring Laboratory* who operate the network on behalf of the *U.K. Department of the Environment*.

References

Altwicker, E.R. and *Mahar, J.T.*, 1984: NH_4/Ca ratio in different forms of atmospheric deposition: interpretative potential. *Atmosph. Environ. 18*, 1875-1883.

ApSimon, H.M., *Kruse, M.* and *Bell, J.N.B.*, 1987: Ammonia emissions and their role in acid deposition. *Atmosph. Environ. 21*, 1939-1946.

Argese, E. and *Bianchini, A.G.*, 1989: Chemical and physical characteristics of rainfall in Venice: influence of the sampling method on the reliability of the data. *Sci. Tot. Environ. 83*, 287-298.

Atkins, D.H.F. and *Lee, D.S.*, 1993: Indoor concentrations of ammonia and the potential contribution of humans to atmospheric budgets. *Atmosph. Environ. 27A*, 1-7.

Butlin, R.N., 1991: Effects of air pollutants on buldings and materials. *Proc. R. Soc. Edin. 97B*, 255-272.

Buttler, T.J., 1988: Composition of particles dry deposited to an inert surface at Ithaca, New York. *Atmosph. Environ. 22*, 895-900.

Casado, H., *Eacinas, D.* and *Lacaux, J.P.*, 1992: The moderating effect of the Ca^{2+} ion on the acidity in precipitation. *Atmosph. Environ. 26*, 1175.

Cauer, H., 1949: Ergebnisse chemisch-meteorologischer Forschung. *Arch.*

Geophys. Bioklimat. S.B.B.I.H, 221-256.

Cauer, H., 1956: Die pH-Werte von Aerosolen und Niederschlägen und ihre lufthygienische und bioklimatische Indikatorbedeutung. *Zeit. Aerosol Forsch. Therapie 6*, 459-509.

Clarke, A.G. and *Karani, G.N.*, 1992: Characterisation of the carbonate content of atmospheric aerosols. *J. Atmosph. Chem. 14*, 119-128.

Clarke, A.G. and *Lambert, D.R.*, 1987: Local factors affecting the chemistry of precipitation. In *Acid Rain: Scientific and Technical Advances* (eds.: *R. Perry, R.M. Harrison, J.N.B. Bell* and *J.N. Lester*). Selper Ltd., London.

Clarke, A.G., Willison, M.J. and *Zeki, E.M.*, 1984: A comparison of urban and rural aerosol composition using dichotomous samplers. *Atmosph. Environ. 18*, 1767-1775.

Davies, T.D., Farmer, G. and *Barthelmie, R.J.*, 1990: Use of simple atmospheric circulation types for the interpretation of precipitation composition at a site (Eskdalemuir) in Scotland, 1978-1984. *Atmosph. Environ. 24A*, 63-72.

DoE, 1990: *Digest of Environmental Protection and Water Statistics No. 12*. Department of the Environment, HMSO, London.

Gatz, D.F., 1991: Urban precipitation chemistry: a review and synthesis. *Atmosph. Environ. 25B*, 1-15.

Gentilizza, M. and *Vadjic, V.*, 1986: The relationship between the mass concentrations of sulphate and sulphur dioxide in air polluted with cement dust. *Sci. Tot. Environ. 48*, 231-237.

Gorham, E., 1955: On the acidity and salinity of rain. *Geochim. et Cosmochim. Acta 7*, 231-239.

Gorham, E., 1958: Atmospheric pollution by hydrochloric acid. *Quart. J. Roy. Meteorol. Soc. 84*, 274-276.

Gorsuch, R.L., 1983: *Factor Analysis*. Lawrence Erlbaum Associates, New Jersey.

Harman, H.H., 1976: *Modern Factor Analysis*. University of Chicago Press, Chicago.

Hooper, R.P. and *Peters, N.E.*, 1989: Use of multivariate analysis for determining sources of solutes found in wet atmospheric deposition in the United States. *Environ. Sci. Technol. 23*, 1263-1268.

Kruse, M., ApSimon, H.M. and *Bell, J.N.B.*, 1989: Validity and uncertainty of an emission inventory for ammonia arising from agriculture in Great Britain. *Environ. Pollut. 56*, 237-257.

Lee, D.S., 1993: The spatial variability of urban precipitation chemistry and deposition; statistical associations between constituents and potential removal processes of precursor species. *Atmosph. Environ. 27B*, 321-337.

Lee, D.S. and *Dollard, G.J.*, 1994: Uncertainties in current estimates of the emissions of ammonia in the United Kingdom. *Environ. Pollut.* (in press).

Lee, D.S. and *Longhurst, J.W.S.*, 1992a: A comparison between wet and bulk deposition at an urban site in the U.K. *Water, Air, and Soil Pollut. 64*, 635-648.

Lee, D.S. and *Longhurst, J.W.S.*, 1992b: A statistical intercomparison between 'urban' and 'rural' precipitation data from Greater Manchester and two nearby secondary national network sites in the United Kingdom. *Atmosph. Environ. 26A*, 2869-2883.

Lee, D.S. and *Longhurst, J.W.S.*, 1993: Estimates of emissions of SO_2, NO_x, HCl and NH_3 from a densely populated region of the U.K. *Environ. Pollut. 79*, 37-44.

Lee, D.S., Nason, P.D. and *Bennett, S.L.*, 1992: Atmospheric ammonia in the vicinity of a sewage treatment plant–results from a preliminary investigation. AEA-EE-0328, AEA Environment and Energy, Harwell Laboratory, Oxon.

Lightowlers, P.J. and *Cape, J.N.* 1988: Sources and fate of atmospheric HCl in the U.K. and western Europe. *Atmosph. Environ. 22*, 7-15.

Lipfert, F.W. and *Dupuis, L.R.*, 1984: Urban and local effects on precipitation chemistry. *Proc. 77th Ann. Meet. Air Pollut. Contr. Assoc.*

Longhurst, J.W.S., Gee, D.R., Lee, D.S. and *Green, S.E.* 1987: The establishment of an urban acid deposition monitoring network. *Environmentalist 7*, 299-307.

Longhurst, J.W.S., Raper, D.W., Lee, D.S., Heath, B.A., Conlan, B. and *King, H.J.*, 1993a: Acid deposition: a select review 1852-1990. 1. Emissions, transport, deposition, effects on freshwater systems and forests. *Fuel 72*, 1261-1280.

Longhurst, J.W.S., Raper, D.W., Lee, D.S., Heath, B.A., Conlan, B. and *King, H. J.*, 1993b: Acid deposition: a select review 1852-1990. 2. Effects on materials and health; abatement strategies and programmes. *Fuel 72*, 1363-1380.

Nicholson, K.W., 1988: A review of particle resuspension. *Atmosph. Environ. 22*, 2639-2651.

Nicholson, K.W. and *Branson, J.R.*, 1990: Factors affecting resuspension by road traffic. *Sci. Tot. Environ. 93*, 349-358.

RGAR, 1983: *Acid Deposition in the United Kingdom.* United Kingdom Review Group on Acid Rain. Warren Spring Laboratory, Stevenage.

RGAR, 1987: *Acid Deposition in the United Kingdom 1981-1985.* A second report of the United Kingdom Review Group on Acid Rain. Warren Spring Laboratory, Stevenage.

RGAR, 1990: *Acid Deposition in the United Kingdom 1986-1988.* A third report of the United Kingdom Review Group on Acid Rain. Warren Spring Laboratory, Stevenage.

Skeffington, R.A., 1984: The chemistry of bulk precipitation at a site in southeast England – I. Small scale spatial variation, frequency distributions and variation with time. *Atmosph. Environ. 18*, 1683-1693.

Smith, R.A., 1852: On the air and rain of Manchester. *Mem. Lit. Phil. Soc. Manchester 10*, 207-217.

Smith, R.A., 1872: *Air and Rain. The Beginnings of a Chemical Climatology.* Longmans Green and Co., London.

Stedman, J.R., Heyes, C.J. and *Irwin, J.G.*, 1990: A comparison of bulk and wet-only precipitation collectors at rural sites in the United Kingdom. *Water, Air, and Soil Pollut. 52*, 377-395.

Van Borm, W.A., Adams, F.C. and *Maenhaut, W.*, 1989: Characterization of individual particles in the Antwerp aerosol. *Atmosph. Environ. 23*, 1139-1151.

Vermette, S.J., Drake, J.J. and *Landsberger, S.*, 1988: Intra-urban precipitation quality: Hamilton, Canada. *Water, Air, and Soil Pollut. 38*, 37-53.

IDŐJÁRÁS

Quarterly Journal of the Hungarian Meteorological Service
Vol. 98, No. 2, April–June 1994

The effect of the droplet size distribution on the reflectivity of boundary layer clouds

I. Csiszár

Satellite Research Laboratory, Hungarian Meteorological Service
P.O. Box 39, H-1675 Budapest, Hungary

(Manuscript received 17 March 1994; in final form 12 May 1994)

Abstract—The principal aim of this study was the assessment of the applicability of the 3.7 μm satellite reflectivity measurements for the retrieval of cloud microphysical properties, with special respect to the *High Resolution Infrared Radiation Sounder* (HIRS) on board the polar orbiter NOAA series. Reflectivities of opaque plane-parallel water clouds have been simulated using a discrete-ordinate radiative transfer model by assuming various droplet size distributions. A small sensitivity to the width of the droplet size spectrum was observed. The effects of the within-cloud horizontal variability were also investigated. The calculations have shown that the fractal re-distribution of the droplet population causes changes in the cloud reflectivity. These phenomena affect not only the effective radius retrieval accuracy, but also have to be taken into account in the parametrization of the near-infrared cloud albedo in general circulation models.

Key-words: radiation balance, cloud microphysics, satellite measurements.

1. Introduction

During the recent years there has been a major concern about the radiative effects of cloudiness on the Earth's energy budget. The net *cloud forcing* (the change of total radiant energy due to the presence of clouds) shows significant variation with cloud type. For example, cirrus clouds exhibit a warming effect because of their high shortwave transmissivity and low longwave emission. Low stratocumulus clouds, on the other hand, reflect large proportion of the shortwave energy with little compensation in the longwave region. Investigations have revealed that 15–20% increase in their amount, 20–35% increase in their liquid water path or 15–20% decrease in their droplet size can balance the radiative perturbation from doubling of the CO_2 content (*Slingo*, 1990). Therefore, the accurate knowledge about these parameters is essential and requires sophisticated retrieval methods.

Meteorological satellites provide a unique opportunity to obtain global information on the state and amount of the cloudiness. The *International Satellite Cloud Climatology Program* (ISCCP, *Rossow* and *Schiffer*, 1991) is aimed at the collection and processing of such data.

In this study we were focusing on the effect of the cloud droplet size distribution on the accuracy of the retrieval of the cloud droplet *effective radius* (r_e). This parameter is the ratio of the total volume to the total surface of the cloud droplets. A commonly used bispectral retrieval approach is based on constructing reflectivity look-up tables by radiative transfer calculations in a visible window and a near-infrared liquid water absorption band for various sun-satellite geometries, cloud optical depth (τ) and effective radius values. Then, the satellite reflectivity measurements at a given viewing geometry provide simultaneously the optical depth and the effective radius of the cloud droplets. However, for relatively thick clouds ($\tau \geq 10$) the reflection in the near-infrared (e.g around 1.65, 2.16 or 3.7 μm) is closely independent of the optical depth (*Nakajima* and *King*, 1990). Hence, in such cases, the effective radius can be directly derived from the near-infrared satellite reflectivity measurements.

Two radiometers on board the polar orbiting operational NOAA satellites carry out measurements in the 3.7 μm band. They are channel 3 of the *Advanced Very High Resolution Radiometer* (AVHRR) and channel 19 of the *High Resolution Infrared Radiation Sounder* (HIRS), having sub-satellite pixel sizes of 1.1 and 17 km, respectively. Both instruments have been used for the retrieval of cloud droplet effective radius (see, for example, *Arking* and *Childs*, 1985; *Gu et al.*, 1992; *Watts*, 1993).

However, the simulated reflectivity values are calculated using several simplifying assumptions. First, the clouds are taken geometrically plane-parallel. Second, within-cloud homogeneity in liquid water content is assumed on a scale comparable to the pixel size of the satellite radiometer. In addition, the effective radius is also taken to be constant on the same scale, and the statistical characteristics of the droplet size spectra in all pixels are fixed. Obviously, in some cases these simplifications are not entirely applicable. Here we will examine the potential error caused by the last assumptions, using in-situ and remote sensing observational data of marine stratocumulus clouds during the *First ISCCP Regional Experiment* (FIRE) off the California Coast in 1987 (*Nakajima et al.*, 1991). We will concentrate on the larger field of view (FOV) of HIRS where the bias is expected to be larger.

In the paper we first introduce the physical basis of the simulation of cloud reflectivities by radiative transfer calculations. After that we investigate the potential retrieval error connected to the assumption of constant droplet spectrum width. In the following section we study the effect of the horizontal cloud inhomogeneity on the reflectivity. That will be followed by some discussion and concluding remarks.

2. *Calculation of simulated reflectivities of opaque plane-parallel water clouds*

In the investigated spectral region the shortwave solar radiation and the longwave terrestrial thermal emission are of comparable magnitude. However, the thermal emission can be easily removed from the measured radiance. Hence, it is sufficient to use the radiative transfer equation for a multiple scattering atmosphere, which describes the change of the radiant intensity I in direction Ω at a given optical depth (*Liou*, 1980)

$$\mu \frac{dI(\tau,\Omega)}{d\tau} = I(\tau,\Omega) - \frac{\varpi}{4\pi} \int_{4\pi} I(\tau,\Omega')\, P(\Omega,\Omega')\, d\Omega' - \frac{\varpi}{4\pi}\, \pi F_0\, P(\Omega, -\Omega_0)\, e^{-\frac{\tau}{\mu_0}}, \tag{1}$$

where $\mu = \cos\Theta$ and $\mu_0 = \cos\Theta_0$ denote the cosines of the observational and solar zenith angles respectively, ϖ is the *single scattering albedo* (the ratio of the scattering and extinction efficiencies), F_0 is the solar flux and P is the *phase function* that describes the angular distribution of the scattering. It is usual to express P in the form of Legendre polynomial expansion:

$$P(\cos\chi) = \sum_{0}^{N} \alpha_l P_l(\cos\chi), \tag{2}$$

where χ is the angle between the incident and scattered beams (scattering angle) and P_l is the lth Legendre polynomial. The first moment of the expansion, α_1 is the *asymmetry factor* (generally denoted as g) that gives at what rate the scattering differs from the isotropic distribution.

In this work the scattering parameters at $\lambda = 3.7$ μm were calculated by the Mie scattering program *MIEV0* developed by *Wiscombe* (1979). This software provides, among other quantities, the single scattering albedo, the asymmetry factor and the coefficients for the Legendre polynomial expansion for a single droplet size and wavelength. To obtain these parameters for a given size distribution an integration over the droplet size spectrum is required. The complex refractive index of water for 3.7 μm was taken from the work by *Paltridge* and *Platt* (1976).

The angular distribution of the radiant intensity on the top of the atmosphere was determined by the discrete-ordinate radiative transfer program *DISORT* (*Stamnes et al.*, 1988), using 24 computational polar angles (streams). A three-layer atmospheric model was applied in which the cloud was located in the middle layer with Rayleigh scattering and weak water vapour absorbtion in the top and bottom layers. The reflectivity was determined from the following formula

$$R(\mu,\mu_0,\Phi) = \frac{\pi I(0,-\mu,\Phi)}{\mu_0 F_0}, \tag{3}$$

in which Φ represents the azimuthal separation of the sun and the satellite. The physical meaning of the reflectivity is what the cloud albedo would be if the reflection were isotropic.

3. Sensitivity of the cloud reflectivity to the width of the droplet size spectrum

Throughout this work it was assumed that the droplet size spectrum of a stratocumulus cloud follows the lognormal distribution. This distribution is understood locally, i.e. the whole spectrum is present in a vertical cloud column having a horizontal dimension that is comparable to or smaller than the pixel (or FOV) size of the satellite sensor. The optical depth of all cloud columns was 32. Since in the case of opaque clouds the remotely sensed cloud microphysical parameter represents the upper third of the cloud (*Nakajima* and *King*, 1990), for simplicity, no vertical inhomogeneity was taken into account. The effects of two parameters were investigated: those of the standard deviation of the lognormal distribution, σ (the width of the spectrum) and the effective radius, r_e that is connected to the mode radius of the lognormal distribution r_0 by the following expression

$$r_e = r_0 \exp(5\sigma^2). \tag{4}$$

Fig. 1 shows the reflectivity pattern between $\Phi = 0°$ and 180° for four effective radii at 60° and 30° solar and satellite zenith angles respectively for standard deviations ranging between 0.20 and 0.50. The strengthening of the forward scattering with the increase of r_e is obvious. It is also clear that the reflectivity is sensitive to the width of the droplet spectrum, which can lead to retrieval errors in extreme situations. For example, at these solar and satellite zenith angles and $\Phi = 0$ the same reflectivity value (R = 21%) corresponds to both $r_e = 5$ μm, $\sigma = 0.20$ and $r_e = 10$ μm, $\sigma = 0.50$. However, using look-up tables calculated assuming a realistic mean value of $\sigma = 0.35$, this potential absolute error at such droplet sizes is generally not larger than 2–3 μm.

In *Fig. 2* the reflectivity pattern is shown as a function of the effective radius at the above viewing geometry and standard deviation (it is hereafter referred to as *reflection function*). With the increase of its slope one may suspect a decrease of the potential retrieval error towards the smaller droplets. This can be easily justified by scrutinizing Fig. 1, where a correspondence similar to the above example is depicted between $r_e = 3$ μm, $\sigma = 0.20$ and $r_e = 5$ μm, $\sigma = 0.50$ (R = 31%).

In addition, by investigating Fig. 1 it can also be observed that the sensi-

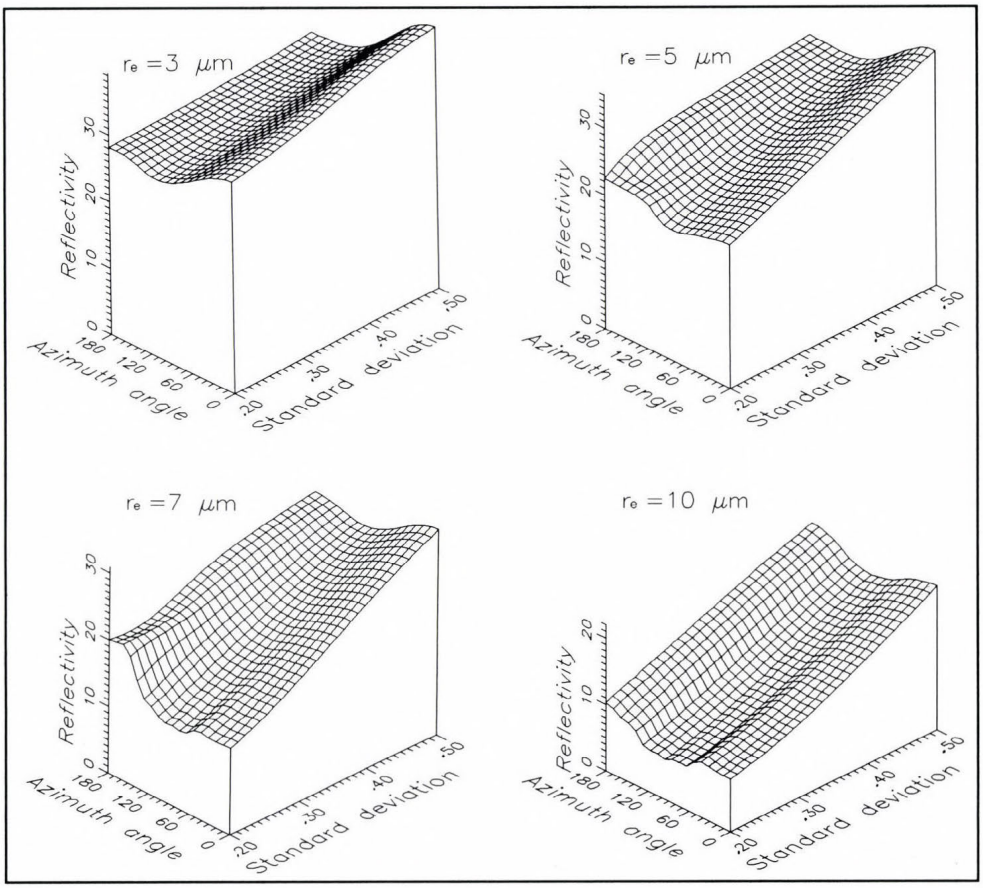

Fig. 1. 3.7 μm reflectivity patterns for lognormal droplet size distributions with $\sigma = 0.35$ and four effective radius values at $\Theta_0 = 60°$ and $\Theta = 30°$.

tivity of the reflectivity to the width of the droplet size spectrum depends on the effective radius itself. From the four cases shown it is highest for $r_e = 7$ μm. The reason of this phenomenon lies in the asymptotic theory developed by *King* (1987). According to this, at the water absorption bands in the near-infrared the reflectivity strongly depends on the single scattering albedo with a weaker dependence on the asymmetry factor. *Fig. 3* illustrates these parameters for three distributions and effective radii from 0.2 μm to 25 μm. There is a high variation of ϖ around 7 μm. This effect seems to be able to counteract the fact that the variability of g has a minimum at approximately the same wavelength. The dependence of the reflectivity on the spectrum width significantly weakens below $r_e = 4$ μm due to the decrease of the variability of ϖ. This results in a further decrease in the potential absolute retrieval error towards the smaller droplets.

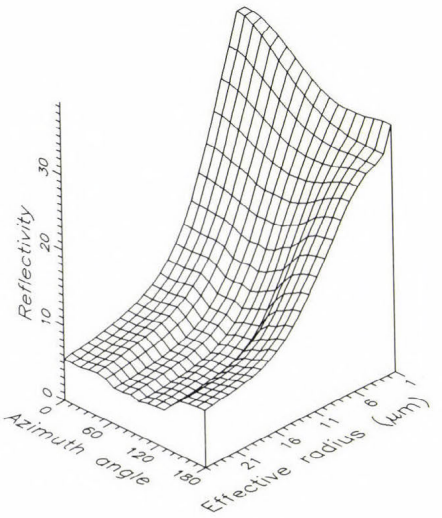

Fig. 2. Reflection function at 3.7 μm for σ = 0.35, Θ_0 = 60° and Θ = 30°, in dependence of the effective radius.

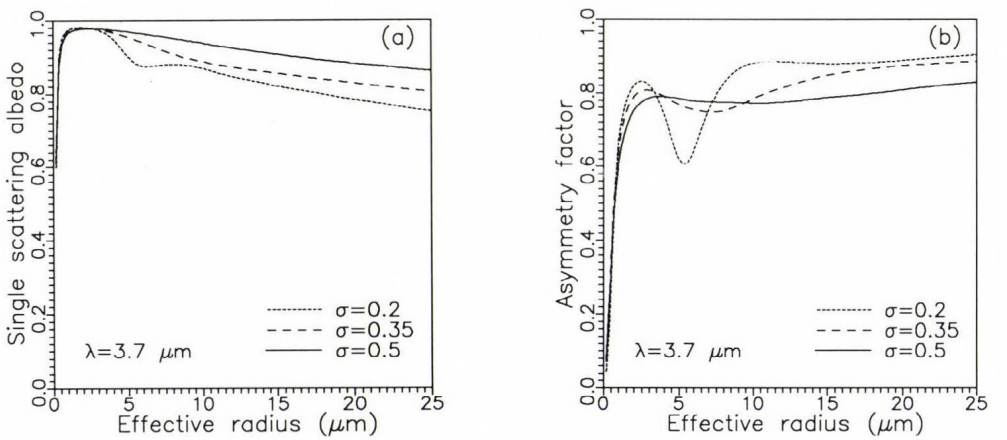

Fig. 3. Single scattering albedo (*a*) and asymmetry factor (*b*) at 3.7 μm as functions of the effective radius for three standard deviations of the lognormal droplet size spectra.

4. The effect of the horizontal cloud inhomogeneity on the remotely sensed reflectivity

Cahalan and *Snider* (1989) revealed that the liquid water path (or optical thickness) of marine stratocumulus clouds has a mesoscale fractal structure that can be characterized either by a lognormal probability density function or by a cascade model. They also showed that this inhomogeneity causes a decrease in the cloud albedo. *Nakajima et al.* (1991) observed a similar within-cloud inhomogeneity in microphysical properties over an area of several hundred square kilometres with no strong correlation between the effective radius and

the optical depth. Since this area is comparable to the HIRS FOV size, it is essential to investigate the effect of such spatial structure on the cloud reflectivity. In the present work the following assumptions were made about the cloud fractal structure and the radiative transfer processes:

— The probability density function of the effective radius is lognormal for an area comparable to the HIRS FOV size.
— The cloud optical thickness is high enough to assume opacity for all vertical cloud columns in the above area.
— There is no net photon transport between the adjacent cloud columns.

Thus, the reflectivity of the HIRS FOV can be obtained by the simple integration of the reflectivities of the separate cloud columns over the effective radius spectrum.

Fig. 4a shows the reflectivity pattern for $\Theta_0 = 60°$ for a FOV in which the horizontal distribution of the effective radius follows a lognormal spectrum with mode radius (r_{e0}) and standard deviation (σ_{e0}) of 10 μm and 0.10, respectively (these values are characteristic to the FIRE clouds). The standard deviation of the droplet spectra in the individual cloud columns was kept at 0.35.

The effective radius of this droplet population is 7.54 μm. If we now compute the reflectivity pattern for a horizontally homogeneous size distribution having $r_e = 7.54$ μm and $\sigma = 0.35$, we can estimate the retrieval error due to the neglect of the fractal structure of the cloud. These reflectivity values shown in *Fig. 4b* are systematically 6–12% higher than in the previous case. Thus, a cloud having the same effective radius but the above fractal structure produces

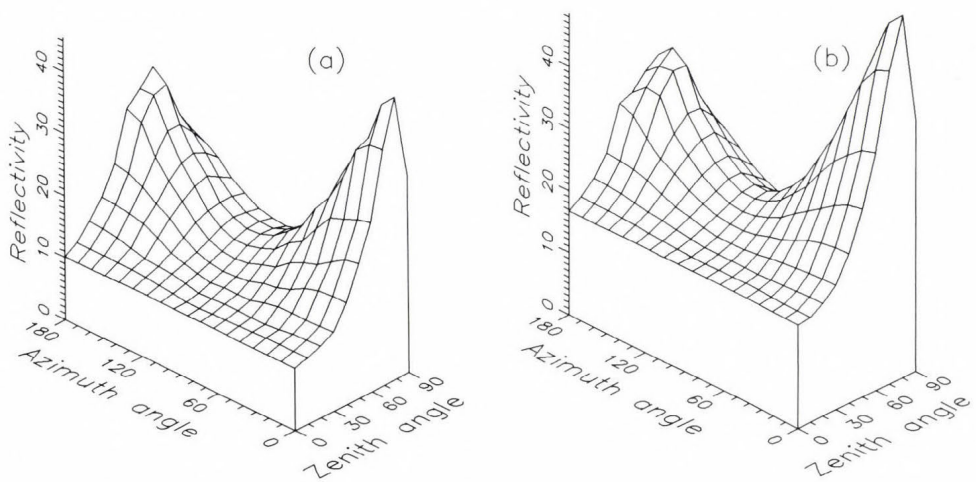

Fig. 4. (*a*) 3.7 μm reflectivity pattern at $\Theta_0 = 60°$ for a horizontally inhomogeneous cloud with $r_{e0} = 10$ μm and $\sigma_{e0} = 0.10$. (*b*) 3.7 μm reflectivity pattern for a homogeneous cloud with r_e=7.54 μm and $\sigma = 0.35$.

a reflectivity value that is lower than the one assigned to that particular effective radius and viewing geometry in the retrieval look-up table. This effect leads to the overestimation of the effective radius. The phenomenon is the consequence of the non-linearity of the reflection function and the asymmetry of the probability density function of the effective radius. Since the slope of the reflection function $\Delta R(\%)/\Delta r_e(\mu m) \approx -2$ in this region, the absolute error in the effective radius retrieval may reach 3–6 μm.

It is also important to see what the cloud reflectivity is if the same population of droplets, instead of having the fractal structure described above, is evenly distributed in the FOV. This may give us an idea of the behaviour of the reflectivity (and albedo) bias caused by the assumption of mesoscale horizontal homogeneity in, for example, general circulation models.

Now we had no assumption about the analytical form of the droplet spectrum; the mean Mie scattering parameters were determined from the normalized relative frequency corresponding to 0.1 μm wide bins of droplet radius. The calculations revealed again a systematic darkening in the case of the fractal cloud. *Fig. 5* shows the relative bias $100*(R_{hom} - R_{fr})/R_{fr}$. As it can be seen, the bias increases towards the higher satellite zenith angles.

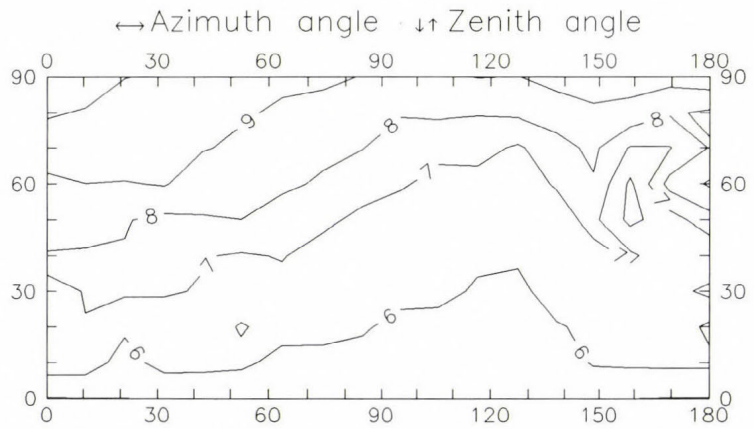

Fig. 5. Relative bias (%) between the 3.7 μm reflectivities of the horizontally inhomogeneous cloud (Fig. 4a) and a cloud containing the same droplet population evenly distributed.

To further clarify this point, we carried out a similar series of calculations for $r_e = 10$ μm and $\sigma = 0.20$. Such a widening of the spectrum may be a result of more intensive within-cloud dynamic processes or of the increase of the FOV size. The comparison of the reflectivity patterns (not shown) for the fractal cloud and the one corresponding to the effective radius of this droplet population (8.13 μm) at $\sigma = 0.35$ indicates a slightly bigger absolute bias

(7–15%) in this case, which results in the further increase of the potential absolute retrieval error.

More striking is, however, the increase in the relative bias between the reflectivities of the fractal and the corresponding homogeneous clouds; its characteristic value is about 25% (*Fig. 6*).

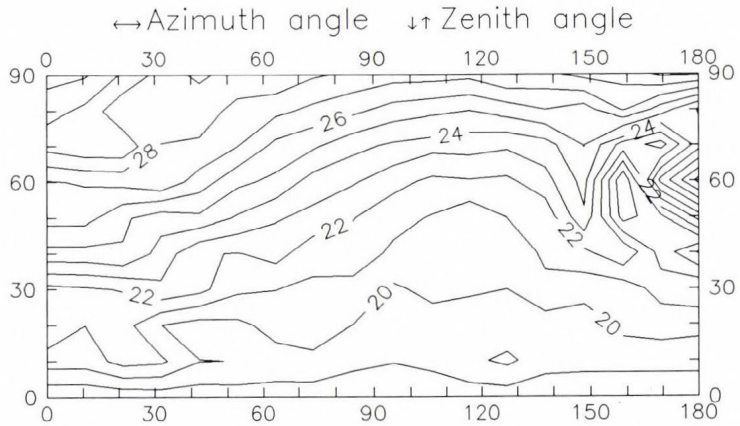

Fig. 6. Relative bias (%) between the 3.7 μm reflectivities of the horizontally inhomogeneous cloud with $r_{e0} = 10$ μm and $\sigma_{e0} = 0.20$ and a cloud containing the same droplet population evenly distributed.

It is also obvious that the magnitude of the reflectivity bias varies with the viewing geometry and r_{e0}. For clouds having larger droplets and hence characterized by a lower variability of the reflectivity the darkening is expected to be smaller. However, in this study these effects have not been investigated in details.

5. Conclusion and plans for the future

The effect of the droplet size distribution was investigated on the reflectivity of geometrically plane-parallel, low-level stratiform clouds. The principal aim of this study was to determine whether the near-infrared reflectivity measurements of the HIRS radiometer can be used for the accurate determination of the microphysical properties of such clouds. The main results can be summarized as follows:

— The cloud reflectivity is sensitive to the width of the droplet size spectrum. This sensitivity depends upon the effective radius, and is determined by the variability of the mean Mie scattering parameters of the droplet population. However, the potential absolute retrieval error caused by this effect is relatively small. This indicates an

acceptable retrieval accuracy whenever the horizontal variability of the effective radius is low on a scale comparable to the radiometer pixel size.

— The within-cloud horizontal inhomogeneity of the microphysical properties causes a darkening in the cloud reflectivity, and probably in the albedo too. This effect has two consequences. First, the use of look-up tables built up by assuming horizontal homogeneity causes a systematic overestimation of the effective radius of the droplet population by the low-resolution HIRS reflectivity measurements. Second, the parametrizations of the mesoscale near-infrared cloud albedo in climate models must also account for the within-cloud fractal structure even if the given gridbox is entirely overcast.

Of course, these results are based only on several simple examples. To achieve a better understanding of the phenomena it may be necessary to revise some of the simplifying assumptions made. For example, the choice of other statistical distributions or the consideration of the geometric inhomogeneity and non-zero cloud transmissivity may lead to a slight modification of the results, probably without changing, however, their main characteristics. Also, more detailed calculations would be needed for the whole range of sun-satellite geometry. The extension of our computational capabilities will hopefully enable us to perform this work.

Acknowledgements—We wish to express our gratitude to the *authors* of *MIEV0* and *DISORT* for making the programs available. The valuable discussions regarding the Mie scattering calculations with *Dr. M. Putsay* are also appreciated. *I. Ihász* and *G. Duska* were of great help in solving many computational problems.

References

Arking, B.A. and *Childs, J.D.*, 1985: Retrieval of cloud cover parameters from multispectral satellite images. *J. Climate Appl. Meteor. 24*, 322-333.

Cahalan, R.F. and *Snider, J.B.*, 1989: Marine stratocumulus fractal structure. *Remote Sens. Environ. 28*, 95-107.

Gu, J., Pincus, R., Austin, P. and *Szczodrak, M.*, 1992: Cloud optical depth estimates from satellite measurements. *Proceedings of the 11th International Conference of Clouds and Precipitation*, Montreal, Canada, 1992, 839-842.

King, M.D., 1987: Determination of the scaled optical thickness of clouds from reflected solar radiation measurements. *J. Atmos. Sci. 44*, 1734-1751.

Liou, K.N., 1980: *An Introduction to Atmospheric Radiation*. Academic Press, New York, London, Toronto, Sydney and San Francisco, 176-182.

Nakajima, T. and *King, M.D.*, 1990: Determination of the optical thickness and effective particle radius of clouds from selected solar radiation measurements. Part I: Theory. *J. Atmos. Sci. 47*, 1878-1893.

Nakajima, T., King, M.D., Spinhirne, J.D. and *Radke, L.F.*, 1991: Determination of the optical thickness and effective particle radius of clouds from selected solar radiation measurements. Part II: Marine stratocumulus observations. *J. Atmos. Sci. 48*, 728-750.

Paltridge, G.W. and *Platt, C.M.R.*, 1976: *Radiative Processes in Meteorology and Climatology*. Elsevier-Scientific Pub. Co., Amsterdam.

Rossow, W.B. and *Schiffer, R.A.*, 1991: ISCCP data products. *Bull. Amer. Meteorol. Soc. 72*, 2-20.

Slingo, A., 1990: Sensitivity of the Earth's radiation budget to changes in low clouds. *Nature 343*, 49-51.

Stamnes, K., Tsay, S.C., Wiscombe, W. and *Jayawera, K.*, 1988: A numerically stable algorithm for discrete-ordinate-method-radiative transfer in multiple scattering and emitting layered media. *Appl. Opt. 27*, 2502-2512.

Watts, P.D., 1993: Cloud microphysical Parameters from TOVS: a practical scheme and geometrical considerations. *Technical Proceedings of the Seventh International TOVS Study Conference*, 10-16 February, Igls, Austria, 543-554.

Wiscombe, W.J., 1979: Mie scattering calculations: advances in technique and fast, vector-speed computer codes. *NCAR Technical Note TN-140+STR*, National Center for Atmospheric Research, Boulder, Colorado.

IDŐJÁRÁS

Quarterly Journal of the Hungarian Meteorological Service
Vol. 98, No. 2, April–June 1994

Assessment of the impacts of climate change on the yields of winter wheat and maize, using crop models

Zs. Bacsi[1] and **M. Hunkár**[2]

[1]*Pannon University of Agricultural Sciences, Georgikon Faculty of Agronomy*
P.O. Box 71, H–8361 Keszthely, Hungary
[2]*Hungarian Meteorological Service, Agrometeorology Research Station*
P.O. Box 80, H–8361 Keszthely, Hungary

(Manuscript received 7 February 1994; in final form 20 May 1994)

Abstract—The climate change induced by the increase in atmospheric CO_2 due to human activities may lead to significant consequences for the human society and economy. Nowadays neither the extent of this climate change nor its effects on agriculture can be predicted with certainty. Many research papers have dealt with the analysis of these impacts on different crops in different regions of the Earth. The present paper aims at assessing the impacts of three well known climate change scenarios—the carbon-dioxide doubling scenarios from the GISS, GFDL and UKMO general circulation models—on wheat and maize yields in Hungary. For this purpose the outputs of the above three GCMs are used to create weather time series for Hungary. These are used together with the CERES-Wheat and the CERES-Maize crop growth simulation models, which simulate the growth and development processes of these crops using daily values of temperature, radiation and precipitation. These crop models facilitate the testing of the results of adaptation strategies such as adjusted sowing date, changed irrigation or fertilization patterns, or choice of a variety capable of better utilizing the environmental conditions of a new climate situation. The present paper uses field observations and weather data from Keszthely (Western Hungary). Simulation results indicate decreases both in winter wheat and maize yields with maturity occurring significantly earlier during the year.

Key-words: climate change impacts, simulation, crop models, wheat, maize, Hungary.

1. Introduction

Many climate scientists agree that the increase in atmospheric carbon-dioxide resulting from human activities will probably lead to changes in the Earth's climate. However, it is not possible at present to accurately forecast either the size or the temporal dynamics of this change. There are several

methods available which help us to estimate, under certain assumptions, the main features of this carbon-dioxide induced change. One of these methods is modelling the Earth's climate using General Circulation Models (GCMs) at various levels of atmospheric carbon-dioxide concentrations. Several such GCMs are known among the climate scientists, and these differ both in the climatic input variables considered and in the output variables produced. Until recently only results from so called 'equilibrium models' were published, that is, model outputs describing the Earth's climate after it has reached an equilibrium state at a given, higher level of atmospheric carbon-dioxide. (GCM results on the dynamics of the increase in the concentration of atmospheric carbon-dioxide—as well as other so-called 'greenhouse gases'—and on the temporal dynamics of the resulting climate change were not published until 1993. The climate research laboratory of the U.K. Meteorological Office at Bracknell has recently completed such a 'transient' model run, but the results of this were not available to the authors at the time of writing this paper.)

For the purposes of this study outputs from three general circulation models were used. Then the climate change scenarios predicted for Western Hungary were linked to wheat and maize simulation models, and the impacts on the development and yield of the two crops were estimated. The results describing the growth and development of the two crops were then compared to the corresponding values from the past 16 years at Keszthely, the location of the study, to analyse the size and direction of the changes.

2. Material and method

For the purposes of the present study daily maximum and minimum temperature values, daily global radiation and daily precipitation amounts were used for the years 1975 to 1990 measured at the Agrometeorology Station at Keszthely (county Zala, Western Hungary). Outputs from three General Circulation Models were used to create climate change weather scenarios. These are:

- GISS (Goddard Institute for Space Studies, New York, U.S.A.; *Hansen et al.*, 1988),
- GFDL (Geophysical and Fluid Dynamics Laboratory, Princeton, U.S.A.; *Wetherald* and *Manabe*, 1986),
- UKMO (United Kingdom Meteorological Office, Bracknell, U.K.; *Wilson* and *Mitchell*, 1987).

The crop growth and development rates were simulated using the CERES-Wheat (*Godwin et al.*, 1989) and the CERES-Maize (*Jones* and *Kiniry*, 1986) crop models.

3. The CERES simulation models

The growth and development of the winter wheat and maize crop were assessed using the Wheat and the Maize models of the CERES model group, developed in the United States. The two crop models are very similar regarding their structure, operation, input data requirements and modelled processes. They are capable of simulating the impacts of the following environmental factors:

- weather variables: daily maximum and minimum temperature values, global radiation and precipitation amount for each day from sowing till harvest;
- soil variables: parameters describing the physical and chemical composition and water holding capacity of each soil layer, and the initial soil water and nutrient content just before sowing;
- plant parameters: 5 parameters are used for maize and 6 parameters for wheat to describe the genetic characteristics of the actual crop variety used, some of these referring to the speed of phenological development, others to the speed of dry matter accumulation;
- agrotechnology data: sowing date, sowing depth, sowing density, date and amount of irrigation and fertilization, if any.

Based on the above input information the CERES crop models simulate the time of the crop's reaching each development stage, the amount of above ground biomass and its distribution among the various crop parts, the growth of the leaf area, the crop grain yield, the water and nitrogen balance of the soil, and the nitrogen content of the various crop parts.

Before starting the climate change experiments it was necessary to assess the performance of the Ceres-Wheat and Ceres-Maize models under the environmental conditions typical to the vicinity of Keszthely, and with crop varieties used in Hungary. For these so-called validation runs, relying on the experiments by *Hunkár* (1994) 3 years were chosen for maize from which field observations were available for a variety popular in Hungary. For winter wheat the field observations from 4 years by the Crop Production Institute of the Pannon University of Agricultural Sciences Keszthely were used. The field observations for both crops were compared to model outputs for Rammann-brown forest soil, the typical soil type around Keszthely, for the maize variety Pioneer 3901 and for the winter wheat variety Martonvásár-4. The results of the validation experiments are shown in *Table 1*.

As the above results show the model works with adequate accuracy, so it is suitable to be used in climate impact assessment studies. It has to be mentioned, that due to the inherent limitations of the simulation models available, the assessment of the climate change impacts has to be limited to the impacts caused by the changed weather characteristics resulting from the

increased carbon-dioxide concentrations, and the direct impacts of this increased carbon-dioxide level on the crop physiological processes (changed photosynthesis, transpiration and respiration) were not considered.

Table 1. Validation results for CERES-Maize and CERES-Wheat with field observations from Keszthely

CERES-Maize: Variety: Pioneer 3901

Difference between simulated and observed values

Year	Silking (day)	Maturity (day)	Grain yield (t/ha)	Biomass (t/ha)
1989	-4	-4	4.3	0.6
1990	-3	-5	0.006	-3.8
1991	-4	-4	-1.5	-1.8

CERES-Wheat: Variety: Martonvásár-4

Difference between simulated and observed values

Year	Anthesis (day)	Maturity (day)	Grain yield (t/ha)	Biomass (t/ha)
1984/85	+11	-3	0.4	-0.5
1985/86	+7	-11	0.6	1.1
1988/89	+1	-8	0.8	-0.4
1989/90	-2	-8	0.2	0.4

4. The creation of the climate change scenarios

All the three applied GCMs have their limitations regarding spatial resolution. The GISS handles the Earth's surface as gridboxes of the size 10° latitude × 7.9°longitude. The climate of each gridbox is considered to be homogeneous, and the climate characteristic are allocated to the gridbox centre. The GFDL works similarly with gridboxes of 4.5°latitude × 7.5°longitude, and the UKMO with gridboxes of 5°latitude × 7.5°longitude. In the present study the gridbox covering the location of Keszthely was used with each GCM, thus for GISS the gridbox with the centre 50°N;20°E, for GFDL the gridbox with the centre 46.7°N;15°E, for UKMO the gridbox with the centre 47.5°N;18.8°E (see *Fig. 1*).

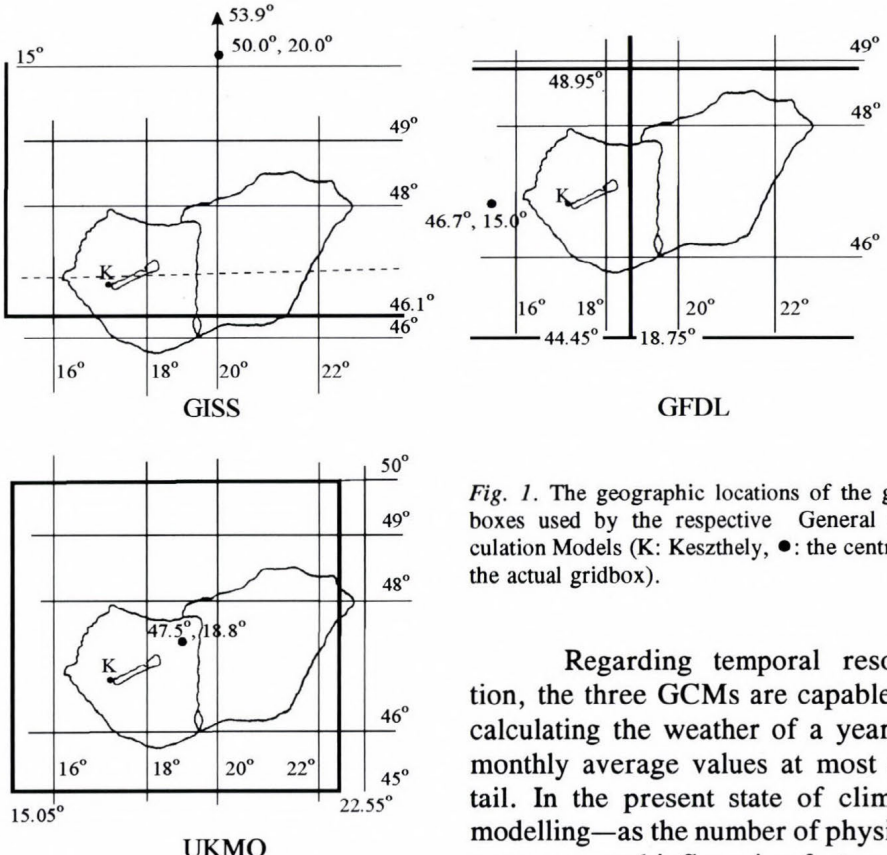

Fig. 1. The geographic locations of the gridboxes used by the respective General Circulation Models (K: Keszthely, •: the centre of the actual gridbox).

Regarding temporal resolution, the three GCMs are capable of calculating the weather of a year as monthly average values at most detail. In the present state of climate modelling—as the number of physical processes, and influencing factors included in the climate models are limited—the predictions coming from climate models are considerably inaccurate, e.g. the results from model experiments aiming at simulating the present climate of the Earth differ considerably from reality. So the climate characteristics simulated under changed greenhouse gas concentrations are also rather unreliable. Nevertheless, the predicted rate of changes can be accepted. For this reason in creating the climate change scenarios for the location of Keszthely a change factor between the modelled present and 'future' climates was generated for the various weather parameters, and then these change factors were used to modify the 'baseline' weather of the period 1975–1990. *Figs. 2* and *3* show the monthly average temperature values and precipitation amounts for the baseline weather in comparison with the same average values for the climatic standard period of 1951–1980. In the computation process of the change factors the 'present' climate means the modelled climate under the CO_2 concentration of the first half of the 1980s (300 ppm for GFDL and UKMO, 315 ppm for GISS), and the 'future' climate the modelled climate under doubled CO_2 concentration. The change factor was calculated as the difference between the

'future' and 'present' values for temperature, and as the ratio of these for radiation and precipitation, in agreement with the recommended methodology of many similar impact assessment studies (*Smith* and *Tirpak*, 1989; *Parry et al.*, 1988; *Adams et al.*, 1990).

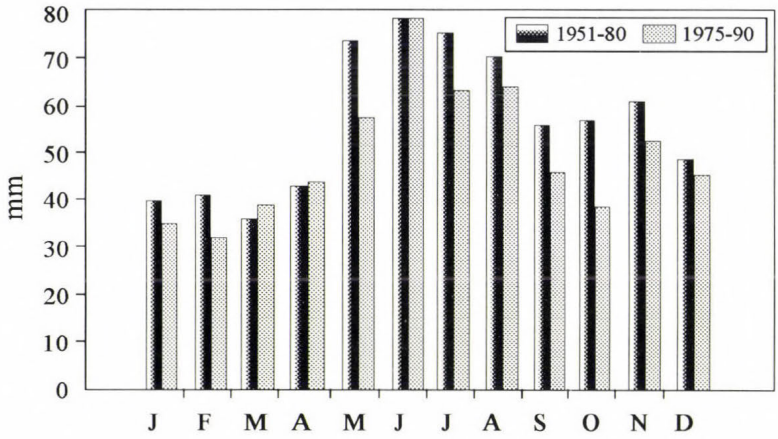

Fig. 2. Average monthly precipitation.

As the crop growth simulation models require daily weather data from sowing till harvest and the climate model outputs present the results only in

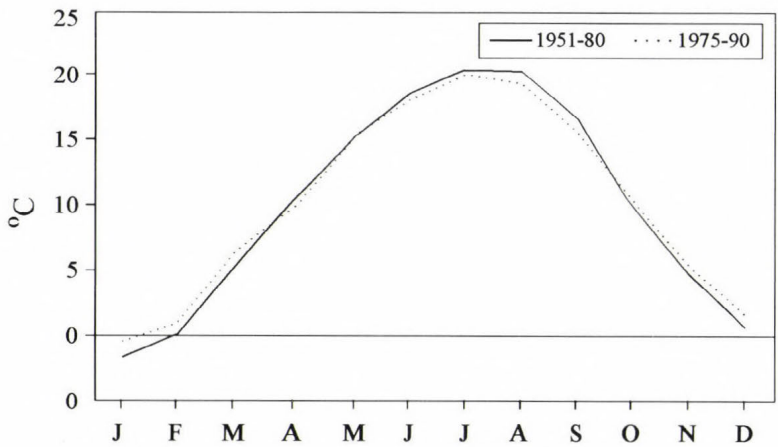

Fig. 3. Average monthly temperature.

monthly resolutions, the baseline daily weather data were modified by the change factor of the corresponding month, to create climate change scenarios with daily resolutions.

The change factors were calculated for each month of the year and for each GCM as follows:

$$\begin{aligned} \Delta T_j &= T_j\,(2 \times CO_2) - T_j\,(1 \times CO_2) && \text{for temperature,} \\ \Delta P_j &= P_j\,(2 \times CO_2) \,/\, P_j\,(1 \times CO_2) && \text{for precipitation,} \\ \Delta R_j &= R_j\,(2 \times CO_2) \,/\, R_j\,(1 \times CO_2) && \text{for radiation,} \end{aligned}$$

where $T_j\,(2 \times CO_2)$, $P_j\,(2 \times CO_2)$, $R_j\,(2 \times CO_2)$ are the average temperature, precipitation and radiation values respectively, calculated by the actual GCM for the month j in question for the modelled climate under doubled carbon-dioxide concentrations, and $T_j\,(1 \times CO_2)$, $P_j\,(1 \times CO_2)$, $R_j\,(1 \times CO_2)$ are the same for the modelled climate under normal carbon-dioxide concentrations, giving 12 sets ($j = 1 \ldots 12$, from January to December) of ΔT_j, ΔP_j and ΔR_j values for each GCM used.

The next step was to generate daily time series using the above change factors and the data of the baseline weather years of 1975–1990. So for all the three GCMs altogether 16 changed weather years were generated with daily maximum and minimum temperature, radiation and precipitation data as follows:

$$\begin{aligned} maxT_i\ (2 \times CO_2) &= maxT_i\ (1 \times CO_2) + \Delta T_j, \\ minT_i\ (2 \times CO_2) &= minT_i\ (1 \times CO_2) + \Delta T_j, \\ P_i\ (2 \times CO_2) &= P_i\,(1 \times CO_2) \times \Delta P_j, \\ R_i\ (2 \times CO_2) &= R_i\,(1 \times CO_2) \times \Delta R_j, \end{aligned}$$

where $maxT_i$, $minT_i$, P_i and R_i are the maximum and minimum temperature values, precipitation and radiation amounts respectively, for the actual day of the year in question, under the present and the doubled CO_2 concentrations. *Figs. 4, 5, 6* and *7* show the monthly average values of the weather variables for the baseline climate and for the doubled CO_2 scenarios from each GCM.

As described above, climate change scenarios were created using the three GCM outputs and the 16 baseline weather years from Keszthely. For the wheat simulation model altogether 15 baseline weather scenarios (from the 1975/76 growing period to the 1989/90 growing period), 15 GISS scenarios, 15 GFDL scenarios and 15 UKMO scenarios, and for the maize simulation model 16 baseline, 16 GISS, 16 GFDL and 16 UKMO scenarios were generated for the purpose of the climate impact assessments.

In order to compare the impact of the changed weather on the crops the agrotechnology was assumed constant for all simulation experiments. In the simulation runs the following agrotechnology parameters were used: sowing on 10 October with Martonvásár-4 winter wheat variety for the wheat model, and sowing on 10 April with Pioneer 3901 variety for the maize model. For both crops optimal nitrogen supply was assumed, and no irrigation was applied.

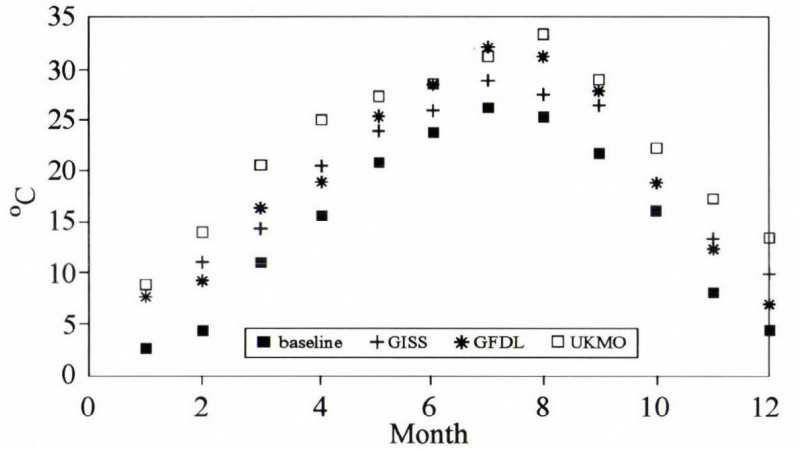

Fig. 4. Monthly averages of daily maximum temperature for 16 years.

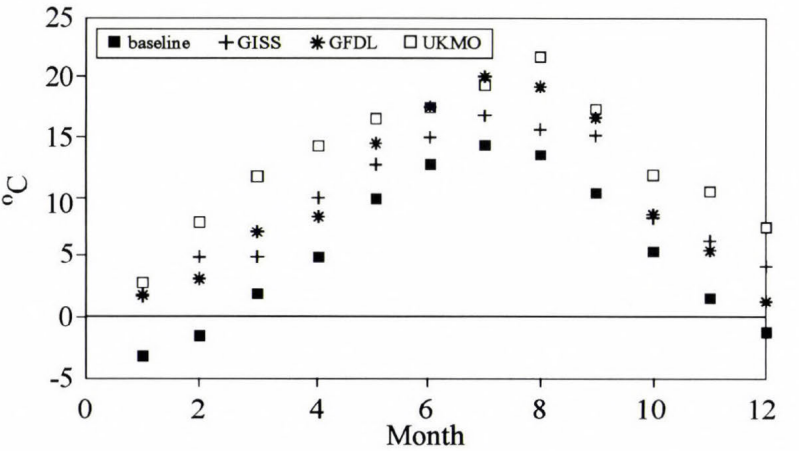

Fig. 5. Monthly averages of daily minimum temperature for 16 years.

5. Results

The outputs from the CERES crop models were used for the impact assessments, that is, for both wheat and maize the simulated values of resultant variables under the baseline weather were compared to the simulated values of the same variables under the climate change weather scenarios generated from the three GCMs.

5.1 Maize

In the maize experiments altogether 16 baseline weather years were available together with 16 GISS-years, 16 GFDL-years and 16 UKMO-years. So

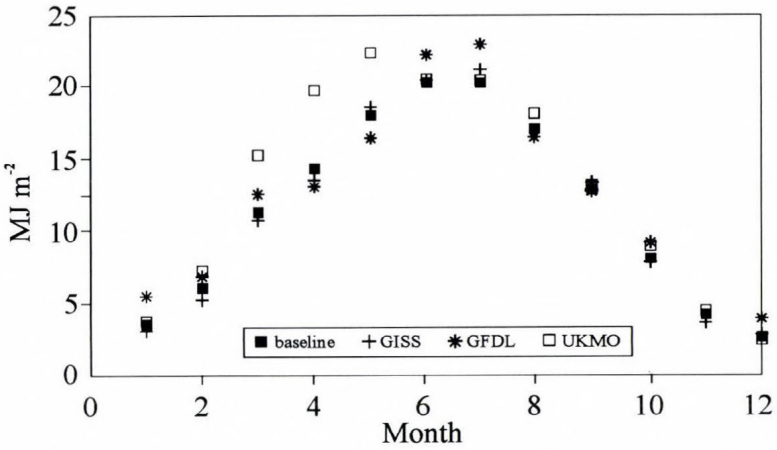

Fig. 6. Monthly averages of daily radiation for 16 years.

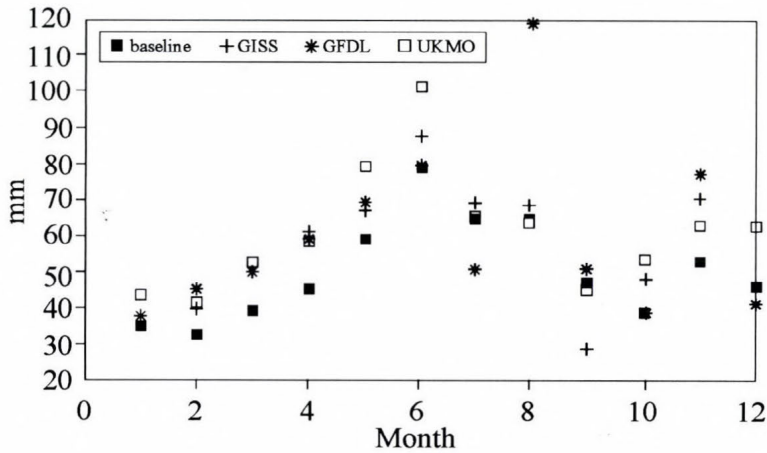

Fig. 7. Average monthly precipitation values for 16 years.

altogether 64 simulation experiments were carried out besides the validation runs described earlier.

The following resultant variables were considered in the assessment:

- the grain yield (t/ha),
- the amount of above ground biomass (t/ha),
- maximum leaf area index (LAI max),
- silking date,
- maturity date.

The climate change scenarios resulted in silking and maturity occurring much earlier, and thus the growing season became significantly shorter for all

the three different GCMs. The maize crop showed the fastest development under the 16 UKMO weather years, with maturity occurring 41 days earlier on average than under the baseline weather years. The GFDL scenario resulted in the crop's maturity occurring 35 days earlier on the average, while under GISS maturity occurred 20 days earlier.

Biomass and grain yield show somewhat less unanimous results. The GISS scenario resulted in a small, 8% yield increase on the average, while the GFDL resulted in a 7%, and the UKMO in a 14% average yield decrease. For all the three GCM scenarios the standard deviations of the yield are somewhat smaller than in the case of the baseline weather, so the yields though smaller, seem to become more stable under the changed weather, especially in the case of the GISS and the GFDL scenario. Biomass results showed similar characteristics to the yield. The average values of the maximum leaf area index increased a little for all the three GCM scenarios, while the standard deviations decreased. These results are shown in *Figs. 8* and *9*.

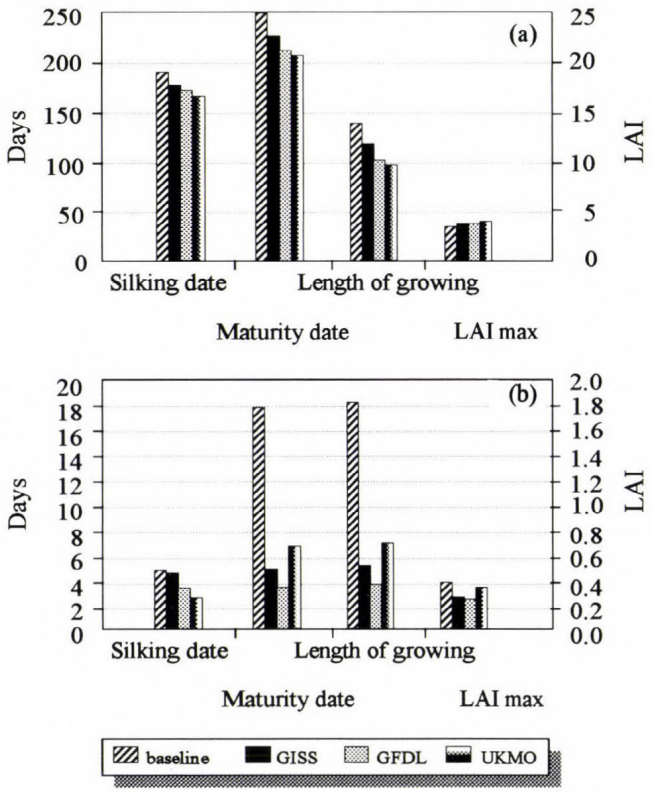

Fig. 8. Averages (*a*) and standard deviations (*b*) for the modelled development variables of maize for the various climate scenarios.

The above results may seem surprising, as maize, being a crop of tropical origin, was expected to utilize the increased temperature better, and produce higher yields under the changed weather, but the shortened growing season and the changed distribution of precipitation under this shorter growing season counteracted the results of the advantageous temperature patterns.

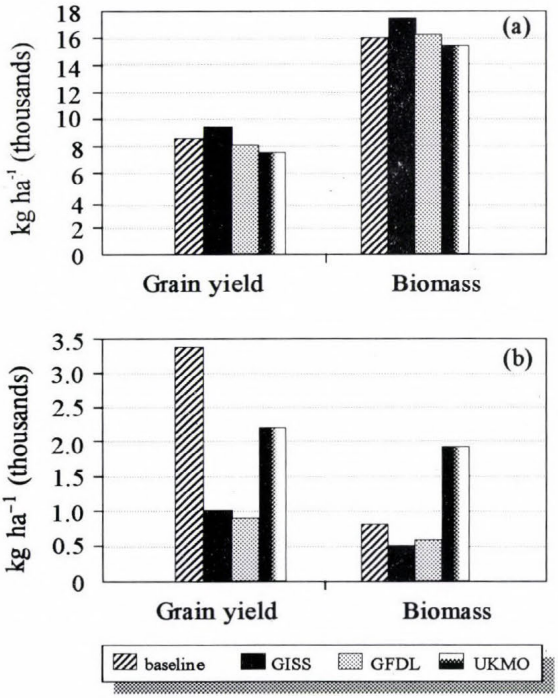

Fig. 9. Averages (*a*) and standard deviations (*b*) for the modelled production variables of maize for the various climate scenarios.

5.2 Wheat

In the wheat experiments altogether 15 baseline weather years were available together with 15 GISS-years, 15 GFDL-years and 15 UKMO-years. So altogether 60 simulation experiments were carried out above the validation runs described earlier.

The following result variables were considered in the assessment:

- the grain yield (t/ha),
- the amount of above ground biomass (t/ha),
- maximum leaf area index (LAI max),
- anthesis date,
- maturity date.

Results showed that similar to maize, the anthesis and maturity dates occurred earlier and the growing season became significantly shorter for all of the climate change scenarios. The fastest crop development occurred in the case of the UKMO scenario, with an average of 42 days shorter period from sowing to maturity in comparison to the baseline, while under the GFDL scenario maturity occurred 25 days earlier on the average, and under the GISS scenario 22 days earlier in average than under the baseline weather.

The average biomass production slightly increased for all the three climate change scenarios, and the standard deviation decreased. In the case of grain yield the GISS scenario resulted in a yield only 87%, the GFDL in a yield 72%, and the UKMO scenario in a yield 75% of the baseline average. It is true again that standard deviations of grain yield decreased for all the climate change scenarios, but it can be explained by the decrease in yield, and does not necessarily suggest more stable yields. It is also true for winter wheat that the 15 year average value for maximum leaf area index slightly increased while the standard deviation was somewhat reduced (see *Figs. 10* and *11*).

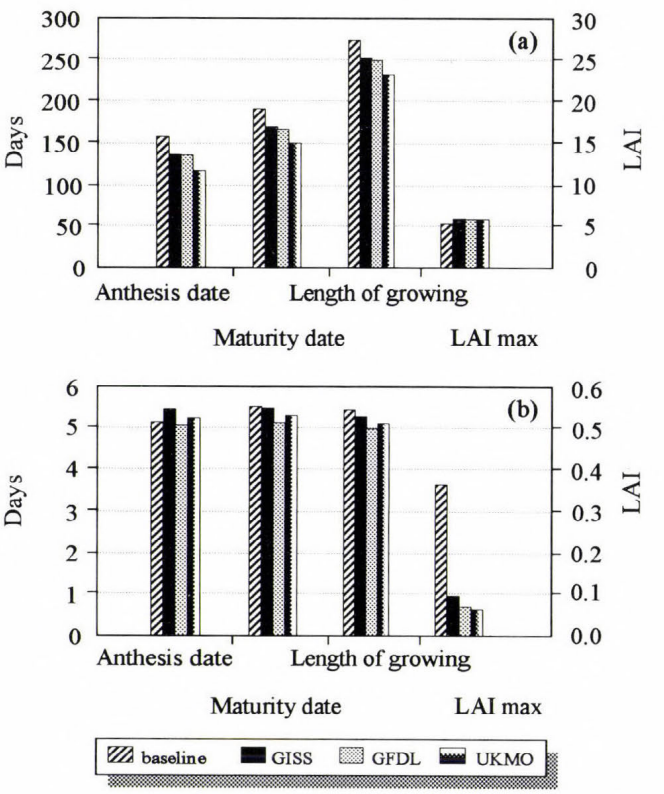

Fig. 10. Averages (*a*) and standard deviations (*b*) for the modelled development variables of wheat for the various climate scenarios.

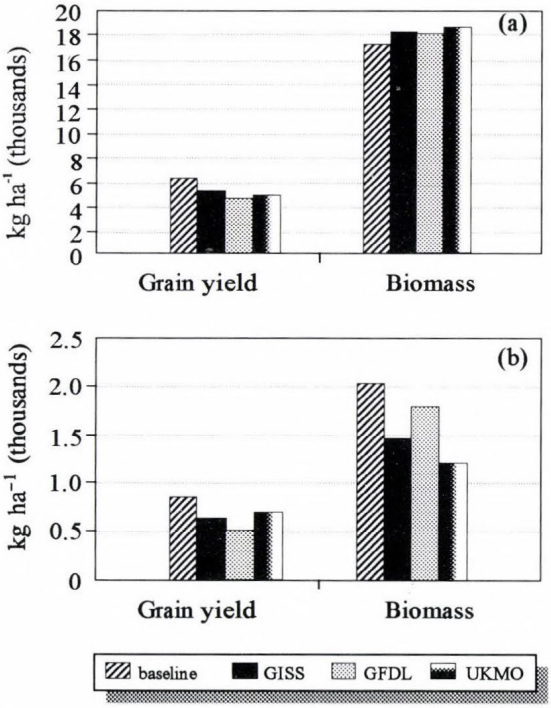

Fig. 11. Averages (*a*) and standard (*b*) deviations for the modelled development variables of wheat for the various climate scenarios.

5.3 Adjustment in agrotechnology to diminish unfavourable consequences

The present study also tried to assess whether modifications in agrotechnology could diminish the disadvantageous consequences of the climate change, or even turn them to advantageous results. These investigations were limited to the maize crop and for adjustments in sowing date and choice of variety.

In the original experiments the sowing date of 20 April and the variety Pioneer 3901 were used. In the sowing date adjustment experiments the impacts of 10 days earlier and 10 days later sowing were assessed.

Surprisingly, the three climate change scenarios produced different results. In the case of the GISS scenario neither the earlier nor the later sowing increased either grain yield or biomass production of the maize crop. For the GFDL scenario the later sowing at 30 April resulted in a slight increase in grain yield, which, however, was still lower than the baseline yield under the original sowing date. For the UKMO scenario the earliest sowing, that is, 10 April resulted in the best yield, but it is also lower, than the original baseline yield of 20 April (see *Table 2*).

In the variety choice experiments Pioneer 3382, a variety of longer growing

Table 2. The effect of sowing date on maize production under various weather scenarios

Variety: Pioneer 3901	Weather scenario			
Sowing date: 10 April	Baseline	GISS	GFDL	UKMO
Maturity date	2 Sep	6 Aug	28 Jul	20 Jul
Grain yield (kg/ha)	8261	8199	7749	7890
cv%	40.6	40.9	43.2	42.5
Biomass (kg/ha)	15726	15895	15655	16307
cv%	5.2	5.1	5.2	5.0
Sowing date: 20 April	Baseline	GISS	GFDL	UKMO
Maturity date	5 Sep	13 Aug	31 Jul	25 Jul
Grain yield (kg/ha)	8567	9285	7961	7354
cv%	39.1	36.1	42.1	45.6
Biomass (kg/ha)	15947	17285	16099	15251
cv%	5.1	4.7	5.1	5.4
Sowing date: 30 April	Baseline	GISS	GFDL	UKMO
Maturity date	13 Sep	18 Aug	5 Aug	2 Aug
Grain yield (kg/ha)	9096	8716	8254	7484
cv%	36.9	38.4	40.6	44.8
Biomass (kg/ha)	16349	16562	16694	16188
cv%	5.0	4.9	4.9	5.0

season was compared to Pioneer 3901 at the sowing date 20 April. Pioneer 3382 produced much higher grain yields and biomass results for all the three climate change scenarios than the baseline yield of Pioneer 3901, but in comparison with the yield of Pioneer 3382 under the baseline climate, only the GISS scenario led to a yield increase (see *Table 3*).

It has to be remarked, that the results of the variety choice experiments have to be handled with caution, because before having compared the performance of the two varieties the genetic parameters defining the variety characteristics should have been carefully tested, validated. The present study could not carry out this task due to lack of field observations for Pioneer 3382. Summarising the results of the present impact assessment it can be stated that adjustments in agrotechnology, such as careful choice of the sowing date and the variety sown, offer a possibility to compensate for, or at least diminish the unfavourable consequences of climate change.

Table 3. The impact of various climate scenarios on various maize varieties

Variety: Pioneer 3901	Weather scenario			
Sowing date: 20 April	Baseline	GISS	GFDL	UKMO
Maturity date	5 Sep	13 Aug	31 Jul	25 Jul
Grain yield (kg/ha)	8567	9285	7961	7354
cv%	39.1	36.1	42.1	45.6
Biomass (kg/ha)	15947	17285	16099	15251
cv%	5.1	4.7	5.1	5.4

Variety: Pioneer 3382	Weather scenario			
Sowing date: 10 April	Baseline	GISS	GFDL	UKMO
Maturity date	4 Oct	5 Sep	18 Aug	9 Aug
Grain yield (kg/ha)	14335	15703	13705	11964
cv%	23.4	21.3	24.4	28.0
Biomass (kg/ha)	21618	23873	22273	20728
cv%	3.8	3.4	3.7	3.9

6. Summary

The above assessment was aimed at assessing the impacts of a possible greenhouse gas-induced climate change on the winter wheat and maize yields in Western Hungary. As the forecasts regarding this future climate change are rather uncertain at present, three different climate change scenarios were used for the present study. There are serious inherent limitations in these climate scenarios, e.g. severe methodological problems arise in creating regional climate change scenarios from the outputs of global climate models. Another problematic issue is to construct daily weather time series from the outputs of climate models which produce results as seasonal, or at most detail, monthly averages for the changed climatic parameters. Another important research area would be to work with so-called 'transient' scenarios instead of the 'equilibrium' scenarios used here, which could describe the expected climate change as a gradual, dynamic process in time.

The application of crop growth simulation models as tools for climate change impact studies also present some difficulties. In the present assessment the location of the study was the Keszthely area, because field observations and historical weather data were available from this region. In order to use crop models for climate impact assessment studies it is necessary to test and validate

the genetic parameters describing the variety dependent characteristics of the crop varieties, and for this purpose many field observations from several locations would be necessary. A further research task could be to evaluate the impacts of nitrogen fertilization and the nitrogen balance of the crop, which may again lead to interesting conclusions under the changed water balance patterns of the changed climate.

A further issue is the choice of statistical methods to compare the present and 'future' performance of the crops in question. The present study used only a simple comparison of averages and standard deviations, though it might be more important to compare the distributions of the crop yield, and to analyse the probabilities of the occurrence of low and high yields. The techniques of risk assessment and stochastic dominance could be suitable tools for these analyses in the future.

References

Adams, R.M., Rosenzweig, C., Peart, R.M., Ritchie, J.T., McCarl, B.A., Glyer, J.D., Curry, R.B., Jones, J.W., Boote, K.J. and *Allen, L.H. Jr.*, 1990: Global climate change and US agriculture. *Nature 345*, 219-224.

Godwin, D.C., Ritchie, J.T., Singh, U. and *Hunt, L.* 1989: *A User's Guide to CERES Wheat-V2.10.* Muscle Shoals, Alabama: International Fertiliser Development Centre.

Hansen, J., Fung, I., Laces, A., Lebedeff, S., Rind, D., Ruedy, R. and *Russet, G.* 1988: Global climate changes as forecast by the GISS 3-D model. *J. Geophys. Res. 93*, 9341-9364.

Hunkár, M., 1994: Validation of crop simulation model CERES-Maize. *Időjárás 98*, 37-46.

Jones, S.A. and *Kiniry, J.R.*, 1986: *CERES-Maize: A Simulation Model of the Growth and Development of Maize.* Texas A&M University Press, College Station, Texas.

Parry, M.L., Carter, T.R. and *Konijn, N.T.* (eds.), 1988: *The Impact of Climatic Variations on Agriculture.* Vol. 1. Kluwer Academic Press.

Smith, J.B. and *Tirpak, J.A.* (eds.), 1989: *The Potential Effects of Global Climate Change on the United States.* EPA, Washington, DC.

Wetherald, R.T. and *Manabe, S.*, 1986: An investigation of cloud cover change in response to thermal forcing. *Climatic Change 8*, 5-23.

Wilson, C.A. and *Mitchell, J.F.B.*, 1987: A $2 \times CO_2$ climate sensitivity experiment with a global climate model including a simple ocean. *J. Geophys. Res. 92*, 13315-13343.

IDŐJÁRÁS

Quarterly Journal of the Hungarian Meteorological Service
Vol. 98, No. 2, April–June 1994

Cloud motion winds derived from METEOSAT infrared images

Á. T. Meszlényi

Satellite Research Laboratory, Hungarian Meteorological Service
P.O. Box 39, H–1675 Budapest, Hungary

(Manuscript received 14 February 1994; in final form 10 May 1994)

Abstract—A few attempts were made in Hungary about ten years ago for the estimation of wind fields from the displacement of clouds in successive METEOSAT infrared images. These techniques were not fully automatic and at that time the image information was converted into digital data. Now sequences of METEOSAT infrared data are available in digital form every half an hour. It enables the automatic derivation of cloud motion winds from carefully aligned successive satellite images. In this paper the first stage of this automatic method elaborated by us is described. The vectors derived from a twenty-day period are compared with radiosonde measurements and results are presented in this study.

Key-words: cloud motion winds, METEOSAT infrared images, automatic derivation.

1. Introduction

The basic principle of wind determination using geostationary satellite image data is quite simple. The starting point is always a sequence of satellite images, all covering the same area of the Earth's surface. These images are then standardized with each other very carefully, so that the coastlines and the earth horizons coincide from image to image. Then following the movement of clouds across the sequence with different techniques, the wind vectors can be derived.

These techniques include direct measurements of cloud motion from projected time lapse film loops, man machine interactive methods and automatic methods. The cloud motion winds were first determined from carefully aligned successive ATS visible pictures with a cross correlation technique by *Leese* and *Novak* (1971). The various stages of the automatic method were described in detail by *Bowen* (1979), *Rákóczi* and *Kovács* (1981), *Schmetz* and *Nuret* (1987), *Schmetz* (1991).

2. *Image data*

The geostationary METEOSAT satellites observe the Earth with an imaging radiometer in three channels:

VIS: solar spectrum between 0.4 and 1.1 μm,

IR: infrared window region between 10.5 and 12.5 μm,

WV: water vapour absorption band between 5.7 and 7.1 μm.

Images are taken at half hourly intervals and the spatial resolution is 2.5 $\times$ 2.5 km^2 in the VIS and 5 $\times$ 5 km^2 in the IR and WV channels.

METEOSAT IR images form the database for the automatic tracking of clouds with a cross-correlation. Three successive IR images are used to determine a wind vector. We used an image at the time 12 UTC and images at times h $\pm$30 min, that is an image at the time 11.30 UTC and an image at the time 12.30 UTC, in order to eschew inaccuracy proceeding from time difference, when the results are compared with radiosonde measurements. The basic square unit of processing is the segment. This is an array of 32 $\times$ 32 IR pixels called target area, which is cut out from the central image. The centre of each segment is always at a fixed geographical location.

Since the wind vectors are derived from the displacement of clouds, it is necessary that lands and seas, where pixels do not contain clouds, are left out of consideration. Empirically estimated threshold values are used for this purpose.

The wind vectors are computed for such locations, where radiosonde measurements are carried out regularly. Thus the inaccuracy proceeding from different locations of the calculated and measured vectors can be avoided, when the cloud motion winds are compared with radiosonde values.

If the wind vector is computed for a given station, the centre of segment is determined by its position. Then the φ, λ coordinates of the station are converted into x, y coordinates of satellite image, which are the coordinates of centre of segment.

3. *Wind vector determination*

The target area is cut out from the central image at time 12 UTC. The search area is an array of 3 $\times$ 3 segments cut out from the subsequent image at time 12.30 UTC. The search area is centered on the same pixel as the target area. The target area is moved stepwise over the search area. Correlation coefficients are computed for two pairs of the successive images.

If the best match is found between the target area and the central segment of the search area then there is a calm. If the match is good enough displaced from the centre, then the clouds have moved during the intervening period, and the displacement from the centre presents the wind velocity.

There are 65 × 65 possible displacements of the target area within the large search area. For each location the correlation coefficient between the target area and search area is computed. These correlation coefficients can be thought of as a correlation surface and its peak gives the best match between the two images. So the highest value of the correlation coefficients is searched. The distance and direction of the peak from the centre indicate the cloud motion wind vector.

Consequently, starting and extreme points of wind vector are known in the satellite image (x_1,y_1 ; x_2,y_2). Converting this coordinates into geographical coordinates x_1,$y_1 \rightarrow \varphi_1$,$\lambda_1$ and x_2,$y_2 \rightarrow \varphi_2$,$\lambda_2$, the speed ($v$) and direction ($\beta$) of the cloud motion wind are given by the following formulas (*Tänczer*, 1988):

$$\cos \varphi_c = \sin \varphi_1 \sin \varphi_2 + \cos \varphi_1 \cos \varphi_2 \cos (\lambda_2 - \lambda_1), \tag{1}$$

$$|v| = \frac{R\varphi_c}{t_2 - t_1}, \tag{2}$$

$$\beta = \arcsin \frac{\sin (\lambda_2 - \lambda_1) \cos \varphi_1}{\sin \varphi_c}, \tag{3}$$

where φ_c is the spherical distance between the two points, R is the Earth's radius, t_1 and t_2 are the image taking times.

4. Symmetry check

However, the cloud patterns can repeat themselves in the successive images, so there is a chance to find wrong local maximum. Therefore use of a quality check based on symmetry criteria is needed. The same process as outlined in the previous chapter is repeated, comparing the image at time h (12 UTC) with the image at time h -30 min (11.30 UTC). This symmetry check rejects all vectors for which the vector pair speeds or directions are not symmetrical within certain thresholds (*Schmetz* and *Nuret*, 1989).

5. Height assignment

The following step is to perform the height assignment of wind vector. The IR radiance is used for cloud height attribution. The brightness value of starting point of the wind vector is converted into a temperature by means of the Planck's relationship. The temperature of the cloud top can be converted into

a pressure or height if the atmospheric profile is known. The height of starting point of wind vector is computed using the TEMP data of the given station.

6. Results and conclusion

A twenty-day overcast period was selected. Each day the TEMP data and IR images at time 11.30 UTC, 12 UTC and 12.30 UTC were used for the study. Fourteen stations were selected in the vicinity of Hungary, where radiosonde measurements are performed regularly at these times. So 280 wind vectors have been produced. From these

— in 42 case there were no TEMP data at the given station;
— in 13 case there was no cloudy pixel in the segment;
— 96 vectors are removed by the symmetry check.

So in all 129 wind vectors have remained for comparing with radiosonde measurements.

It is remarkable that the use of a symmetry check has decreased the number of wind vectors from 225 to 129. Our examinations, however, prove that values removed by symmetry check are really very different from radiosonde values. If the calculations are performed to all segments of a greater area, then after the symmetry check enough wind vectors will remain to characterize the wind field.

The results obtained by comparing of the cloud motion winds and radiosonde measurements are presented in figures.

In *Fig. 1* the frequency distribution of differences between the wind speeds derived from images and measured by radiosonde can be seen. Small differences are observable in most cases, although large differences also occur (24 m/s $< \Delta v <$ 26 m/s) in some cases. The largest frequency of the distribution falls in to the interval of 2–4 m/s. So the peak is shifted to positive direction.

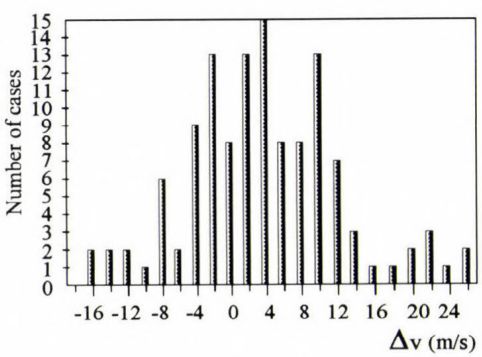

Fig. 1. Frequency distribution of differences (Δv (m/s)) between wind speeds from cloud motion and radiosonde in all cases of our examination.

Fig. 2 shows frequency distribution of differences in case of different level winds derived from low (<2000 m), medium (2000–7000 m) and high-level (>7000 m) clouds. The peak is shifted to positive direction in case of low-level clouds, however, the result cannot be considered too characteristic because of the small number of cases. The peak is situated closer to the 0 in the case

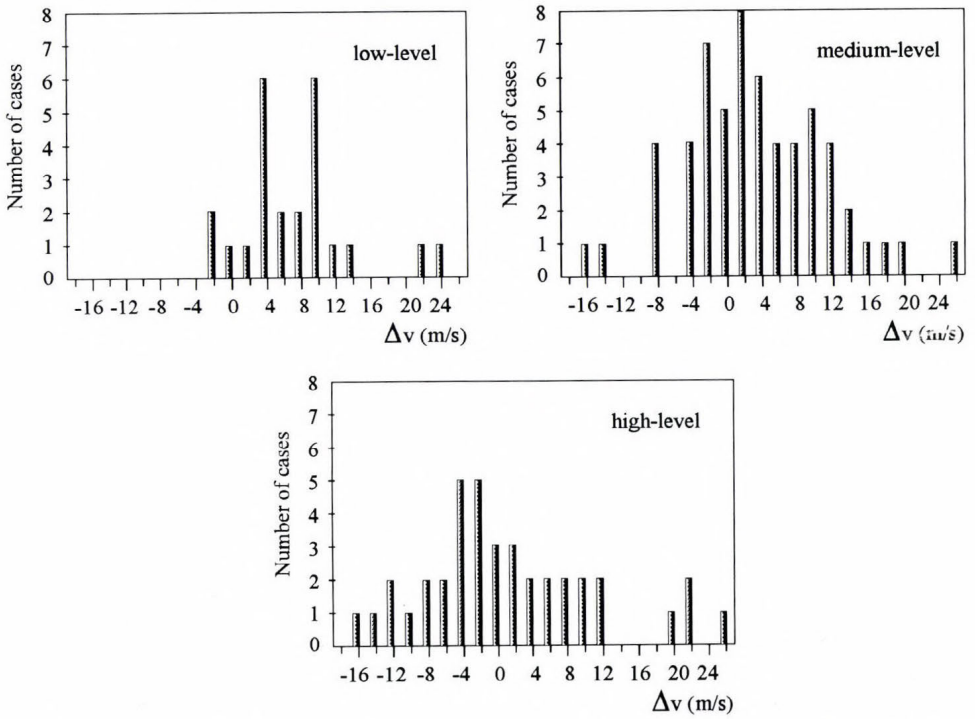

Fig. 2. Frequency distribution of differences (Δv (m/s)) between wind speeds from cloud motion and radiosonde in cases computed from low-level (< 2000 m), medium-level (2000–7000 m), high-level (> 7000 m) clouds.

of medium-level clouds comparing with Fig. 1. The smaller windspeed differences occur more frequently, but the great differences only in a few cases. It means that our calculation gives more accurate results in case of medium-level winds. There is a less significant peak of the windspeed differences in case of high-level clouds, which tends to negative direction, so the high-level winds are slightly underestimated.

The frequency distribution was examined in different windspeed categories (0–10 m/s, 10–20 m/s, 20–30 m/s) as well, which can be seen in *Fig. 3.* General shift to positive direction can be observed in case of windspeed under 10 m/s. The peak is between –4 m/s and –2 m/s in case of medium wind speed, but two secondary maximum occur at 4 m/s and 8 m/s. The shift to negative direction in case of strong winds follows from the underestimation of the high-level winds.

Frequency distribution of differences of the wind direction is represented in *Fig. 4.* Nevertheless, in *Fig. 5* the same is shown in cases of low, medium and high-level winds. The differences of wind directions are close to a normal

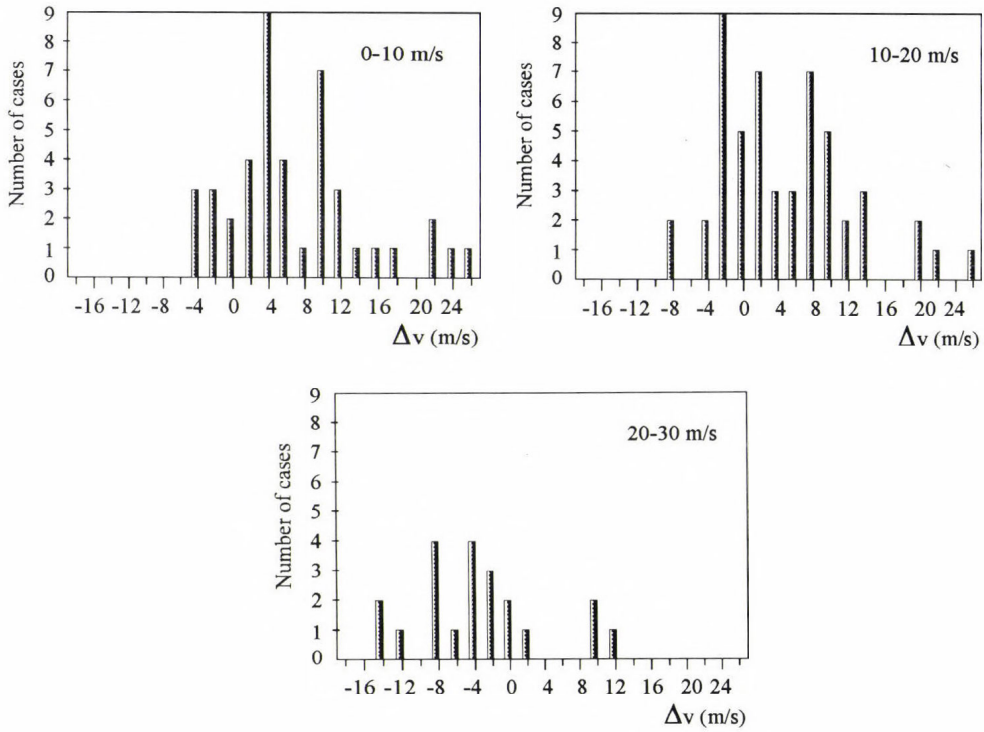

Fig. 3. Frequency distribution of differences (Δv (m/s)) between wind speeds from cloud motion and radiosonde in cases of measured wind speeds ranging 0–10 m/s, 10–20 m/s, 20–30 m/s.

distribution with a peak at 0. The separation of the three levels did not give more characteristic results.

Considering the simplicity of this method, rather good results have been achieved. Further improvement of the results can be expected by means of development of the method, for instance: application of multispectral image analysis and radiance slicing technique, refining the location of the peak on the correlation surface.

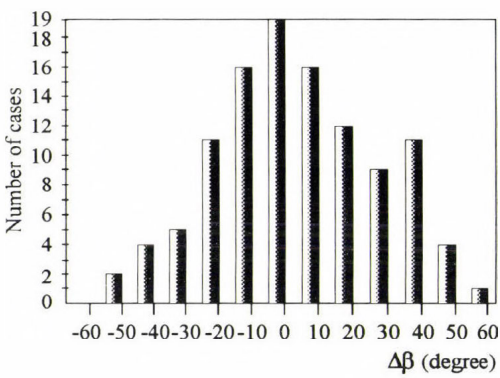

Fig. 4. Frequency distribution of differences (Δβ (degree)) between wind directions from cloud motion and radiosonde in all cases of our examination.

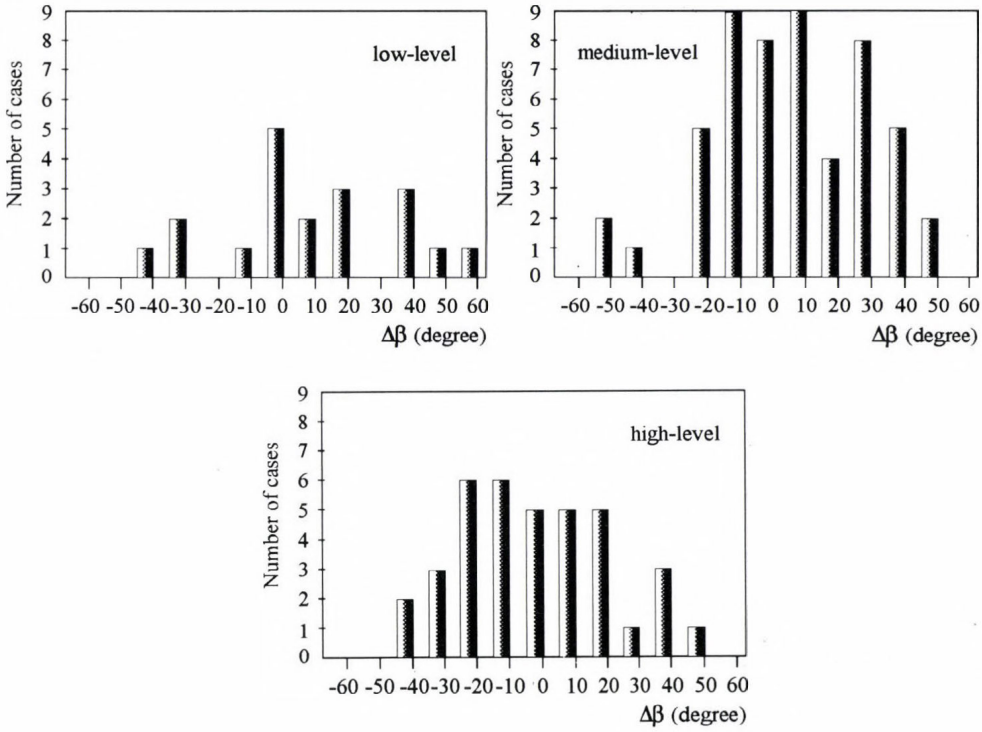

Fig. 5. Frequency distribution of differences ($\Delta\beta$ (degree)) between wind directions from cloud motion and radiosonde in cases computed from low-level (< 2000 m), medium-level (2000-7000 m), high-level (> 7000 m) clouds.

References

Bowen, R., Fusco, L., Morgan, J. and *Roeska, K.O.*, 1979: Operational production of cloud motion vectors (satellite winds) from METEOSAT image data. In *Proc. Use of Data from Meteorological Satellites*, ESA SP-143, 65-75.

Leese, L., Novak, S. and *Clark, B.*, 1971: An automated technique for obtaining cloud motion from geosynchronous satellite data using crosscorrelation. *J. Appl. Meteorol. 10*, 118-132.

Rákóczi, F. and *Kovács, E.*, 1981: Wind-field analysis on the basis of METEOSAT images. *Adv. in Space Research 1*, 133-137.

Schmetz, J., 1991: Cloud motion winds from METEOSAT: performance of an operational system. *Palaeogeogr., Palaeoclimatol., Palaeoecol.* (Global Planet. Change Sect.), 90, 151-156.

Schmetz, J. and *Nuret, M.*, 1987: Automatic tracking of high-level clouds in METEOSAT infrared images with a radiance windowing technique. *ESA Journal 11*, 275-286.

Schmetz, J. and *Nuret, M.*, 1989: Cloud motion wind estimates in Europe. In *The Use of Satellite Data in Operational Numerical Weather Prediction 1989-1993*. Proceedings of a workshop held at ECMWF, 9-12 May 1989, Vol. II, October 1989, 263-273.

Tänczer, T., 1988: *Műholdmeteorológia*. Akadémiai Kiadó, Budapest.

BOOK REVIEW

Meadows, D. H., Meadows, D. L. and *Randers, J.*: **Beyond the Limits**. Chelsea Green Publishing Company, Vermont (USA), 1992. pp. XIX and 300. ISBN 0-930031-55-5 (hard cover): 19.95 $.

More than twenty years ago the same authors published an international best-seller entitled '*The Limits to Growths*'. This book was sold 9 million copies in 29 languages. In this famous volume it was argued that the world economy goes towards its limits. In other words: if everything remains unchanged, the limits to physical growth on the planet-Earth would be reached during the next century. In the present book the authors express their view that in many respects the limit has already overshot: we are '*Beyond the Limits*'. They conclude, however, that the decline is not inevitable: a *sustainable society* is still technically and economically possible.

In the first chapter of the book the definition of the overshoot is given: it means that one goes beyond limits inadvertently, without meaning to do so. In the second chapter it is explained that the overshoot is due to exponential growth in world population and world industry. In many parts of the planet the population growth has resulted in poverty. There is a positive feedback between population growth and poverty. The situation is the worst in Africa, where the food production per capita has decreased since 1960.

The limits are overshot when the balance between sources and sinks is deteriorated. The problem is caused by the fact (Chapter 3) that both population and industrial capital (hardware, machines, factories etc.) have a potential for self-reproduction. For this, people need food, water, air and nutrients to grow, while machines need energy, water and air, minerals, chemicals and biological materials to produce goods and to make more machines. The quantity of these is limited in the Earth, more exactly it is in equilibrium because of the interaction of sources and sinks.

The sustainability is destroyed if the renewable resources are not regenerated, or the nonrenewable resources are not substituted by renewable resources at the rate of their use (e.g. when we use oil and the profit is not invested in solar collectors or in tree planting). Further, for a pollutant a sustainable rate of emission must be below the rate at which the pollutant is recycled. This indicates that we have to learn the dynamics of growth in a finite world as it is discussed in Chapter 4.

Chapter 5 of the book is devoted to the ozone story since the use of freons has already destroyed the balance of the formation and natural removal of stratospheric ozone. This example is applied by the authors to explain what does it mean that we are beyond the limit and how we can restore the natural state.

Chapter 6 is entitled: 'Technology, markets, and overshoot'. The main message of this chapter is that technology and free market can not solve alone the problem we face in spite of the spectacular development of technology and successes of the free market. This is illustrated by using a computer model called World3 elaborated by the authors. Thus, it is concluded that we have only two possibilities: the overshoot and collapse or 'controlled reduction of throughput by deliberate social choice'.

Chapter 7 of the book is interesting in particular. The meaning of a sustainable system is presented in detail. The authors cite the memorable words of the World Commission on Environment and Development according to which a sustainable society is one that 'meets the needs of the present without compromising the ability of future generations to meet their own needs'. In such a society the properties of the human heart and soul are different to the present ones. Thus, we have to change not the technologies, markets or governments but our own mentality. Finally, in the last chapter the authors express the hope of all of us that mankind is not before a collapse, but before the realization of a sustainable economic and social system.

It goes without saying that the present book can be proposed to everybody who cares about our present and future. Although the authors are economists, the text is readable by any educated person. The volume is recommended particularly to those meteorologists who are interested in climate variations and their relationships with world population and economic development.

E. Mészáros

NEWS

Scientific aspects of sustainable development

On the occasion of the General Assembly of the Hungarian Academy of Sciences a joint conference was organized on May 11, 1994 by the Department of Earth Sciences and the Commission of the Environmental Science of the Academy for discussing the scientific aspects of the concept of sustainable development. At the meeting Hungarian scientists of different disciplines outlined their view on the subject.

As it is known a *sustainable society* satisfies its needs in harmony with the environment. It can persist and makes the life for future generations possible. This simple definition becomes rather complicated if we want to define the word 'need'. The question is even more complex if one intends to say exactly what does 'development' mean. It is certain that a sustainable society cannot be poor. However, to cease the poverty on the Earth it would be necessary to increase considerably the standard of life of less developed part of the world. People in these country need a lot of energy, food and goods. How it is possible to meet this requirement without destroying further the environment, the biosphere and natural resources? On the other hand, how it is possible that people in more developed countries moderate their consumption without decreasing significantly the quality of their life? In other words: is the sustainable development a real concept?

During the conference it was more or less agreed that the evolution of our planet has been controlled by the presence of the biosphere. On the basis of physical and chemical principles we cannot simply explain why the planet-Earth is habitable (this point was stressed by *G. Marx*). It follows from this argument that the protection of the biosphere is of crucial interest for mankind. Thus, the conservation of the biodiversity is one of our most important tasks (*G. Vida*) for future. An other essential problem is to mitigate the global air pollution which can cause inadvertent climate modification. In this respect the scientific problems of climate forecasting was discussed. *G. Major* concluded that, beside the influence of greenhouse gases, anthropogenic changes in planetary albedo should also be considered to foresee more precisely climate of the next century.

Several speakers expressed the view that the continuation of the present growth in population and economy and – consequently – the present modification of the environment will lead to serious world-wide problems. Possible solutions were proposed to solve the economy-environment dilemma. *G. Vajda* spoke about the improvement of the energy production and air-cleaning technologies as well as about the necessity of a more efficient energy and material use. *G. Enyedy* stressed the need for a new taxation system which takes into account

the environmental effects of the production. The view generally accepted by the participants was formulated by *R. Czelnai* who argued that the concept of sustainable development is realizable only if the mentality of people can be modified. Such an 'impractical' philosophy is necessary which gives sense to human life without the continuous accumulation of material goods.

The conference was closed by *I. Láng*, session chairman, who mentioned, among other things, the difficulties of the present Hungarian economy which make the environmental management in the country even more complicated. However, he expressed his hope that the coming new Hungarian administration will do everything possible to take part in international efforts aiming to move human societies towards the realization of sustainable development.

E. Mészáros

ATMOSPHERIC ENVIRONMENT

an international journal

To promote the distribution of Atmospheric Environment *Időjárás* publishes regularly the *contents* of this important journal. For further information the interested reader is asked to contact *Dr. P. Brimblecombe,* School for Environmental Sciences, University of East Anglia, Norwich NR 7TJ, U.K.

Volume 28 Number 3 1994

A.J. Policastro, W.E. Dunn and *R.A. Carhart*: A model for seasonal and annula cooling tower impacts, 379-395.

R.N. Colvile, T.W. Choularton, M.W. Gallagher, A.J. Wicks, R.M. Downer, B.J. Tyler, K.J. Storeton-West, D. Fowler, J.N. Cape, G.J. Dollard, T.J. Davies, B.M.R. Jones, S.A. Penkett, B.J. Bandy and *R.A. Burgess*: Observation on Great Dun Fell of the pathways by which oxides of nitrogen are converted to nitrate, 397-408.

R.L. Bennett, L. Stockburger and *H.M. Barnes*: Comparison of sulfur measurements from a regional Fine Particle Network with concurrent Acid MODES network results, 409-419.

G.D. Hayman, M.E. Jenkin, T.P. Murrells and *C.E. Johnson*: Tropospheric degradation chemistry of HCFC-123 (CF_3CHCl_2): a proposed replacement chlorofluorocarbon, 421-437.

H. Elias, U. Götz and *K.J. Wannowius*: Kinetics and mechanism of the oxidation of sulfur (IV) by peroxomonosulfuric acid anion, 439-448.

R. Sempéré and *K. Kawamura*: Comparative distribution of dicarboxylic acids and related polar compounds in snow, rain and aerosols from urban atmosphere, 449-459.

J.S. Bower, G.F.J. Broughton, J.R. Stedman and *M.L. Williams*: A winter NO_2 smog episode in the U.K., 461-475.

G.W. Campbell, J.R. Stedman and *K. Stevenson*: A survey of nitrogen dioxide concentrations in the United Kingdom using diffusion tubes, July-December 1991, 477-486.

J.W. Erisman, B.G. van Elzakker, M.G. Mennen, J. Hogenkamp, E. Zwart, L. van de Beld, F.G. Römer, R. Bobbink, H. Heil, M. Raessen, J.H. Duyzer, H. Verhage, G.P. Wyers, R.P. Otjes and *J.J. Möls*: The Elspeetsche Veld experiment on surface exchange of trace gases: summary of results, 487-496.

R.M. Harrison, Z. Zlatev and *C.J. Ottley*: A comparison of the predictions of an Eulerian atmospheric transport-chemistry model with experimental measurements over the North Sea, 497-516.

F. Martin, F. Valero and *J.A. García-Miguel*: On the response of the background atmospheric CO_2 growth rate to the anomalies of the sea-surface temperature in the equatorial Pacific Oceans, 517-530.

A.S. Wexler, F.W. Lurmann and *J.H. Seinfeld*: Modelling urban and regional aerosols—I. Model development, 531-546.

R.l. Falconer and *T.F. Bidleman*: Vapor pressure and predicted particle/gas distributions of polychlorinated biphenyl congeners as functions of temperature and ortho-chlorine substitution, 547-554.

O.R. Bullock Jr: A computationally efficient method for the characterization of sub-grid-scale precipitation variability for sulfur wet removal estimates, 555-566.

Volume 28 Number 4 1994

D.W. Clow and *G.P. Ingersoll*: Particulate carbonate matter in snow from selected sites in the south-central Rocky Mountains, 575-589.

H. Kauppa, J. Towara and *M.S. McLachlan*: Distribution of polychlorinated dibenzo-*p*-dioxins and dibenzofurans in atmospheric particulate matter with respect to particle size, 585-593.
S.F. Mueller and *R.E. Imhoff*: Estimates of particle formation and growth in coal-fired boiler exhaust—I. Observations, 595-602.
S.F. Mueller and *R.E. Imhoff*: Estimates of particle formation and growth in coal-fired boiler exhaust—II. Theory and model simulations, 603-610.
T. Tirabassi and *U. Rizza*: Applied disperion modelling for ground-level concentrations from elevated sources, 611-615.
B. Dupré, Ph. Négrel, F. Seimbille and *C.J. Allegre*: $^{87}Sr/^{86}Sr$ ratio variation during a rain event, 617-620.
H. Horvath, G. Metzig, O. Preining and *R.F. Pueschel*: Observation of a blue sun over New Mexico, U.S.A., on 19 April 1991, 621-630.
H. Nitta, M. Ichikawa, M. Sato, S. Konishi and *M. Ono*: A new approach based on a covariance structure model to source apportionment of indoor fine particles in Tokyo, 631-636.
R.G. Harrison and *H.M. ApSimon*: Krypton-85 pollution and atmospheric electricity, 637-648.
H.M. ApSimon, R.F. Warren and *J.J.N. Wilson*: The abatement strategies assessment model – ASAM: applications to reductions of sulphur dioxide emissions across Europe, 649-663.
H.M. ApSimon, B.M. Barker and *S. Kayin*: Modelling studies of the atmospheric release and transport of ammonia in anticyclonic episodes, 665-678.
R.W. Allott, M. Kelly and *C.N. Hewitt*: A model of environmental behaviour of contaminated dust and its application to determining dust fluxes and residence times, 679-687.
Zhao Dianwu and *Wang Anpu*: Estimation of anthropogenic ammonia emissions in Asia, 689-694.
C.P. Wake, J.E. Dibb, P.A. Mayewski, Li Zhongqin and *Xie Zichu*: The chemical compositon of aerosols over the eastern Himalayas and Tibetan plateau during low dust periods, 695-704.
C.M. Romo-Kröger, J.R. Morales, M.I. Dinator, F. Llona and *L.C. Eaton*: Heavy metals in the atmosphere coming from a copper smelter in Chile, 705-711.
K.J. Allwine and *C.D. Whiteman*: Single-station integral measures of atmospheric stagnation, recirculation and ventilation, 713-721.
R.H. Myrick, S.K. Sakiyama, R.P. Angle and *H.S. Sandhu*: Seasonal mixing heights and inversions at Edmonton, Alberta, 723-729.
D.H. Lowenthal, B. Zielinska, J.C. Chow, J.G. Watson, M. Gautam, D.H. Ferguson, G.R. Neuroth and *K.D. Stevens*: Characterization of heavy-duty diesel vehicle emissions, 731-743.

Volume 28 Number 5 1994

Conference on Visibility and Fine Particles, Vienna, Austria, 15-18 September 1992

H. Horvath: Conference on Visibility and Fine Particles, Vienna, Austria, 15-18 September 1992: an overview, 755-756.
H. Horvath: Remarks and suggestions on nomenclature and symbols in atmospheric optics, 757-759.

Section I: Atmospheric optics and image transfer
I.L. Katsev and *E.P. Zege*: The modern theory of black object visibility and meteorological visibility range, 763-767.
C. Rozé, B. Maheu, G. Gréhan and *J. Ménard*: Evaluations of the sighting distance in a foggy atmosphere by Monte Carlo simulation, 769-775.
M. Kocifaj: Solving the diffusion of solar radiation in the atmosphere and identifying the aerosol structure, 777-783.
M. Wendisch and *W. von Hoyningen-Huene*: Possibility of refractive index determination of atmospheric aerosol particles by ground-based solar extinction and scattering measurements, 785-792.

Section II: In-cloud transformation of particles

V. Ulevičus, S. Trakumas and *A. Girgždys*: Aerosol size distribution transformation in fog, 795-800.

Section III: Humidity influence on particle growth and visibility

W.E. Wilson and *P.C. Reist*: A PC-based Mie scattering program for theoretical investigations of the optical properties of atmospheric aerosols as a function of composition and relative humidity, 803-809.

E.-M. Uhlig, M. Stettler and *W. von Hoyningen-Huene*: Experimental studies on the variability of the extinction coefficient by different air masses, 811-814.

B.A. Nilsson: Model of the relation between aerosol extinction and meteorological parameters, 815-825.

M.L. Pitchford and *P.H. McMurry*: Relationship between measured water vapor growth and chemistry of atmospheric aerosol for Grand Canyon, Arizona, in winter 1990, 827-839.

K.A. Gebhart, W.C. Malm and *D. Day*: Examination of the effects of sulfate acidity and relative humidity on light scattering at Shenandoah National Park, 841-849.

J.F. Sisler and *W.C. Malm*: The relative importance of soluble aerosols to spatial and seasonal trends of impaired visibility in the United States, 851-862.

Section IV: Light absorption by aerosol particles

T. Raunemaa, U. Kikas and *T. Bernotas*: Observations of submicron aerosol, black carbon and visibility degradation in remote area at temoerature range from –24 to 20°C, 865-871.

G.W. Mulholland and *N.P. Bryner*: Radiometric model of the transmission cellreciprocal nephelometer, 873-887.

R.A. Dobbins, G.W. Mulholland and *N.P. Bryner*: Comparison of a fractal smoke optics model with light extinction measurements, 889-897.

Section V: Measuring methods and networks

M. Gazzi, V. Vicentini and *U. Bonafé:* A field experiment on contrast reduction law, 901-907.

W.H. White, E.S. Macias, R.C. Nininger and *D. Schorran*: Size-resolved measurements of light scattering by ambient particles in the southwestern U.S.A., 909-921.

W. von Hoyningen-Huene and *M. Wendisch*: Variability of aerosol optical parameters by advective processes, 923-933.

A. Thomas and *J. Gebhart*: Correlations between gravimetry and light scattering photometry for atmospheric aerosols, 935-938.

H. Tang, E.A. Lewis, D.J. Eatough, R.M. Burton and *R.J. Farber*: Determination of the particle size distribution and chemical composition of semi-volatile organic compounds in atmospheric fine particles with a diffusion denuder sampling system, 939-947.

Section VI: Airplane and space observations, solar photometry

R.F. Pueschel, J.M. Livingston, G.V. Ferry and *T.E. DeFelice*: Aerosol abundances and optical characteristics in the Pacific Basin free troposphere, 951-960.

J. Lukáč: Trend of solar radiation attenuation by atmospheric aerosols, 961-962.

V.E. Cachorro and *A.M. de Frutos*: Retrieval of atmospheric aerosol characteristics for visible extinction data at Valladolid (Spain), 963-971.

A.A. Galal and *R.H. Hamid*: On the instability of atmospheric optics in polluted areas, 973-976.

V. Cuomo, C. Serio, F. Esposito and *G. Pavese*: A differential absorption technique in the near infrared to determine precipitable water, 977-987.

Section VII: Trends in visibility and fine particles, including urban data

A. Trier and *L. Firinguetti*: A time series investigation of visibility in an urban atmosphere–I, 991-996.

V.N. Aref'ev and *V.K. Semenov*: Spectral transparency of the atmosphere in the center of the European-Asian continent, 997-999.

R.A. Stuart and *R.M. Hoff*: Airport visibility in Canada–revisited, 1001-1007.

R.A. Eldred and *T.A. Cahill*: Trends in elemental concentrations of fine particles at remote sites in the United States of America, 1009-1019.

Section VIII: Response of visibility to emission changes

W.C. Malm, J. Trijonis, J. Sisler, M. Pitchford and *R.L. Dennis*: Assessing the effect of SO_2 emission changes on visibility, 1023-1034.

W.H. White, E.S. Macias, J.D. Kahl, P.J. Samson, J.V. Molenar and *W.C. Malm*: On the potential of regional-scale emissions zoning as an air quality management tool for the Grand Canyon, 1035-1045.

Section IX: Physiological optics

M.L. Pitchford and *W.C. Malm*: Development and applications of a standard visual index, 1049-1054.

J.V. Molenar, W.C. Malm and *C.E. Johnson*: Visual air quality simulation techniques, 1055-1063.

R.C. Henry, T. Shibata and *D. Chitwood*: Construction and operation of a video-based visual colorimeter for atmospheric research, 1065-1069.

Section X: Physics of aerosols

N. Zhang, Y.C. Chang, R.V. Calabrese and *J.W. Gentry*: The potential use of sequences of Fibonacci series to simulate breakage and agglomeration, 1073-1080.

Volume 28 Number 6 1994

A. Karlsson, K. Irgum and *P. Lindgren*: Trace-level standard for gaseous nitric acid based on sublimation of ammonium nitrate, 1083-1087.

R.M. Harrison and *A.-M. N. Kitto*: Evidence for a surface of atmospheric nitrous acid, 1089-1094.

H. Boudries, G. Toupance and *A.L. Dutot*: Seasonal variation of atmospheric nonmethane hydrocarbons on the western coast of Brittany, France, 1095-1117.

R.L. Tanner and *B. Zielinska*: Determination of the biogenic emission rates of species contributing to VOC in the San Joaquin Valley of California, 1113-1120.

M.A. Nilles, J.D. Gordon and *L.J. Schroder*: The precision of wet atmospheric deposition data from National Atmospheric Deposition Program/National Trends Network sites determined with collocated samplers, 1121-1128.

D.-S. Kim, V.P. Aneja and *W.P. Robarge*: Characterization of nitrogen oxide fluxes from soil of a fallow field in the central Piedmont of North Carolina, 1129-1137.

J.L. Jaffrezo, M.P. Clain and *P. Masclet*: Polycyclic aromatic hydrocarbons in the polar ice of Greenland. Geochemical use of these atmospheric tracers, 1139-1145.

M.L. Sánchez and *J. Sanz*: Application of discriminant analysis to interpret the behaviour of photochemical oxidants in an urban area, 1147-1157.

D.E. Oram and *S.A. Penkett*: Observations in eastern England of elevated methyl iodide concentrations in air of Atlantic origin, 1159-1174.

B.J. Johnson, S.C. Huang, M. LeCave and *M. Porterfield*: Seasonal trends of nitric acid, particulate nitrate, and particulate sulfate concentrations at a southwestern U.S. mountain site, 1175-1179.

O. Klemm, A.S. Bachmeier, R.W. Talbot and *K.I. Klemm*: Fog chemistry at the New England coast: influence of air mass history, 1181-1188.

E.O. Edney, D.J. Driscoll, E.W. Corse and *F.T. Blanchard*: Laboratory investigations of interactions of irradiated *o*-xylene/NO_x/SO_2/air mixtures with aqueous media containing sodium fluoride, sodium trifluoroacetate, ammonium nitrate and hydrogen peroxide, 1189-1196.

A. Guenther, P. Zimmerman and *M. Wildermuth*: Natural volatile organic compound emission rate estimates for U.S. woodland landscapes, 1197-1210.

Shuming Du, J.D. Wilson and *E. Yee*: Probability density functions for velocity in the convective boundary layer, and implied trajectory models, 1211-1217.

NOTES TO CONTRIBUTORS

The purpose of *Időjárás* is to publish papers in the field of theoretical and applied meteorology. These may be reports on new results of scientific investigations, critical review articles summarizing current problems in certain subject, or shorter contributions dealing with a specific question. Authors may be of any nationality but papers are published only in English.

Papers will be subjected to constructive criticism by unidentified referees.

* * *

The manuscript should meet the following formal requirements:

Title should contain the title of the paper, the names(s) of the author(s) with indication of the name and address of employment.

The title should be followed by an *abstract* containing the aim, method and conclusions of the scientific investigation. After the abstract, the *key-words* of the content of the paper must be given.

Three copies of the manuscript, typed with double space, should be sent to the Editor-in-Chief: *P.O. Box 39, H-1675 Budapest,* Hungary.

References: The text citation should contain the name(s) of the author(s) in Italic letter or underlined and the year of publication. In case of one author: *Miller* (1989), or if the name of the author cannot be fitted into the text: *(Miller,* 1989); in the case of two authors: *Gamov* and *Cleveland* (1973); if there are more than two authors: *Smith et al.* (1990). When referring to several papers published in the same year by the same author, the year of publication should be followed by letters a,b etc. At the end of the paper the list of references should be arranged alphabetically. For an article: the name(s) of author(s) in Italics or underlined, year, title of article, name of journal, volume number (the latter two in Italics or underlined) and pages. E.g. *Nathan, K. K.,* 1986: A note on the relationship between photosynthetically active radiation and cloud amount. *Időjárás 90,* 10-13. For a book: the name(s) of author(s), year, title of the book (all in Italics or underlined with except of the year), publisher and place of publication. E.g. *Junge, C. E.,* 1963: *Air Chemistry and Radioactivity.* Academic Press, New York and London.

Figures should be prepared entirely in black India ink upon transparent paper or copied by a good quality copier. A series of figures should be attached to each copy of the manuscript. The legends of figures should be given on a separate sheet. Photographs of good quality may be provided in black and white.

Tables should be marked by Arabic numbers and provided on separate sheets together with relevant captions. In one table the column number is maximum 13 if possible. One column should not contain more than five characters.

Mathematical formulas and *symbols:* non-Latin letters and hand-written marks should be explained by making marginal notes in pencil.

The final text should be submitted both in manuscript form and on *diskette.* Use standard 3.5" or 5.25" DOS formatted diskettes for this purpose. The following word processors are supported: WordPerfect 5.1, WordPerfect for Windows 5.1, Microsoft Word 5.5, Microsoft Word for Windows 2.0. In all other cases the preferred text format is ASCII.

* * *

Authors receive 30 *reprints* free of charge. Additional reprints may be ordered at the authors' expense when sending back the proofs to the Editorial Office.

Published by the Hungarian Meteorological Service

Budapest, Hungary

INDEX: 26 361

HU ISSN 0324-6329